ADSORPTION REFRIGERATION CYCLE WITH MASS AND HEAT RECOVERY

by

Kadir Yiğit Yıldız

B.S., in Mechanical Engineering, İstanbul Technical University, 2010

Submitted to the Institute for Graduate Studies in

Science and Engineering in partial fulfillment of

the requirements for the degree of

Master of Science

Graduate Program in Mechanical Engineering

Boğaziçi University

2014

ADSORPTION REFRIGERATION CYCLE WITH MASS AND HEAT RECOVERY

APPROVED BY:

Assoc. Prof. Hasan Bedir .....

(Thesis Supervisor)

Assoc. Prof. Kunt Atalık .....

Prof. Ramazan Yıldırım .....

DATE OF APPROVAL: 24.01.2014

to my family

ACKNOWLEDGEMENTS

I would like to express my truthful gratitude to my thesis supervisor Assoc. Prof. Hasan Bedir for his collaboration, endeavor and consultancy that he has provided so far. It was a pleasure and honor for me to work together on this thesis study. I also thank to Assoc. Prof. Kunt Atalık and Prof. Ramazan Yıldırım who enlist me by their valuable comment and submission.

I would also like to take this opportunity to thank my family for their peerless support during my thesis study which is devoted to them.

I hope this thesis study will provide the reader access to the relevant literature and promote further research toward improving and developing adsorption refrigeration systems.

ABSTRACT

ADSORPTION REFRIGERATION CYCLE WITH MASS AND HEAT RECOVERY

A non-uniform temperature/uniform pressure mathematical model of a combined mass and heat recovery adsorption cooling cycle based on activated carbon/methanol working pair is examined and numerically solved under certain assumptions and operating conditions in this thesis study. The one dimensional model describes the transient heat and mass transfer phenomena within an external-heated generator containing a porous medium in detail by utilizing Dubinin-Astakhov adsorption equilibrium. Mathematical model was programmed with an algorithm in MATLAB software by using forward time centered space finite difference explicit method. Stability and convergence analysis are performed by changing grid size of the domain in order to ensure utilized numerical method reliability. Dynamic sorption amount and temperature development within adsorbent bed are obtained, and consequently system performance is calculated for several working pairs such as activated carbon/ammonia, activated carbon/methanol, silica gel/water, and zeolite/water in terms of coefficient of performance and specific cooling power. Then parametric analysis is carried out by searching heat source temperature, condenser temperature, evaporator temperature, adsorbent porosity, and adsorbent bed geometry effect on system performance. As an outcome of the analysis done, activated carbon/methanol is selected as an appropriate working pair for the combined mass and heat recovery adsorption refrigeration cycle. Mass recovery and heat recovery's performance enhancement effect are analyzed and 25% improvement is obtained on both coefficient of performance and specific cooling power. By performing a cycle time optimization analysis, it is showed that total cycle time can be reduced 77.8% for basic adsorption cooling cycle utilizing activated carbon/methanol and consequently the performance enhancement can be promoted for the combined mass and heat recovery adsorption cooling cycle.

ÖZET

KÜTLE VE ISI İYİLEŞTİRMELİ SOĞURMALI SOĞUTMA ÇEVRİMİ

Bu tez çalışmasında, aktif karbon/metanol çiftini kullanan kütle ve ısı iyileştirmeli soğurmalı soğutma çevrimi homojen olmayan sıcaklık ve homojen basınç matematik modeli kullanılarak incelenmiş ve nümerik olarak çözülmüştür. Bir boyutlu bu model Dubinin-Astakhov soğurma dengesini kullanarak içinde boşluklu ortam bulunduran dıştan ısıtmalı üretici içindeki süreksiz ısı ve kütle transferini tanımlamaktadır. Matematik model, ileri zaman ve merkez aralık sonlu farklar yöntemini kullanarak MATLAB yazılımında programlanmıştır. Soğurma yatağının aralık ölçüsü değiştirilerek kullanılan nümerik metodun güvenilirliğini temin etmek amacıyla kararlılık ve yakınsaklık analizi yapılmıştır. Soğurma yatağı içerisindeki dinamik soğrulma miktarı ve sıcaklık gelişimi elde edilmiş ve sonuç olarak aktif karbon/amonyak, aktif karbon/metanol, silika jel/su ve zeolite/su çalışma çiftleri için sistem performansı, performans katsayısı ve soğutma gücü cinsinden hesaplanmıştır. Parametrik analiz ile ısı kaynağı sıcaklığı, buharlaştırıcı sıcaklığı, yoğuşturucu sıcaklığı, soğurma yatağı boşluk miktarı ve soğurma yatağı geometrik ölçülerinin sistem performansı üzerine etkisi araştırılmıştır. Yapılan analizlerin sonucunda kütle ve ısı iyileştirmeli soğurmalı soğutma çevrimi için aktif karbon/metanol çifti seçilmiştir. Kütle ve ısı iyileştirmesi incelenerek hem sistem performans katsayısı hem de soğutma gücü üzerinde %25 iyileştirici etkisi bulunduğu ortaya konmuştur. Gerçekleştirilen çevrim zamanı optimizasyonu ile toplam çevrim süresinin aktif karbon/metanol çiftini kullanan temel soğurmalı soğutma çevrimi için %77.8 azaldığı gösterilmiş ve sonuç olarak kütle ve ısı iyileştirmeli soğurmalı soğutma çevrimi performansının bu yöntemle daha da artabileceği gösterilmiştir.

TABLE OF CONTENTS

LIST OF FIGURES

LIST OF TABLES

LIST OF ACRONYMS/ABBREVIATIONS

AC	Activated carbon
CFC	Chlorofluorocarbons
COP	Coefficient of performance
D-A	Dubinin-Astakhov
HCFC	Hydro chlorofluorocarbons
HFC	Hydro fluorocarbons
SCP	Specific cooling power

LIST OF SYMBOLS

a	Adsorbed phase
avg	Average
$a_1, a_2, a_3, g_1, g_2, g_3, a_1', g_1'$	States on Clausius-Clapeyron diagram
c	Cycle
c_p	Specific heat at constant pressure
c_v	Specific heat at constant volume
con	Condenser, Concentrated
cw	Heat sink
dil	Diluted
D_s	Surface diffusivity
e	Equilibrium
E_a	Activation energy of surface diffusion
ev	Evaporator
Fo	Fourier number
h_a	Heat of adsorption
hw	Heat source
in	Initial
i, j	Grid points in mesh domain
Ja	Jakob number
k_D	Real (inherent) permeability of the adsorbent bed
k_{eq}	Equivalent thermal conductivity
L_e	Latent heat of vaporization
m	Mass
min	Minimum
p	Pressure
Pe	Peclet number
Q	Energy input/output
Q_e	Refrigeration energy
r	Recovery, Radius
R_0	Specific gas constant of adsorbate

r_{in}	Inner radius of adsorbent bed
r_{out}	Outer radius of adsorbent bed
r_p	Radius of adsorbent particle
s	Solid phase
sat	Saturation
t	Time
T	Temperature
u_v	Vapor velocity
v	Vapor phase
α	Thermal diffusivity
δx	Concentration increase during mass recovery phase
ΔG	Gibbs free energy change
Δr	Incremental radial length
ΔS	Entropy change
Δt	Incremental time
Δx	Concentration change
ε	Adsorbent macro porosity
ε_t	Total porosity of the adsorbent bed
η_{II}	Second law efficiency
μ	Dynamic viscosity
ρ	Density
x	Concentration of adsorbed adsorbate

1. INTRODUCTION

Chlorofluorocarbons (CFCs), used in traditional vapor compression refrigeration systems are not environment friendly because they contribute to the depletion of the ozone layer and have a role in the greenhouse effect. Although other alternatives such as hydro chlorofluorocarbons (HCFCs) and hydro fluorocarbons (HFCs) have less ozone layer depletion effect, they do have the potential of global warming. These environmental protection reasons intensify the research efforts on the development of both ozone layer and global warming safe refrigeration technology [1].

The environmental friendly adsorption cooling system, which employs natural refrigerants like water, ammonia, methanol etc., is an attractive alternative to the conventional vapor compression cooling system for both civil and industrial applications. In addition, the adsorption systems have the benefits of simpler control, no vibration and lower operation costs, if compared with mechanical vapor compression systems. In comparison with the absorption systems, they do not need a solution pump or rectifier for the refrigerant, do not present corrosion problems due to the working pairs normally used, they are less sensitive to shocks and to the installation position [2]. Unlike absorption systems, which use chemical reaction and the substances absorbed actually enter into the crystal lattice of the absorbing material, the adsorption systems use physical phenomenon, which is somewhat similar to the process of condensation. Equilibrium between the solid surface and the gas molecules is usually rapidly attained and easily reversible because the energy requirements are small [3]. Adsorption cooling machines consist essentially of an evaporator, condenser, valves, adsorbent fluid and a generator containing a porous medium (adsorbent bed).

Utilization of waste heat and solar energy is one of the main research fields. Large quantity of stable waste heat can be found in chemical plants, power stations and diesel engines [4]. The adsorption cycle can be driven by this low-grade temperature thermal energy (80-140 °C) as energy source. As a result, it has special advantages in energy saving and environment protection. A great deal of research work has been done over many years, and it is developing more and more rapidly.

As it is known, however, the main drawbacks of adsorption systems are its low coefficient of performance (COP), small specific cooling power (SCP), and long cycle time. These drawbacks are mainly caused by the poor heat and mass transfer conditions in the adsorber. Therefore, much research work is being carried out at present, mainly focused on how to enhance the cycle performance, by several means such as [5]:

- find new better working pairs and improve the adsorption performance
- propose new types of adsorption cycle
- intensify the heat and mass transfer in the adsorber
- decrease the cycle time

New types of adsorption cycle, much has been discussed besides the basic cycle, such as two-adsorber continuous cycle, continuous heat recovery cycle, thermal wave cycle, convective thermal wave cycle, and cascading cycle, which are [6]

- The basic cycle is suitable for recovering heat from intermittent heat sources, like solar energy.
- The two adsorber continuous cycle and continuous heat recovery cycle may be used to recover low-grade thermal energy and will provide continuous cooling effect with a higher thermal efficiency. The heat recovery cycle is practical as the system has reasonable COP and is not so complicated.
- Thermal wave cycle, in which it is assumed that a big temperature gradient exists along an adsorption bed. For a two bed system, high temperature thermal fluid flows into the adsorber, exchanges heat with the bed, and the temperature goes down along the bed rapidly, thus the outlet temperature will be close to ambient. After being cooled by ambient surroundings, the fluid flows into another adsorption bed, adsorbers supply heat to the heat transfer fluid, and the temperature of the fluid goes up. At the exit of this bed, the thermal fluid temperature will be very close to the temperature of heat source. In this case, only less heat is added to the system, and less heat released to the environment, thus heat recovery ratio is high and the COP is of course significantly increased. The thermal wave cycle has the highest theoretical COP, but it is difficult to be realized in a prototype system. It also needs very high thermal conductivity which is not easy for adsorbents to reach. In addition, the thermal fluid velocity is restricted, which reduces specific cooling power.

- Convective thermal wave cycle, the concept is the same as thermal wave cycle, however the thermal fluid for heating or cooling to the bed is initiated by the refrigerant itself, thus the heat transfer between thermal fluid and adsorption bed is direct contact heat transfer, which is incorporated with mass transfer in the system.
- Cascading cycle, in which zeolite/water, activated carbon/methanol, silica gel/water are usually used for cascading. The high temperature heat source (i.e., 200 °C) is used to drive the high temperature stage adsorption refrigeration cycle. The low temperature stage adsorption refrigeration is driven by the sensible heat and heat of adsorption of high temperature stage. But the system will be a complicated one and not suitable for actual engineering application, which prevents it from wide use.

In thesis the combined cycle with mass and heat recovery will be analyzed to enhance the cycle performance. The continuous cycle, which incorporates heat and mass recovery cycles, is verified to be a simple and effective method to improve the thermal performance. The function of the heat recovery cycle is to recover the thermal energy from the temperature difference between the two adsorbent beds, while mass recovery can increase the cycled refrigerant mass, which leads to improved performance. In order to achieve higher performance, mass recovery and heat regeneration can be simultaneously employed. The thermodynamic investigation of a two-bed heat and mass recovery adsorption cycle has been carried out in recent years by several researchers [1]. Although they obtained some good results, their models gave only the COP values without any information of the transient heat and mass transfer.

2. LITERATURE SURVEY

2.1. Adsorption Mechanism on a Solid Surface

Whatever the nature of the forces holding a solid together, it can be regarded as producing a field of force around each ion, atom, or molecule. At the surface of solid, these forces cannot suddenly disappear and thus reach out in space beyond the surface of solid. Due to these unsaturated and unbalanced forces, the solid has a tendency to attract and retain on its surface molecules and ions of other substances with which it comes into contact. Thus, when a solid surface comes in contact with a gas or a liquid, the concentration of the gas or liquid is always greater on the surface of the solid than in the bulk gas or liquid phase [7]. The process by which this surface excess is created is called adsorption. The balance of the forces is partially restored by the adsorption of the gas or the liquid on the surface of the solid. The substance attached to the surface is called adsorbate, and the substance to which it is attached is known as the adsorbent.

Adsorption of a gas on a solid or liquid surface is a spontaneous process. It is, therefore, accompanied by a decrease in free energy of the system. Furthermore, the gaseous molecules in the adsorbed state have fewer degrees of freedom than in the gaseous state. This results in decrease in entropy during adsorption. Using the thermodynamic relationship:

$$\Delta G = \Delta H - T\Delta S \tag{2.1}$$

is obtained, and it follows that the term ΔH, which is the heat of adsorption, must be negative indicating that adsorption is always an exothermic process, respective of the nature of the forces involved in the adsorption process.

Depending upon the nature of the forces involved, the adsorption is of two types as physical or Van der Waals adsorption, and chemisorption or chemical adsorption. In the case of physical adsorption, the adsorbate is bound to the surface by relatively weak Van der Waals forces to identical with molecular forces of cohesion that are involved in the condensation of vapors into liquids. Chemisorption, on the other hand, involves exchange or sharing of electrons between the adsorbate molecules and the surface of the adsorbent,

resulting in a chemical reaction. The bond formed between the adsorbate and the adsorbent is essentially a chemical bond and is thus much stronger than in physical adsorption.

The most common difference between the two kinds of adsorption is the magnitude of the heat of adsorption. In the case of physical adsorption, the heat of adsorption is of the same as the heat of condensation and does not usually exceed 10 to 20 kJ per mole, whereas in chemisorption the heat of adsorption is usually 40 to 400 kJ per mole. Physisorption does not require any activation energy so that the rate of adsorption is very high even at low temperatures. The chemisorption, on the other hand, requires activation energy; the rate of adsorption is low and depends upon the temperature of adsorption. Physical adsorption is nonspecific and occurs between any adsorbate-adsorbent systems, while chemisorption is specific. Another point of difference between physisorption and chemisorption is the thickness of the adsorbed phase. The thickness is multimolecular in physisorption, whereas it is monomolecular in chemisorption. All these comparisons are listed in Table 2.1 [8].

The type of adsorption that takes place in adsorbate-adsorbent system depends upon the reactivity of the surface, the nature of the adsorbate, the nature of the adsorbent, and the temperature of adsorption.

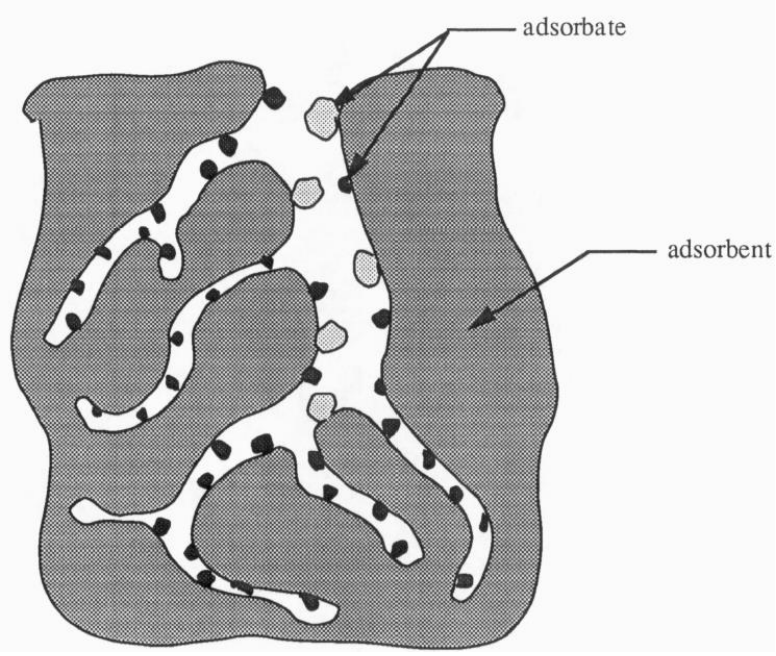

Figure 2.1. Adsorption of particles on a typical adsorbent surface [8].

Table 2.1. Comparison of physical and chemical adsorption.

	Physical Adsorption	**Chemical Adsorption**
Heat of Adsorption	Less latent heat of evaporation	Higher latent heat of evaporation
Frequency of Occurrence	Readily occurs between various adsorbate and adsorbent	Only occurs between specific adsorbate and adsorbent
Adsorbate Thickness	Monolayer or multilayer	Monolayer only
Speed of Adsorption	Rapid	May be slow
Bond Strength	Weak	Strong
Reversibility	Generally reversible	Generally not reversible
Bonding Process	Exothermic from gas phase	May be endothermic

2.2. Adsorption Equilibrium

When a solid surface is exposed to a gas, the molecules of the gas strike the surface of the solid. Some of the striking molecules stick to the solid surface and become adsorbed while the others rebound. Initially the rate of adsorption is large as the whole surface is bare but as more and more of the surface becomes covered by the molecules of the gas, the available bare surface decreases and so does the rate of adsorption. However the rate of desorption, which is the rate at which adsorbed molecules rebound from the surface, increases because desorption takes place from the covered surface. As time passes, the rate of adsorption continues to decrease while the rate of desorption increases until an equilibrium is reached between the rate of adsorption and the rate of desorption. As this stage the solid is in adsorption equilibrium with gas, and the rate of adsorption is equal to rate of desorption. It is a dynamic equilibrium because the number of molecules sticking to the surface is equal to the number of molecules rebounding from the surface [7].

For a given adsorbate-adsorbent system, the equilibrium amount adsorbed $\frac{x}{m}$ is a function of pressure and temperature; i.e.,

$$\frac{x}{m} = f(p, T) \tag{2.2}$$

where $\frac{x}{m}$ is the mass concentration of adsorbate per unit mass of the adsorbent [kg/kg] at the equilibrium pressure p and T is the temperature of adsorption. The adsorption equilibrium can be approached in three different ways.

2.2.1. Isothermal Adsorption

If the temperature is kept constant, then for a given adsorbent-adsorbate system $\frac{x}{m}$ depends on the equilibrium pressure, and the equilibrium can be represented as:

$$\frac{x}{m} = f(p)_T \tag{2.3}$$

2.2.2. Isobaric Adsorption

When pressure is kept constant and temperature is varied, an isobar is obtained, and the equilibrium can be represented as:

$$\frac{x}{m} = f(T)_p \tag{2.4}$$

2.2.3. Isosteric Adsorption

An isostere is obtained when, for a constant equilibrium amount adsorbed, the temperature is varied and the pressure essential to keep $\frac{x}{m}$ being constant is a function of the temperature, and the equilibrium can be represented as:

$$p = f(T)_{\frac{x}{m}} \tag{2.5}$$

These three adsorption lines can be interchanged; however they are used for different situations. Isothermal adsorption is mainly applied in micro-porous adsorption in industrial equipment. Isobaric adsorption is used in the operation design of generation processes. Isosteric adsorption is suitable for the calculation of heat of adsorption and desorption.

2.3. Adsorption Isotherm Equations

The adsorption isotherm is the most extensively employed methods for representing the equilibrium states of an adsorption system. It can give useful information regarding the adsorbate, the adsorbent, and the adsorption process. It helps in the determination of the surface area of the adsorbent, the volume of the pores, and their size distribution, the heat of adsorption, and the relative adsorb ability of a gas or a vapor on a given adsorbent.

The most important adsorption isotherms are the Langmuir, the Freundlich, the Temkin, the Brunauer-Emmett-Teller (BET), and the Dubinin equations. Langmuir, Freundlich and Dubinin equations are very important for analysis of the physical adsorption of gases and vapors on porous adsorbents.

Most adsorption refrigeration research is focused on physical adsorption, because of its reversible property, almost unlimited operation time and ease of operation. The adsorption equations for physical adsorption can be classified into three types:

- Adsorption equation based on adsorption speed, which is based upon single molecular layer adsorption; thereby it is a Langmuir-type equation.
- Thermodynamic adsorption equation, which is based on Polanyi adsorption potential theory and the Dubinin mini-pore filling theory. A lot of literature [9] shows that the adsorption of vapor on activated carbon can be well described by such an equation.
- Adsorption equation based on capillary condensing theory, which does not consider the effect of energy distribution around the adsorbent surface, but treating the mini-pores as capillaries. A good example is the Kelvin equation.

There are three possible theoretical approaches for deriving adsorption isotherms [7]:

- The kinetic approach
- The statistical approach
- The thermodynamic approach

In the kinetic approach, the condition of the equilibrium is that the rate of adsorption is equal to the rate of desorption at equilibrium. Equating the two rates in an isotherm equation can be obtained. In the statistical approach, the equilibrium constant is represented by a ratio of partition functions of vacant sites, adsorbed molecules, and the gas phase molecules. The isotherm equation can be obtained by equating this ratio to the corresponding ratio of concentrations. This approach has the advantage that it gives numerical value to the constants that cannot be evaluated by the kinetic approach. The equilibrium can be also approached thermodynamically, using either the conditions that the

work done in transferring an infinitesimal amount of gas from the gas phase to the surface at constant temperature is zero, or alternatively the Gibbs adsorption equation.

2.3.1. Langmuir Isotherm Equation

The Langmuir isotherm equation is the first theoretically developed adsorption isotherm. Langmuir isotherm equation is based on some certain assumptions:

- The adsorbed entities (atoms or molecules or ions) are attached to the surface at definite localized sites.
- Each site accommodates one and only one adsorbed entity.
- The energy state of each adsorbed entity is the same at all sites on the surface independent of the presence or absence of other adsorbed entities at neighboring sites. Thus the Langmuir model (also called localized model) assumes that the surface is perfectly smooth and homogenous and that lateral interactions between the adsorbed entities are negligible.

One practical working form of Langmuir equation can be expressed as follows:

$$x = PK_0' exp\left(\frac{Q_{st}}{TR_0}\right) \tag{2.6}$$

where x is the concentration of adsorbed adsorbate [kg/kg], P is the adsorption pressure [Pa], K_0' is the adsorption constant that can be determined experimentally [1/Pa], Q_{st} is the adsorption heat that can be determined experimentally [kJ/kg], R_0 is specific gas constant [kJ/kgK], T is the temperature of adsorbent [K].

2.3.2. Freundlich Equation

Freundlich equation is an empirical equation and exhibits considerable accuracy in describing physical adsorption within range where adsorbate concentration is relatively high. For solid-vapor adsorption, Freundlich equation can be given as:

$$x = x_0 \left(\frac{P}{P_{sat}}\right)^{\frac{1}{n}} \tag{2.7}$$

where x is the concentration of adsorbed adsorbate [kg/kg], x_0 is theoretical maximum adsorption capacity [kg/kg], P is system adsorption pressure [Pa], P_{sat} is saturation

pressure at adsorbent temperature [Pa], n and x_0 are two parameters that can be determined experimentally.

2.3.3. Dubinin-Astakhov Equation

Dubinin-Astakhov (D-A) equation is isobaric adsorption equation used to research mini-pore adsorption phenomena, which is simple, applicable for various pore sizes, and have good agreement for a wide range of temperature and pressure for uniform pore size adsorbent [9].

The equilibrium adsorption/desorption quantity of physical adsorption in micro pores is usually calculated by the Dubinin– Astakhov (D–A) equation, which is expressed as:

$$x = x_0 exp\left(-k\left(\frac{\varepsilon}{\beta}\right)^2\right) \tag{2.8}$$

where x_0 limiting adsorption capacity, k constant determined by the structure of the adsorbent, ε is adsorption potential energy, β is affinity coefficent which is determined by the adsorbent-adsorbate pair.

The reformed equation can be expressed as:

$$w = w_0 exp\left(-D\left(Tln\frac{p_{sat}}{p}\right)^n\right) \tag{2.9}$$

$$x = x_0 exp\left(-K\left(\frac{T}{T_{sat}} - 1\right)^n\right) \tag{2.10}$$

where w and x represent the volume adsorption and mass adsorption, respectively at temperature T and pressure p in terms of adsorbed liquid volume [l/kg] and the adsorbed liquid mass [kg/kg] per unit mass of adsorbent. In the above equations p_{sat} is the saturated vapor pressure corresponding to the adsorption temperature T, p is the adsorption pressure which is saturated pressure corresponding to the saturated refrigerant liquid temperature T_{sat}. D, K, n are the adsorption parameters depending on the adsorption refrigeration pair. w_0 and x_0 are the maximum adsorbed liquid volume and adsorbed liquid mass per unit mass of adsorbent, respectively. The correlations of the above two equations are as the following:

$$x_0 = \rho w_0 \tag{2.11}$$

$$K = DA^n \tag{2.12}$$

The above D-A equations are widely adopted in adsorption refrigeration research for the most studied physical adsorption working pairs are activated carbon (or activated carbon fibre)/methanol, activated carbon (or activated carbon fibre)/ammonia, silica gel/water, zeolite/water.

Below table lists experimentally determined adsorption parameters, which define volume pore filling with respect to pressure and temperature, existing in D-A equations for the most studied working pairs.

Table 2.2. Coefficients for D-A equations [10].

	x_0	**K**	**D**	**n**
Activated carbon/Methanol	0.45	13.38		1.5
Activated carbon/Ammonia	0.29	3.57		1.38
Silica gel/Water	0.35		$6x10^6$	1.7
Zeolite/Water	0.261	5.36		1.73

2.4 Heat of Adsorption

Ideal sorption (desorption and adsorption) is considered to be a phase transformation process between vapor phase and liquid phase at constant pressure [11]. The latent heat of the phase transformation of desorption and adsorption process can be described with a Clapeyron equation as follows:

$$\frac{dP}{dT} = \frac{h_0^\beta - h_0^\alpha}{T(\vartheta^\beta - \vartheta^\alpha)} \tag{2.13}$$

where the superscripts α and β represent the coexisting phase vapor and liquid; and symbols h and ϑ represent the specific enthalpy and specific volume, respectively. Since the pressure of the adsorption system is relatively low, the volume of vapor is far bigger

than that of liquid refrigerant trapped by the adsorbent. Therefore, the volume of the liquid is negligible and the volume of the vapor can be described using the ideal gas law:

$$\vartheta'' P = R_0 T \tag{2.14}$$

where P is pressure [Pa], ϑ'' is specific volume of vapor [m³/kg], R_0 is the specific gas constant of adsorbate [J/kgK], T is temperature [K].

The superscript symbols $''$ and $'$ represent saturated gaseous phase and saturated liquid phase, respectively. Symbol H is used to represent latent entalphy of the phase transfromation. The Clapeyron equation can be simplified into following equation:

$$\frac{dP}{dT} = \frac{h'' - h'}{T(\vartheta'' - \vartheta')} = \frac{H}{T(\vartheta'' - \vartheta')} \approx \frac{H}{T\vartheta''} = \frac{PH}{R_0 T^2} \tag{2.15}$$

The latent heat of adsorption or desorption h_a or h_d is the isosteric heat of adsorption or desorption. Clapeyron equation can be written in the following form [12]:

$$\left[\frac{d(\ln P)}{dT}\right]_{x=cst} = \frac{h_a}{R_0 T^2} = -\frac{h_d}{R_0 T^2} \tag{2.16}$$

For the desorption process the value of h_d is negative value indicating that desorption process is in fact a heat absorption process.

It is obvious that h_a and h_d are the function of temperature and pressure and they are defined as the heat necessary to adsorb or desorb a unit mass of adsorbate, respectively. By using D-A equation below:

$$x = x_0 exp\left(-K\left(\frac{T}{T_{sat}} - 1\right)^n\right) \tag{2.17}$$

It is obtained that

$$\frac{1}{T_{sat}} = \frac{1}{T}\left[\left(\frac{lnx_0 - lnx}{K}\right)^{\frac{1}{n}} + 1\right] \tag{2.18}$$

The correlation between $\ln P$ and -1/ T_{sat} for saturated liquid adsorbate is given by the following Clausius-Clapeyron equation:

$$lnP = A - \frac{C}{T_{sat}} \tag{2.19}$$

where A and C are depend on the adsorbate.

By using last two equations, we can obtain an expression for lnP as the following:

$$lnP = A - \frac{C}{T}\left[\left(\frac{lnx_0 - lnx}{K}\right)^{\frac{1}{n}} + 1\right] \tag{2.20}$$

when x remains constant, the differentiating the last equation gives:

$$\left[\frac{d(\ln P)}{dT}\right]_{x=cst} = \frac{C}{T^2}\left[\left(\frac{lnx_0 - lnx}{K}\right)^{\frac{1}{n}} + 1\right] = \frac{C}{T_{sat}T} \tag{2.21}$$

Thus, the latent heat of adsorption, h_a is

$$h_a(T, T_{sat}) = R_0 C \frac{T}{T_{sat}} \tag{2.22}$$

and that of desorption is

$$h_d(T, T_{sat}) = -R_0 C \frac{T}{T_{sat}} \tag{2.23}$$

Therefore, the total heat of adsorption and desorption become per unit mass of adsorbent are given as the following, respectively:

$$H_a = \int_{T_{a_2}}^{T_{a_1}} h_a \frac{\partial x(T, T_{ev})}{\partial T} dT \tag{2.24}$$

$$H_d = \int_{T_{g_1}}^{T_{g_2}} h_d \frac{\partial x(T, T_{con})}{\partial T} dT \tag{2.25}$$

2.5. Working Pair

When designing an adsorption refrigeration system, the selection of a working pair (i.e., adsorbent and adsorbate) is crucial since the system's performance largely depends on adsorptive properties of the working pairs employed. Measuring and determining a pair's adsorptive property is normally determining the correlations of the adsorbent and adsorbate using a pressure-temperature-concentration (i.e., p-T-x) relationship.

In investigations of common working pairs, numerous adsorbent-adsorbate combinations have been applied and compared [11]. Most research has been done using activated carbon/methanol, activated carbon/ammonia, zeolite/water, silica gel/methanol, silica gel/water as working pair. According to comparative studies, activated carbon-methanol and silica gel-water have been recognized as two appropriate working pairs in the application of a low-temperature driven system, because both of these two working pairs can be normally be driven by a low temperature heat source (below 100 °C), while a working pair with zeolite normally needs temperature of a heat source to be 200 °C.

For any refrigerating application, the adsorbent must have high adsorptive capacity at ambient temperatures and low pressures but less adsorptive capacity at high temperatures and high pressures. Adsorbents are first characterized by surface properties such as surface area and polarity. A large specific surface area is preferable for providing large adsorption capacity, and hence an increase in internal surface area in a limited volume inevitably gives rise to large number of small sized pores between adsorption surfaces. The size of the micro pores determines the effectiveness of adsorptivity and therefore distribution of micro pores is another important property for characterizing adsorptivity of adsorbents.

Based on the above discussion, before the adsorbent and adsorbate choice, some critical factors should be taken into consideration.

2.5.1. Choice of Adsorbent

The important considerations influencing the choice of a suitable adsorbent are [13, 14]:

- Adsorption of large amount of the adsorbate under low temperature conditions to yield good coefficient of performance (COP)
- Desorption of most of the adsorbate when exposed to thermal energy
- Good thermal conductivity in order to shorten the cycle time
- Possession of high latent heat of adsorption compared to sensible heat
- No deterioration with age or use
- Non-toxic and non-corrosive
- Low cost and widely available
- Low specific heat capacity
- Chemically compatible with the chosen refrigerant

2.5.2. Choice of Adsorbate

The selected adsorbate must have most of the following desirable thermodynamics and heat transfer properties [13, 14]:

- Evaporation temperature below 0 °C
- Small molecular size to enable it to be adsorbed into the adsorbent
- High latent heat of vaporization to minimize the adsorbent needed thus minimizing the sensible heat requirement of the adsorbent and low specific volume
- Thermally stable with the adsorbent at the cycle operating temperature ranges
- Non-toxic, non-corrosive and non-flammable
- Low saturation pressures (slightly above atmospheric) at normal operating temperature
- Molecular dimensions should be small enough to allow easy adsorption
- High thermal conductivity
- Good thermal stability
- Low viscosity
- Low specific heat

2.6. Activated Carbon

Activated carbons are unique and versatile adsorbents. Their adsorbent properties are essentially attributed to their large interparticulate surface area, universal adsorption effect, high adsorption capacity, a high degree of surface reactivity and a favorable pore size which makes the internal surface accessible and enhances the adsorption rate. The mostly widely used activated carbons have a surface area of about 800 to 1500 m^2/g [7]. This surface area is contained predominantly within micro pores which have the effective diameter less than 2 nm. In fact, a particulate of activated carbon is made up of a complex network of pores that have been classified into micro pores (diameter < 2 nm), mesopores (diameter between 2 and 50 nm), and macro pores (diameter > 50 nm).

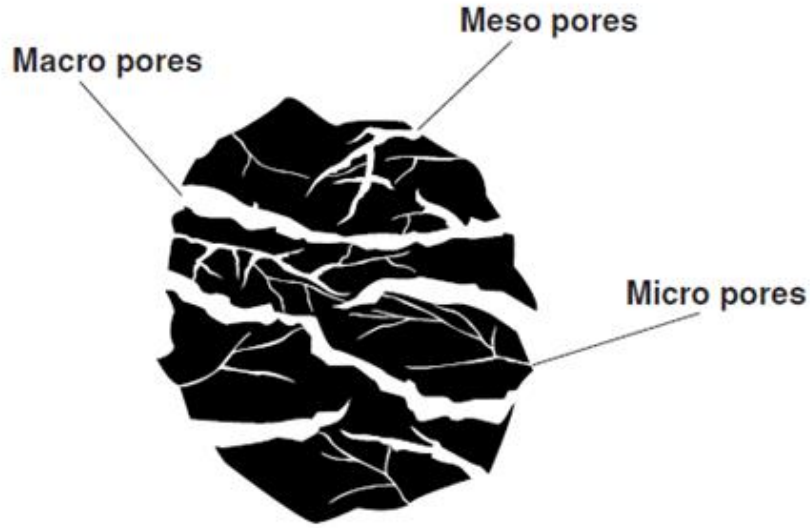

Figure 2.2. Pore types [15].

Most of the adsorption on active carbons takes place in micro pores and only small amount in mesopores, the macro pores acting only as conduits for the passage of the adsorbate into the interior mesopores and the micro pore surface. The pore size distribution in a given carbon depends on the type of the raw material and the method and conditions under which the carbon has been prepared.

Figure 2.3 shows the electron micrograph as an example of porous media taken at Warwick University of the charcoal 208C produced by Sutcliffe Speakman [16].

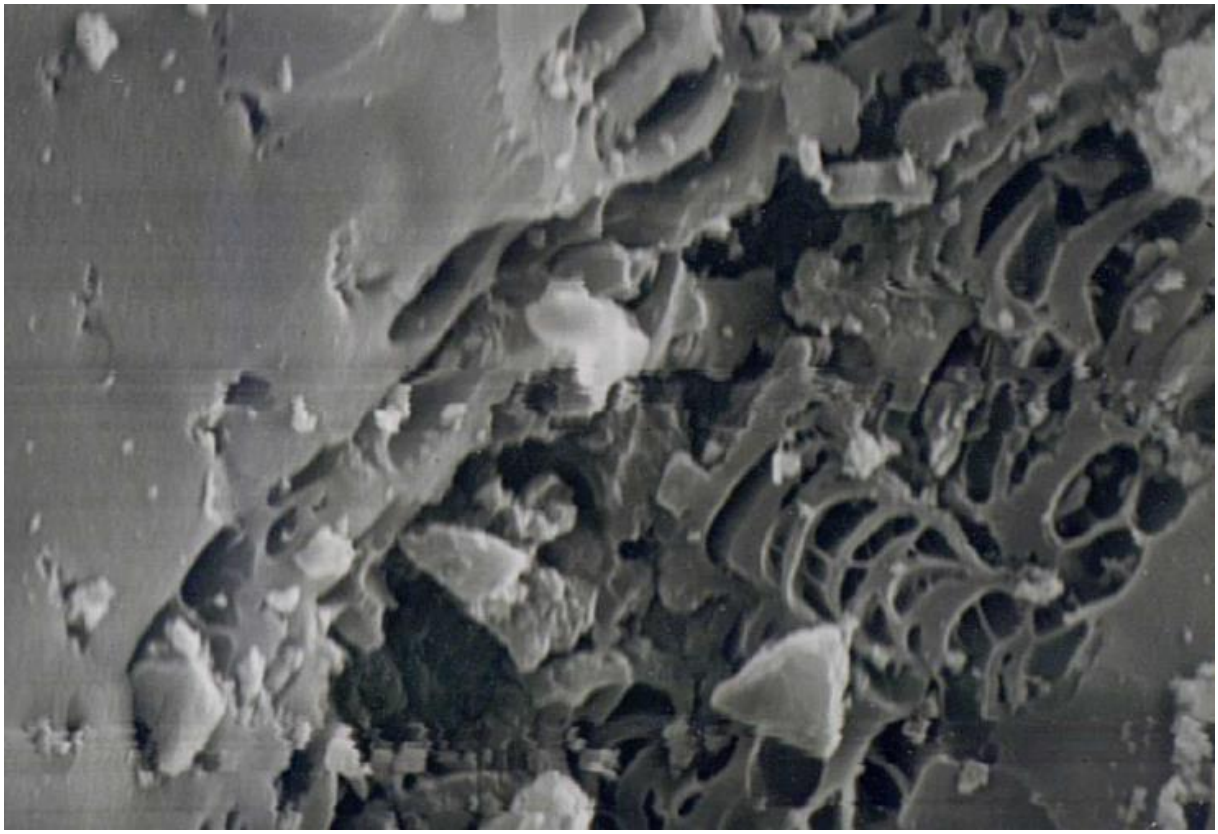

Figure 2.3. Porous media [16].

2.7. Cycle Types

2.7.1. Basic Cycle

The basic cycle is easy to apply and is very suitable for solar refrigeration and also for waste heat recovery refrigeration. Basic cycle is an intermittent refrigeration cycle, in other words, the evaporating process is going on only in a half cycle, if operated with one bed. Continuous refrigeration can be only achieved with two or more beds to shift the heating-cooling phases. When there are two adsorbent beds, they can be easily operated out of phase. The two-bed continuous cycle employs two adsorbent beds to provide continuous cooling power. These are in fact two parallel basic cycles that operate out of phase. Therefore, it is not much different from the basic one from this point of view.

The basic adsorption refrigeration cycle consists of four processes as shown in Figure 2.4.

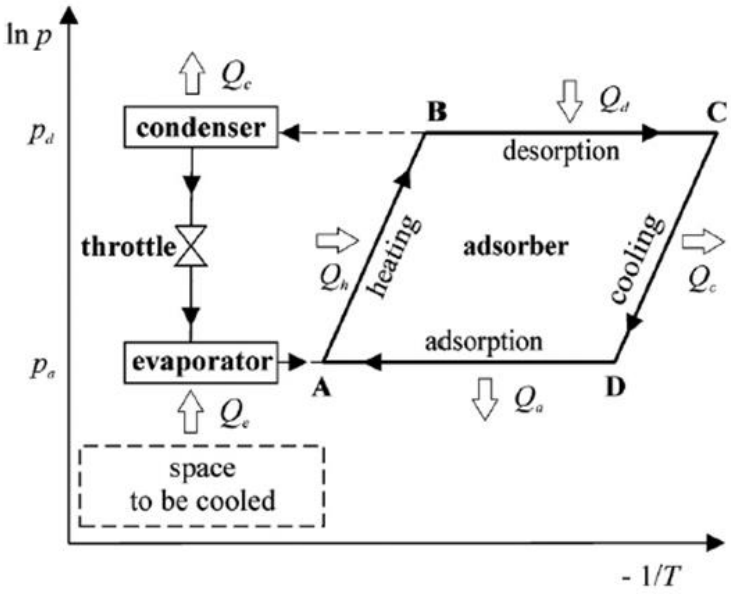

Figure 2.4. Basic adsorption refrigeration cycle [17].

During phase A to B, the adsorbent bed containing a high concentration of adsorbate receives heat while being closed (connection to condenser/evaporator is broken). The pressure increases whereas the adsorbed mass remains constant. This phase is described as isosteric-heating or isosteric-pressurization.

When energy losses in heat transfer and heat supplied to the metal tube which includes adsorbent bed are not taken into account, energy input in this process can be calculated by the following equation:

$$Q_{A-B} = m_s(c_{vs} + x_A c_{va})(T_B - T_A) \tag{2.26}$$

where Q_{A-B} [J] is heat supplied to heat up the adsorbent and refrigerant from point A to point B. c_{vs} and c_{va} represent specific heat at constant volume of the adsorbent and the adsorbed refrigerant (liquid phase), respectively [J/kgK] and are assumed to be constant. m_s is the mass of adsorbent [kg].

It is assumed that [16]

- No desorption takes place until the condensing pressure is reached.
- Sensible heating to the adsorbate gas contained within the bed volume is negligible.
- Heating the bed along an isostere is considered to be a constant volume process.

During phase B to C, when adsorbent bed pressure reaches the saturation pressure P_{con} of the pure refrigerant at the condenser's temperature, adsorbent bed and condenser are connected. The desorption begins and the pressure remains constant until the adsorbent reaches its maximum desorption temperature where the refrigerant condenses. It is the isobaric condensation-desorption phase. It is assumed that [12] the refrigerant gas enters the condenser as soon as it is desorbed from the adsorbent bed, i.e. no cooling of the gas takes place within the adsorbent bed itself. During the first two phases, the external heat system provides an amount of heat Q_h $(Q_{A-B} + Q_{B-C})$. As the maximum temperature of the cycle is reached, the valve is closed and the next phase begins.

In this process, heat supplied does not only increase the bed's temperature, but also drives the desorption of adsorbate out of adsorbent as desorption heat. Energy input can be calculated by using following equation:

$$Q_{B-C} = m_s \left\{ \int_{T_B}^{T_C} \left(c_{ps} + c_{pa} x(T) \right) dT + \int_{x_B}^{x_C} h_d \, dx \right\} \tag{2.27}$$

where Q_{B-C} is the heat supplied to heat up the adsorbent and refrigerant, leading to desorption.

During phase C to D, the adsorbent bed, which has a weak concentration of refrigerant, is cooled, and consequently the pressure decreases and follows an isoster. It is the isosteric-cooling or isosteric-depressurisation phase. The pressure of the adsorber bed (vapor pressure) decreases until it reaches the pressure of the evaporator.

In this process, sensible heat is removed by an external cooling source and energy balance can be expressed as:

$$Q_{C-D} = m_s (c_{vs} + x_C c_{va})(T_C - T_D) \tag{2.28}$$

where Q_{C-D} is heat removed from the adsorbent and adsorbate by external cooling source.

It is assumed that [16]

- No adsorption takes place until the evaporating pressure is reached.

- Sensible cooling to the adsorbate gas contained within the bed volume is negligible.
- Cooling the bed along an isostere is considered to be a constant volume process.

During phase D to A, the adsorbent bed starts to adsorb the refrigerant gas provided by the evaporation process of the refrigerant in the evaporator at a constant pressure P_{ev}, while the adsorbent bed cools down continuously. It is the isobaric evaporation-adsorption phase.

This is the heat energy rejected from the bed as the gaseous adsorbate is readsorbed. It is also the heat loss required for sensible cooling of the adsorbent and adsorbed refrigerant between the adsorption temperature T_D and the initial temperature T_A (can be taken as ambient temperature). Finally, as the adsorbate gas is reintroduced to the bed it is at a lower temperature and therefore has a cooling effect on the adsorbent.

$$\begin{aligned} Q_{D-A} &= Q_{ad} \\ &= m_s \left\{ \int_{T_A}^{T_D} \left(c_{ps} + c_{pa} x(T) \right) dT + \int_{x_D}^{x_A} h_a \, dx \right. \\ &\left. - \int_{T_A}^{T_D} c_{pv} \Delta x d (T - T_{ev}) \right\} \end{aligned} \tag{2.29}$$

It is assumed that [16]

- Adsorption along an isobar is a constant pressure process.
- Saturated vapor leaves the evaporator i.e., no superheating of the refrigerant takes place.

The heat of adsorption and the concentration are found for every degree K from their corresponding equations and summed between T_D and T_A.

It is also useful to describe condensation energy and refrigeration output. Condensation energy is the required heat rejection from the system to allow the hot adsorbate gaseous to cool and condensate to a saturated liquid at condensing pressure, P_{con}. Condensation energy is described as:

$$Q_{con} = \int_{T_B}^{T_C} c_{pv} m_s \Delta x d(T - T_c) + (x_{conc} - x_{dil}) m_s L_e \tag{2.30}$$

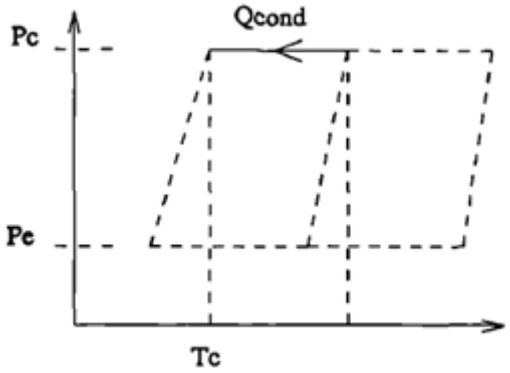

Figure 2.5. Condensation energy [16].

Refrigeration output can be approximately calculated using the following Equation 2.31, in which the first term in the right hand of the equation represents the gross refrigeration capacity while the second term represents the refrigeration power loss due to its self-cooling from condensing temperature to evaporating temperature.

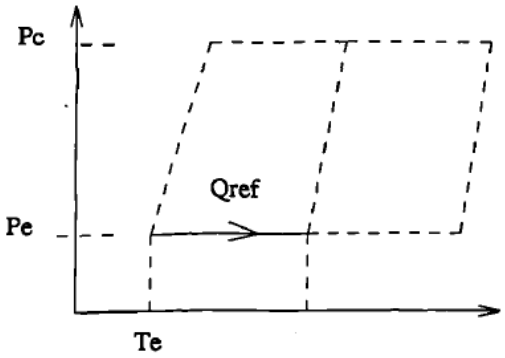

Figure 2.6. Refrigeration output [16].

$$Q_{ref} = Q_{ev} = m_s(x_A - x_D)\left(L_e - \int_{T_{ev}}^{T_{con}} c_{pa} dT\right) \tag{2.31}$$

where L_e is the latent heat of vaporization of refrigerant [kJ/kg] (treated as a constant in ideal case analysis), T_{ev} and T_{con} are evaporation and condensing temperatures [K], respectively.

Two parameters, namely, the coefficient of performance (COP) and the specific cooling power (SCP) are used to assess the performance of the system. These are defined as follows:

$$COP = \frac{useful\ refrigeration\ energy}{sensible\ bed\ heat + desorption\ energy} = \frac{Q_{ev}}{Q_h} = \frac{Q_e}{Q_{A-B} + Q_{B-C}} \quad (2.32)$$

$$SCP = \frac{Q_{ev}}{m_s t_c} \quad (2.33)$$

where Q_h is the heat for generation corresponding to the two processes (isosteric and isobaric), Q_{ev} is cooling production (refrigeration output) at the evaporator, m_s and t_c are the total mass of adsorbent [kg] and cycle time [s], respectively.

2.7.2. Heat Recovery Cycle

There are two adsorbers in this type of cycle, which are operated out of phase. At the end of each half cycle, one adsorber is at point a_2 with a low temperature, and the other is at g_2 with a high temperature. Heat can be easily recovered between the two adsorbers because of this temperature difference. By circulating the external heat transfer fluid between the two adsorbers adiabatically, the energy efficiency will thus be increased significantly [5, 6]. In an ideal heat recovery process, the two adsorbers will reach the same temperature (equilibrium temperature), one is at point e and the other is at e'. Therefore, the thermal load for heating can be decreased by $Q_{a_2-g_1-e}$. After this sub-period of heat recovery, one adsorber is heated up by the external heat source while the other one is cooled down by the heat sink. In this case, the concentration change is determined by the concentration variation between points g_1 and g_2. That means the concentration change, *(*Δx*)*; in the heat recovery cycle is the same as that in the basic cycle.

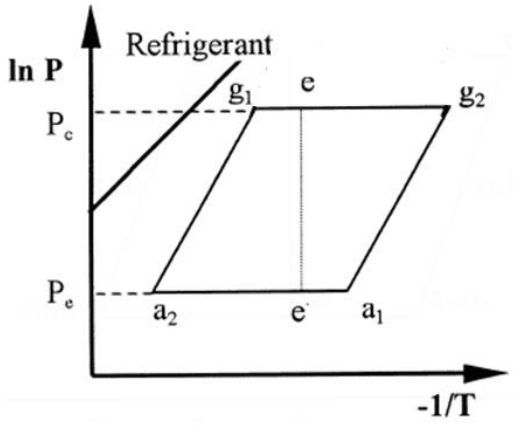

Figure 2.7. Heat recovery cycle Clausius-Clapeyron diagram [6].

The heat recovery may include sensible heat recovery and adsorption heat recovery. [18] Regarding the different heat recovery (sensible heat and adsorption heat recovery), it is easily explained by the p-T-x diagram for the adsorption system. If the heat recovery temperature (equilibrium temperature) T_e is bigger than T_{a_1}, no adsorption heat can be recovered, but if T_e is less than T_{a_1}, the heat of adsorption at the evaporation pressure and in the temperature range [T_e, T_{a_1}] exists and thereby can be possibly recovered in addition to the sensible heat recovery. A separating point for sensible heat recovery or sensible heat and adsorption heat recovery happens when the desorption temperature T_{g_2}, is large enough which causes $T_{a_1} > T_e$. Whether the heat of adsorption can be recovered is dependent on the valve operation between the two beds during the heat recovery process, when the bed temperature is less than T_{a_1} and if the adsorber is not connected to the evaporator, no heat of adsorption happened and thus no adsorption heat recovery. But if the adsorber is connected to the evaporator, the heat of adsorption will thereby be generated in the adsorber bed and thus will be possible to transfer to the bed of generation for recovery.

The coefficient of performance (COP) for a two-bed heat recovery cycle can be expressed as:

$$COP = \frac{Q_{ev}}{Q_h + Q_g - Q_r} \tag{2.34}$$

where Q_r is the heat recovered and is calculated by using energy balance equation between hot and cool adsorbent beds as per below in equation:

$$Q_r = \int_{T_{a_2}}^{T_e} m_s\left(c_{ps} + x_{con}c_{pa}\right) dT = \int_{T_e}^{T_{g_2}} m_s\left(c_{ps} + x_{dil}c_{pa}\right) dT \tag{2.35}$$

Q_h and Q_g are the heats for generation corresponding to the two process isosteric and isobaric, respectively.

Q_{ev} is cooling production (refrigeration output) at the evaporator and is thus given as:

$$Q_{ev} = m_s(x_{con} - x_{dil})\left(L_e - \int_{T_{ev}}^{T_{con}} c_{pa}dT\right) \tag{2.36}$$

which is the latent heat L_e multiplied by the cycle refrigerant. However, some of the cooling quantity will be consumed to cool the refrigerant liquid from condensing temperature T_{con} to evaporation temperature T_{ev}.

It should be highlighted that in contrast to the ideal heat recovery, it requires long time to reach an equilibrium temperature; therefore, it is beneficial to leave a temperature difference ΔT between two adsorber beds at the end of heat recovery. As expected, the COP increases as ΔT decreases. On the other hand, the specific power increases with increasing ΔT because of the shortening of the cycle time. It is possible to find a good compromise between these two tendencies, depending upon the type of application that could require the maximization of the COP or, alternatively, of the power. For different systems, the COP and SCP may be assigned different weights depending on their relative importance. For systems utilizing waste heat, the SCP is more important as the user is only concerned with the cooling power produced since the cost of producing the heat is almost zero [1]. For other systems, the COP may be more important compared to SCP. Thus the selection of the operating conditions should consider the specific demands of the system.

2.7.3. Mass Recovery Cycle

This kind of cycle employs two adsorbers which work out of phase. At the end of each half cycle, one adsorber is hot with high pressure (P_{con}, g_2) and the other is cold with low pressure (P_{ev}, a_2). After that, the high pressure adsorber needs to be cooled down and depressurized while the low pressure one needs to be heated up and pressurized. Then the

two adsorbers can be inter-connected directly with a mass recovery valve. The refrigerant vapor will then flow from the high pressure adsorber to the low pressure one. This is called the mass recovery process. The pressure of Adsorber 2 will decrease due to mass outflow and this will again promote desorption of Adsorber 2. Meanwhile the pressure of Adsorber 1 increases due to mass inflow and will promote further adsorption. The mass recovery is assumed to be an ideal process [6]. That is to say, the final pressures of the two adsorbers in mass recovery are equal, so the process is maintained until the two adsorbers reach an equilibrium pressure. Then the connection is broken and each adsorber goes on with the heating and cooling process just as in the basic cycle. During the mass recovery process, the adsorbers, the condenser, and the evaporator are disconnected. Therefore, the refrigerant flow outside the adsorbers stops during the mass recovery process. In other words, the total mass flux for the system is zero. The process, which only involves direct mass flow and the pressure balance is much faster than temperature balance via heat transfer medium, operates very quickly, so the pressure swing in the condenser and the evaporator is negligible and mass recovery duration is therefore negligible when compared to the whole cycle period [5].

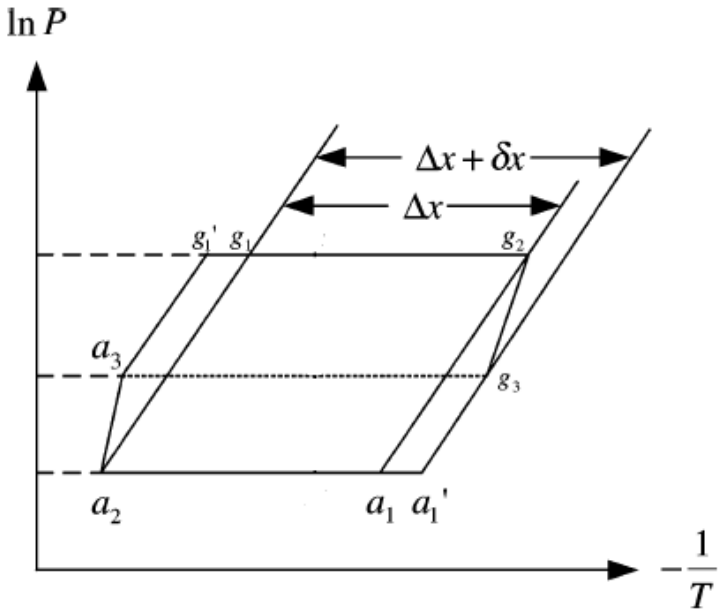

Figure 2.8. Mass recovery cycle Clausius-Clapeyron diagram [11].

For the mass recovery cycle, concentration change is determined by the concentration variation between g_1' and g_2 (or alternatively a_1' and a_2). The concentration change of a basic cycle is determined by g_1 and g_2. So the enlarges the concentration change of the refrigerant in a cycle, δx which causes the refrigeration effect to increase.

The mass recovery process is able to enhance the specific cooling power (SCP) but not to greatly affect the COP. For a given cycle period the quantity of evaporated refrigerant (cycled mass) is enhanced by this process; therefore, the cooling power is increased. On the other hand, the isobaric desorption process $g_1 - g_2$ becomes $g_1' - g_2$. Because the desorption process is prolonged and the desorbed refrigerant is increased, the desorption heat is also enlarged. Therefore, the heating system must supply an additive energy for desorbing this larger quantity of vapor. As a consequence, the COP is almost unchanged [19].

The process is divided into two parts operating in two beds as $a_2 - a_3$ and $g_2 - g_3$. The process can be simulated and calculated utilizing the following model [18].

The vapor desorbed from high pressure bed is entirely re-adsorbed by the low pressure bed. That is

$$\Delta x_{a_2 - a_3} = \Delta x_{g_2 - g_3} \tag{2.37}$$

The mass recovery is assumed to be adiabatic. The temperature variation is caused by adsorption or desorption:

$$\int_{T_{a_2}}^{T_{a_3}} \left(c_{ps} + x_{con} c_{pa}\right) dT = \int_{T_{a_3}}^{T_{a_2}} h_a \frac{\partial x}{\partial T} dT \tag{2.38}$$

$$\int_{T_{g_2}}^{T_{g_3}} \left(c_{ps} + x_{dil} c_{pa}\right) dT = \int_{T_{g_2}}^{T_{g_3}} h_d \frac{\partial x}{\partial T} dT \tag{2.39}$$

where c_{ps} and c_{pa} are the specific heat of solid adsorbent and liquid adsorbate, respectively.

Here the void volume of the two adsorbers is assumed to be equal and neglected, and heat of adsorption/desorption is assumed as a constant at the corresponding averaged pressure. The amount of vapor in the connection pipe lines is negligible and the energy is brought by the vapor of mass recovery is negligible [5]. It means that

$$x_{con} \cong x_{a_2} \tag{2.40}$$

$$x_{dil} \cong x_{g_2} \tag{2.41}$$

The final pressure of the two beds should be equal to each other:

$$P_{a_3} = P_{g_3} \tag{2.42}$$

The iterative calculation method can be used by supposing a final equilibrium pressure at the first, and calculate the temperature and concentration change of each bed. Then modify the supposed pressure if necessary to satisfy the following equation:

$$\Delta x_{a_2-a_3} = \Delta x_{g_2-g_3} \tag{2.43}$$

During the isosteric processes, the concentration of the adsorber does not change. That is

$$x_{a_3} = x_{g_1} \tag{2.44}$$

$$x_{g_3} = x_{a_1} \tag{2.45}$$

$$x_{a_2} = x_{g_1} \tag{2.46}$$

$$x_{g_2} = x_{a_1} \tag{2.47}$$

The pressure of the isobaric processes g_1'-g_2, and a_1'-a_2 does not change for the adsorbers are connected to the condenser or the evaporator:

$$P_{g_1'-g_2} = P_{con} \tag{2.48}$$

$$P_{a_1'-a_2} = P_{ev} \tag{2.49}$$

The COP of the system is calculated by:

$$COP = \frac{Q_{ev}}{Q_{a_3-g_1'} + Q_{g_1'-g_2}} \tag{2.50}$$

2.7.4. The Combined Mass and Heat Recovery Cycle

This system consists of six major components including two adsorbers, external heat and cooling systems, a condenser and an evaporator. Compared to the one adsorber system, a two-adsorber cycle provides cooling on a more continuous basis. At the beginning of this two-bed cooling cycle, the adsorbent bed is at the state of point *a* and

another bed is at the state of point *c*. The mass recovery phase then starts. The two adsorbers are interconnected directly and the refrigerant vapor will flow from the high-pressure to the low-pressure adsorber. This process is maintained until the two beds reach the same pressure (points *e* and e') and the two adsorbers are disconnected. Subsequently, the heat recovery phase is carried out from point *e* to point *f* for adsorbent bed 1 and from point e' to point f' for the other bed. During this phase, no heat is supplied by the external heating systems and the amount of heat of Q_r is exchanged between the two adsorbers. Finally the two adsorbent beds are connected to the external heating or cooling system, respectively. It can be seen in Figure 2.9 that the cycle refrigerant mass will increase through the mass recovery cycle compared with the basic cycle, which leads to an increased value of Q_{ev}. Figure 2.9 also shows that the amount of heat from external heat source $Q_h$will decrease by using a heat recovery phase between the two adsorbers. Therefore, the COP will be increased for the combined heat and mass recovery cycle compared to the basic cycle.

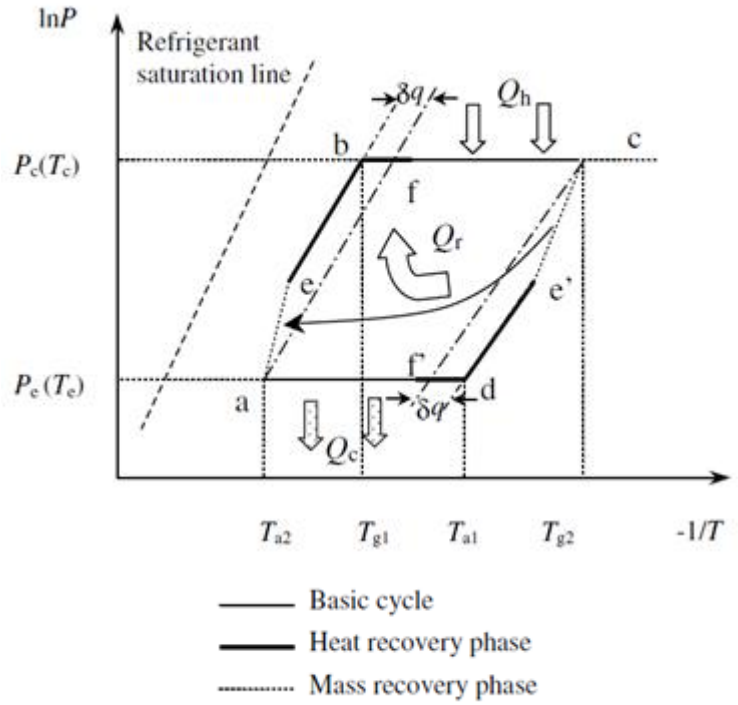

Figure 2.9. Mass and heat recovery cycle Clausius-Clapeyron diagram [1].

Temperature increases rapidly during the mass recovery phase. The adsorption process carried out during the mass recovery phase and the adsorption heat released to adsorbent has caused the adsorbent temperature to increase. The slope of the temperature

with respect to time regarding to the heat recovery phase will be lower than that of the basic cycle phase [1]. Since, for the heat recovery phase, the temperature gap between the two adsorbers is not high compared to the gap between the adsorber and external heat source or heat sink. Hence, the heat exchange rate during the heat recovery phase is small compared to the basic cycle. The total cycle time will then increase with an increase in the heat recovery time leading to a penalty in terms of a reduction in SCP. The variation of pressure is expected to be similar to the ideal case. The pressure becomes a constant after a rapid and significant change for every half cycle. The adsorbed amount will be almost a constant after mass recovery until the adsorber is connected to either the evaporator or condenser. In fact, the pressure is not a constant during the isobaric adsorption phase for the basic cycle Marletta et al. [20] suggested that this phenomenon may be the result of mass transfer limitation. However, for a cycle incorporating a combined heat and mass recovery phase, this phenomenon is not obvious. The effect of mass transfer limitation is reduced. When the adsorber is connected to the evaporator, the temperature gap between adsorber with heat transfer fluid for heat and mass recovery cycle is smaller than that for a basic cycle. Hence, the mass flux of vapor from the evaporator to the adsorber of this advanced cycle is smaller than that of the basic cycle. Based on the same permeability, the pressure gradient in the adsorbent bed of this advanced cycle is also smaller than that of basic cycle. Thus, the average pressure in the heat and mass recovery cycle is closer to the ideal pressure which tends to be constant during adsorption process.

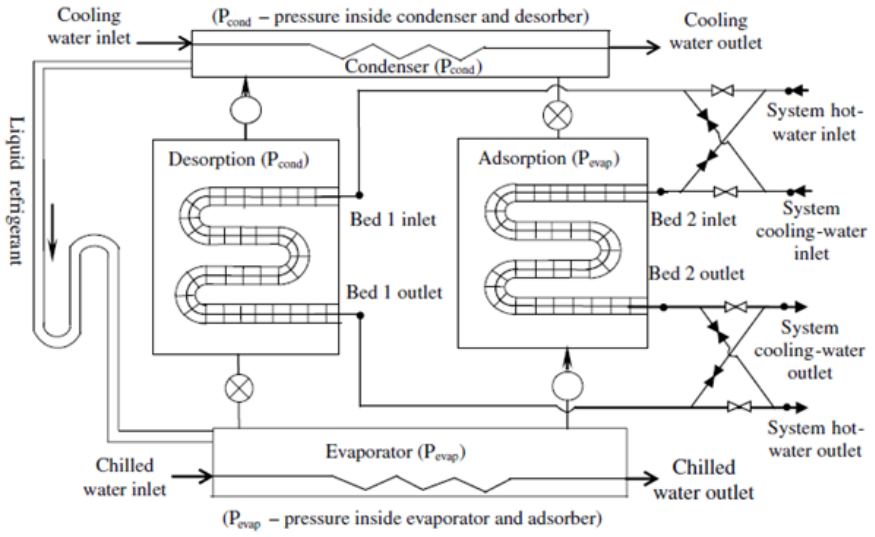

(⋈: opened water valve; ⋈: closed water valve; ⊗: closed gas valve; ○: opened gas valve).

Figure 2.10. Schematic of the two bed adsorption chiller [21].

3. MATHEMATICAL MODELLING

The aim of this chapter is to propose a mathematical model, able to describe in a proper way the heat and mass transfer occurring in the bed for the adsorbate/adsorbent pair. In terms of dynamic models four categories of mathematical models, i.e., uniform temperature-uniform pressure, uniform temperature-non-uniform pressure, non-uniform temperature-uniform pressure, non-uniform temperature-non uniform pressure were proposed and investigated in literature [20].

Solid adsorption refrigeration is basically an adsorption phenomenon involving heat and mass transfer processes, the modelling work mainly includes establishing heat transfer model, mass transfer model and adsorption model.

3.1. Heat Transfer Model

Treatment of heat transfer model in modelling of adsorption refrigeration system includes two streams, i.e. uniform temperature and non-uniform temperature [11].

The model is based on the assumption of uniform temperature in order to study of thermal performance adsorption refrigeration systems is not able to examine temperature profile within the adsorbent bed [14]. Since typical adsorbents have very poor thermal conductivity, temperature within an adsorbent bed can be fairly significant, especially when the adsorbent bed is thick or the system is rapidly cycled.

Compared to uniform temperature treatment, non-uniform temperature model is able to study the detailed temperature profile within the adsorbent bed [22, 23]. However, the non-uniform temperature based models does not examine the effect of temperature profile on the system performance, but instead studies system performance using an average bed temperature.

On the other hand, as assumption of local thermal equilibrium that is adopted by almost all existing models [20] may need sufficient experimental validations. In circumstances where there is fast desorption heat sink and adsorption heat generation, local

thermal non-equilibrium between solid adsorbent and gaseous adsorbate can be employed to develop a more accurate model.

3.2. Mass Transfer Model

The mechanism of mass transfer within an adsorbent bed is considered to be the pressure gradient causing mass flow. Hence, the mass resistance is considered using the non-uniform pressure model while the uniform pressure model does not take the mass transfer resistance into account [24].

For an adsorption refrigeration system, which has a long cycle time, mass transfer resistance may be neglected since the sorption process lasts for a long time.

3.3. Adsorption Model

Equilibrium-based adsorption models and non-equilibrium-based adsorption models are the two streams used when an adsorption refrigeration cycle is mathematically modelled. In equilibrium-based adsorption models Dubinin-Astakhov (D-A), Langmuir equation and Freundlich equation are typically employed in various mathematical models [25]. Compared to equilibrium-based adsorption equations, non-equilibrium adsorption models, i.e., Linear Driving Force (LDF) based model is employed. When the cycle time is short, COP based on the non-equilibrium model is much lower than the calculated using the equilibrium adsorption model [26].

3.4. Bed Structure

Figure 3.1 illustrates a type of external-heated generator examined by Hu [25], Dai and Sumathy [13], Cortes et al. [23], Fadar et al. [2]. In this configuration, the adsorbent is packed inside the center tube can be heated up or cooled down through external heat transfer fluid. Refrigerant vapor can flow between the condenser/evaporator and the adsorbent bed via mass transfer channel. Compared to the center-heated generator, this kind of external-heated generator can be modified into a solar radiation powered generator by removing the water jacket.

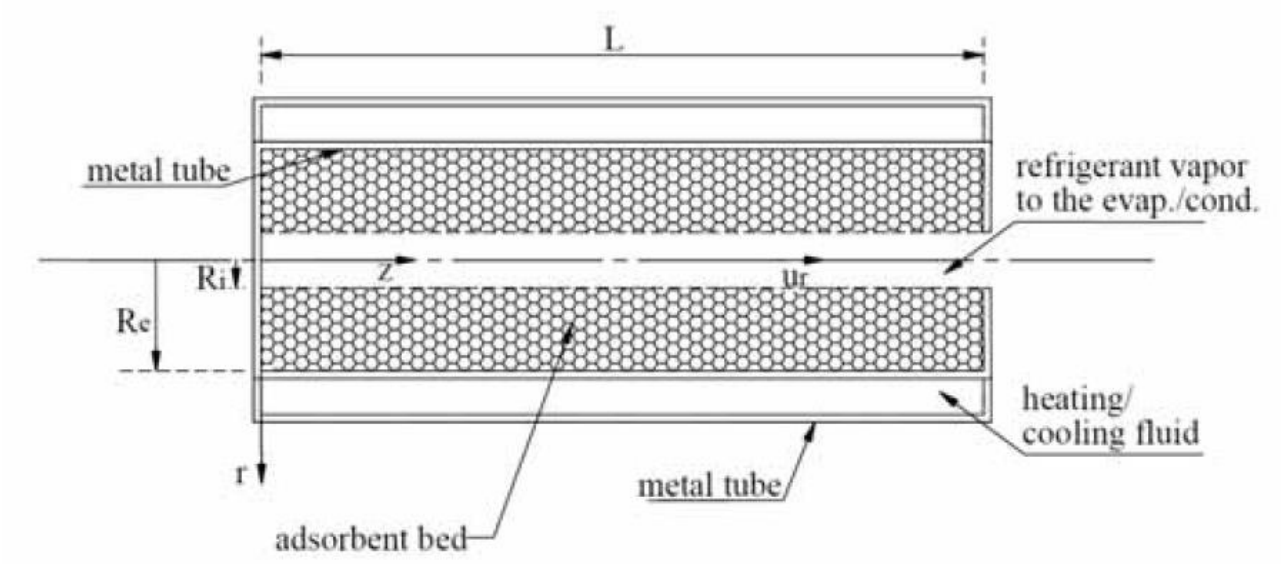

Figure 3.1. External heated adsorbent bed structure [11].

3.5. Governing Equations

3.5.1. Mass Transfer Kinetics and Mass Conservation Equation

Three models are generally used to describe refrigerant transfer between gaseous and solid phases, i.e., the equilibrium model, the solid diffusion model and the Linear Driven Force (LDF) model [27].

The principle of heat and mass transfer inside the porous bed can be described as follows when the bed is exposed to heat exchange, an inhomogeneity of temperature appears, that induces by adsorption/desorption process a mass transfer and consequently a gradient of concentration of adsorbed refrigerant. Because of the exothermic character of adsorption phenomena, this mass transfer affects the mechanism of heat transfer in the medium. For short cycle times (cycle with high power density), the resistance to mass diffusion has a significant effect on the distribution of concentration of adsorbed refrigerant, then when the refrigerant is a slow diffusing adsorbate, the application of the equilibrium model (without mass transfer limitations) will result in an overestimation of the performance of the machine [28]. On the other hand, for long cycle times, as the case of solar refrigeration cycle (cycle with low power density), this limitation of mass transfer can be ignored, because the intraparticle mass transfer is assumed to be sufficiently rapid so that no concentration gradient can exist in adsorbent particles. The gaseous and solid

phases are thermodynamically in equilibrium. The adsorbed amount is simply related to the gas pressure and the adsorbent temperature.

The equilibrium model considers no mass transfer limitations between solid and gas phases, i.e., they are in thermodynamic equilibrium [27]. The adsorption mass transfer rate is only related to gaseous pressure and adsorbent temperature through the following adsorption equilibrium equation:

$$\frac{\partial x}{\partial t} = \frac{\partial x^*}{\partial t} \tag{3.1}$$

where the adsorption capacity x represents the concentration of refrigerant adsorbed in bed at temperature T and pressure p. x^* is the equilibrium adsorption capacity of adsorber, which can be given by a modified Dubinin-Astakhov equation [26]:

$$x^* = x_0 exp\left(-K\left(\frac{T}{T_{sat}} - 1\right)^n\right) \tag{3.2}$$

Solid diffusion and LDF models consider that due to diffusion through intraparticle macro pores and micro pores, which is a slow process, the two phases of gas and solid could not reach equilibrium instantly, but only after a certain time, depending on the adsorbent-adsorbate pair used. For this reason, mass transfer kinetics should be incorporated into the model to verify whether the equilibrium assumption is justified. The LDF model can be used to describe mass transfer between moving and stationary phases in adsorption processes, which is derived from the solid diffusion model based on the assumption made by Gluekauf [27] who assumed that the LDF model could be simplified by a common approximation of the solid diffusion model. The mathematical simplification of the model yields directly the even adsorbed concentration within the particle, thus avoiding numerical integration over the whole particle required by the solid diffusion model. The LDF model is given as:

$$\frac{\partial x}{\partial t} = \frac{15 D_s}{r_p^2}(x^* - x) \tag{3.3}$$

where r_p is the radius of particle, x is the mean adsorbed concentration within the particle, x^* is the adsorbed phase concentration in equilibrium, D_s is the surface diffusivity of particles, which can be calculated by the following equation:

$$D_s = D_0 exp(-E_a/RT_s) \tag{3.4}$$

where D_0 is pre-exponent constant in m²/s unit and E_a activation energy of surface diffusion in kJ/kg unit can be obtained from experimental data available in literature [9].

The overall mass conservation equation in the adsorber is given below:

$$\varepsilon_t \frac{\partial \rho_v}{\partial t} + \boldsymbol{\nabla}.(\rho_v \boldsymbol{u_v}) + (1-\varepsilon_t)\rho_s \frac{\partial x}{\partial t} = 0 \tag{3.5}$$

where ε_t is the total porosity of the adsorbent bed, including the interspaces of the adsorbent itself and the porosity of adsorbent particles. ρ_v and ρ_s are the densities of refrigerant vapor and adsorbent, respectively.

According to Darcy's law, the flow velocity of gaseous phase among the particles in the adsorbent bed can be obtained for Reynolds number less than 10 from the following equation:

$$\boldsymbol{u_v} = -\frac{k_D}{\mu} \boldsymbol{\nabla} P_v \tag{3.6}$$

where μ is the dynamic viscosity of refrigerant gas, and k_D is the real (inherent) permeability of the adsorbent bed which can be calculated from the semi-empirical Blake-Kozeny equation [1]:

$$k_D = \frac{d_p^2 \varepsilon^2}{150(1-\varepsilon)^2} \tag{3.7}$$

where d_p is the diamater of adsorbent particle, ε is the adsorbent macroporosity.

3.5.2. Energy Transfer Kinetics and Energy Conservation Equation

The energy conservation equation can be represented by:

$$\left[\rho_s\left(c_{ps}+c_{pa}x\right)(1-\varepsilon_t)+\varepsilon_t\rho_v c_{pv}\right]\frac{\partial T_s}{\partial t}+\boldsymbol{\nabla}.\left(\varepsilon_t\rho_v c_{pv}\boldsymbol{u_v}T_s\right) = \boldsymbol{\nabla}.\left(k_{eq}\boldsymbol{\nabla}T_s\right)+(1-\varepsilon_t)\rho_s h_a\frac{\partial x}{\partial t} \tag{3.8}$$

where k_{eq} is the equivalent thermal conductivity of adsorber, ρ_s is the adsorbent density, c_p is the specific heat and subscripts *s, a, v* denote to solid adsorbent, adsorbed liquid refrigerant and vapor phases, respectively.

In the convection and diffusion equations, Peclet number ($Pe=\frac{uL}{\alpha}$, where u is velocity, L is characteristic length and α is thermal diffusivity) can reflect the relative magnitude of convection and diffusion actions. For the adsorption cooling system, because it is a low pressure system (for the systems which use the working pairs such as activated carbon-methanol, zeolite-water, silica gel-water) and the dimension of the bed is small, the interior pressure gradient and mass transfer velocity are negligible (see Eqn. 3.6 and Eqn. 3.7), thus the absolute value of *Pe* number is very small, which means that the effect of convection action in the energy equation is very little and can be neglected when solving the temperature field. Therefore equations can be solved under uniform pressure field, leading to simplification of energy conservation equation such as:

$$\left[\rho_s\left(c_{ps}+c_{pa}x\right)(1-\varepsilon_t)+\varepsilon_t\rho_v c_{pv}\right]\frac{\partial T_s}{\partial t}=\boldsymbol{\nabla}.\left(k_{eq}\boldsymbol{\nabla}T_s\right)+(1-\varepsilon_t)\rho_s h_a\frac{\partial x}{\partial t} \tag{3.9}$$

which can be rewritten as the following two-dimensional form in cylindrical coordinate:

$$\left[\rho_s\left(c_{ps}+c_{pa}x\right)(1-\varepsilon_t)+\varepsilon_t\rho_v c_{pv}\right]\frac{\partial T_s}{\partial t} = \frac{1}{r}\frac{\partial}{\partial r}\left(k_{eq}r\frac{\partial T_s}{\partial r}\right)+\frac{\partial}{\partial z}\left(k_{eq}\frac{\partial T_s}{\partial z}\right)+(1-\varepsilon_t)\rho_s h_a\frac{\partial x}{\partial t} \tag{3.10}$$

3.6. Modelling Assumptions

- The adsorbed phase is considered as a liquid, and the adsorbate gas is assumed to be an ideal gas.
- All thermal losses are negligible.
- The thermal resistance between the metal tube and the adsorbent bed is neglected.
- The two adsorbers have identical thermo-physical, structural and geometrical characteristics.
- All the adsorbent particles have the same properties (including shape and size); they are uniformly distributed throughout the adsorbent, and in local thermal equilibrium with the adsorbate and the surrounding gaseous phase. In other words, the porous medium is treated as an equivalent medium; the three phases (solid (*s*), adsorbed phase (a) and vapor (v)) are considered at an equivalent temperature which yields $T_s = T$, adsorption kinetics is very fast.
- The temperatures of heat source, heat sink, condenser and evaporator are fixed and constant (ideal heat sources). The condenser and evaporator are ideal, i.e., they have a constant temperature during the isobaric phases. Because the volume of bed is relatively small, and its heat consumption is much smaller compared with the total heat capacity of outside fluid, therefore the heating/cooling fluid is considered as even and constant temperature body; therefore, temperature gradient within adsorbent bed in axial direction can be neglected.
- The thermodynamic properties (i.e., specific heat and density) of adsorbate and vapor are assumed to be constant.
- Liquid phase is incompressible, and is a single component; its viscosity dissipation energy can be neglected.
- No desorption and adsorption takes place until the condensing pressure and the condensing pressure is reached, respectively.
- The adsorbent bed is considered as a continuous medium and the conduction heat transfer in the medium can be characterized by an equivalent thermal conductivity, k_{eq}.
- The adsorption/desorption process is an isobaric process.
- The adsorption/desorption enthalpy is considered constant as often occurs in literature [29].

- The equilibrium adsorption model has been assumed and the mass transfer resistance between solid and adsorbate gas phase intra-particles is neglected and therefore consider a uniform pressure treatment inside the porous medium.
- The porous medium properties have a cylindrical symmetry and the bed porosity is a constant.
- Time during desorption and adsorption is assumed to be equal while performance of the cycle is analyzed.

3.7. Initial and Boundary Conditions

3.7.1. Initial Condition

At the beginning temperature within adsorbent bed is equal to an initial temperature which can be expressed as:

$$T = T_{in} = T_{a2} \ @ \ t = 0 \ for \ Bed \ 1 \tag{3.11}$$

$$T = T_{in} = T_{g2} \ @ \ t = 0 \ for \ Bed \ 2 \tag{3.12}$$

3.7.2. Boundary Conditions

Boundary conditions of the present mathematical model refer to the adsorbent temperature $T_s = T$ which has two boundary conditions at r_{in} and r_{out}, repectively. The boundary condition of *T* at r_{out} applies Dirchlet boundary condition since the heat transfer resistance of metal water jacket is negligible compared to heat transfer resistance within the adsorbent bed. The heat conductivity of metal tube is normally about 50-150 W/mK while that of activated carbon is about 0.1-0.45 W/mK depending on the refrigerant used. On the other hand, the boundary condition of *T* at r_{in} applies adiabatic boundary condition while the surface is permeable.

Mathematically, the boundary conditions can be expressed as the following:

$$T = T_{hw} \ @ \ r = r_{out} \ while \ heating \ condition \tag{3.13}$$

$$T = T_{cw} \ @ \ r = r_{out} \ while \ cooling \ condition \tag{3.14}$$

$$\frac{\partial T}{\partial r} = 0 \ @ \ r = r_{in} \ for \ both \ conditions \tag{3.15}$$

In order to assess performance of the modelling system an average temperature and an average concentration are described as the following:

$$T_{avg}(t) = \frac{\int_{r_{in}}^{r_{out}} 2\pi r T(r,t) dr}{\pi(r_{out}^2 - r_{in}^2)} \tag{3.16}$$

$$x_{avg}(t) = \frac{\int_{r_{in}}^{r_{out}} 2\pi r x(r,t) dr}{\pi(r_{out}^2 - r_{in}^2)} \tag{3.17}$$

4. NUMERICAL SOLUTION

The governing heat transfer equation, which is second-order non-linear partial differential equation (PDE), take into account detail adsorption phenomena is solved numerically by the forward-time centered-space (FTCS) method in the time and radial space domain by taking account stability and convergence.

The objective is to transform a calculus problem into an algebra problem by

- Discretizing the continuous physical domain into a discrete difference grid.
- Approximating the individual exact partial derivatives in the partial differential equation (PDE) by algebraic finite difference approximations (FDAs).
- Substituting the FDAs into the PDE to obtain an algebraic finite difference equation (FDE).
- Solving the resulting algebraic FDE.

In general, two types of FDEs can be developed, depending on the base point chosen for FDAs. If the grid point (i, j), where *i* refers to the radial spatial domain while *j* is referring time domain, is chosen as the base point of the FDAs, then the FDE can be solved directly for f(i, j+1). Such FDEs are called explicit FDEs. Because the solution at each point is specified explicitly in terms of the known solution at neighboring points at time level j. This situation is illustrated in Figure 4.1 where the solution at point P at time level j+1 depends only on the solution at neighboring points at time level j while having a finite numerical information propagation speed, $c = \frac{\Delta r}{\Delta t}$.

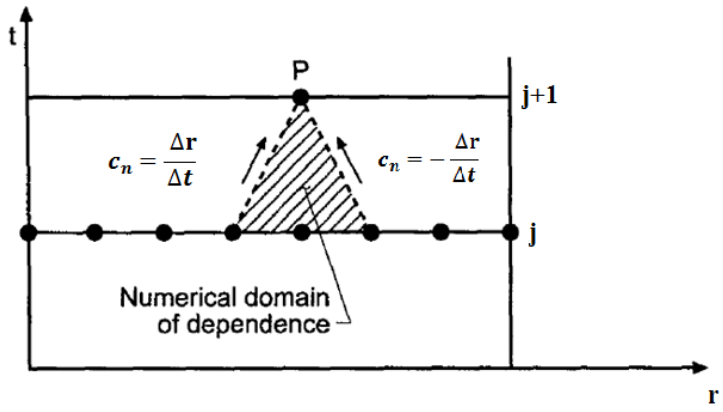

Figure 4.1. Numerical domain of dependence of explicit methods [30].

However, if the grid point (i, j+1) is chosen as the base point of the FDAs, f(i, j+1) cannot be solved directly, since f(i, j+1) depends on f(i+1, j+1) and f(i-1, j+1), which are also unknown. Such FDEs are called implicit FDEs. Because the solution at each point is specified implicitly in terms of the unknown solution at neighboring points at time level j+1 and result in a system of finite difference equations which must be solved at each time level. This situation is illustrated in Figure 4.2 where the solution at point P at time level j+1 depends on the solution at neighboring points at time level j+1 as well as the solution at time level j while having an infinite numerical information propagation speed $c = \frac{\Delta r}{\Delta t} = \pm\infty$.

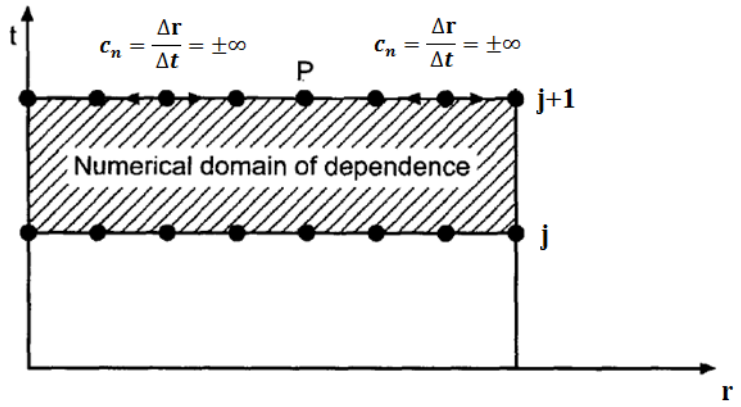

Figure 4.2. Numerical domain of dependence of implicit methods [30].

Explicit FDEs are obviously easier to be evaluated numerically than implicit FDEs. However, there are advantages and disadvantages of both explicit and implicit FDEs. The major difference is that the numerical information propagation speed for explicit methods is finite, whereas the numerical information propagation speed for implicit methods is infinite. Explicit methods are computationally faster than implicit methods because there is no system of finite difference equations to solve. Table 4.1 lists the comparison of two methods.

Table 4.1. Comparison of explicit and implicit method.

	Explicit Method	**Implicit Method**
Advantage	Simple solution algorithm	Stability maintained over larger Δt, fewer time steps required
Disadvantage	For a given Δr, stability constraints impose a maximum limit on Δt, many time steps required	More involved procedure More time consuming due to matrix manipulations involved in the algorithm Due to larger Δt, truncation error is also larger

4.1. Forward Time Centered Space Method

FTCS method is one of the explicit method forms to solve a partial differential equation (PDE). In FTCS method, the base point for the finite difference approximation (FDA) of the partial differential equation (PDE) is grid point (i, j). The finite difference equation approximates the exact partial time derivative by the first-order forward difference approximation, the exact first and second order partial spatial derivatives by centered difference approximation by writing Taylor series for the dependent variables. Taylor series expansion of $T(i+1,j)$, $T(i-1,j)$, and $T(i,j+1)$ are given in Appendix A. When the expansions are put into governing heat transfer equation, below algebraic finite difference equation (FDE) is obtained:

$$\left[\rho_s(1-\varepsilon_t)\left(c_{ps}+c_{pa}x-h_a\frac{\partial x}{\partial T}\right)+\varepsilon_t\rho_v c_{pv}\right]\frac{T(i,j+1)-T(i,j)}{\Delta t}$$

$$=k_{eq}\left[\frac{T(i+1,j)-2T(i,j)+T(i-1,j)}{(\Delta r)^2}\right. \tag{4.1}$$

$$\left.+\frac{1}{r(i)}\frac{T(i+1,j)-T(i-1,j)}{2\Delta r}\right]$$

where *x* is given as:

$$x = x_0 exp\left(-K\left(\frac{T(i,j)}{T_{sat}} - 1\right)^n\right) \tag{4.2}$$

x is only temperature dependent due to one of the approximations stated as uniform pressure throughout the porous medium, so

$$\frac{\partial x}{\partial T} = -x_0 exp\left(-K\left(\frac{T(i,j)}{T_{sat}} - 1\right)^n\right)\frac{Kn}{T_{sat}}\left(\frac{T(i,j)}{T_{sat}} - 1\right)^{n-1} \tag{4.3}$$

ρ_s is the density of activated carbon

c_{ps} is the specific heat of activated carbon

c_{pa} is the specific heat of liquid methanol

h_a is the heat of adsorption for activated carbon/methanol pair

ε_t is the total porosity of activated carbon

ρ_v is the density of liquid methanol

c_{pv} is the specific heat of liquid methanol

k_{eq} is the equivalent thermal conductivity of the porous medium

r_{in} is the inner radius of the adsorbent bed

r_{out} is the outer radius of the adsorbent bed

Δt is the incremental time

Δr is the incremental radial length

T_{sat} is the saturation temperature and equal to condenser temperature and evaporator temperature during desorption and adsorption, respectively.

All these coefficients are given in Appendix B for activated carbon/ammonia, activated carbon/methanol, silica gel/water, and zeolite/water.

The same principle must be used for the initial and the boundary conditions. In other words, finite different approximations must be obtained.

For the adsorbent bed 1, which is at the minimum bed temperature as initial state (at the end of adsorption, point a_2), initial condition is given as:

$$T(i,1) = 298\ K, \qquad \text{i} = 1{:}\ nr \tag{4.4}$$

where nr is the number of grid in radial direction and which is given as:

$$nr = \frac{r_{out} - r_{in}}{\Delta r} + 1 \tag{4.5}$$

Boundary conditions are

$$T(nr, j+1) = T_{hw}\ @\ r = r_{out}, \qquad \text{j} = 1{:}\ nt - 1 \tag{4.6}$$

where T_{hw} is the heat source temperature, 90 °C, nt is the number of grid in time domain and which is given as:

$$nt = \frac{t_{final}}{\Delta t} + 1 \tag{4.7}$$

t_{final} depends on the convergence of average bed temperature to T_{hw} and T_{cw} during heating and cooling phase, respectively.

$$\frac{\partial T(i,j)}{\partial r} = \frac{T(i+1,j) - T(i-1,j)}{2\Delta r} = 0\ @\ r = r_{in} \tag{4.8}$$

then $T(i+1,j)$ becomes equal to $T(i-1,j)$ at the inner radius. If the governing equation is rearranged, at the inner radius it becomes in the following form:

$$\left[\rho_s(1-\varepsilon_t)\left(c_{ps} + c_{pa}x - h_a\frac{\partial x}{\partial T}\right) + \varepsilon_t\rho_v c_{pv}\right]\frac{T(i,j+1) - T(i,j)}{\Delta t} = 2k_{eq}\left[\frac{T(i+1,j) - T(i,j)}{(\Delta r)^2}\right] \tag{4.9}$$

and $r = r_{in}$ corresponds to i=1; therefore,

$$\left[\rho_s(1-\varepsilon_t)\left(c_{ps} + c_{pa}x - h_a\frac{\partial x}{\partial T}\right) + \varepsilon_t\rho_v c_{pv}\right]\frac{T(1,j+1) - T(1,j)}{\Delta t} = 2k_{eq}\left[\frac{T(2,j) - T(1,j)}{(\Delta r)^2}\right], \qquad \text{j} = 1{:}\ nt - 1 \tag{4.10}$$

It should be noted that r_{in} is not equal to zero.

For the adsorbent bed 2, the result can be obtained by the same approach, except it is at the maximum bed temperature as initial state (at the end of desorption, point g_2). It means:

$$T(i,1) = 363\ K \tag{4.11}$$

and it is exposed to cooling; therefore,

$$T(nr, j+1) = T_{cw}\ @\ r = r_{out} \tag{4.12}$$

where T_{cw} is the heat sink temperature, 25 ° C

The basic disadvantage of explicit methods, it requires many time steps. Since when a too large value of the time step is considered or when the number of grid subdivision is not adequate, the result shows instability. Based on this consideration, an adequate time and spatial step in radial direction Δt and Δr, respectively should be chosen to warrant the consistence of the results. In the following sections consistency and stability of FTCS method will be analyzed.

4.2. Consistency

A finite difference equation is consistent with a partial differential equation if the difference between the FDE and the PDE (i.e., the truncation error of exact partial derivatives) vanishes as the sizes of the grid spacing go to zero independently. Consistency of FTCS is analyzed by expressing each term in the finite difference equation by a Taylor series with a particular base point (i, j) in Appendix C.

As Δt and Δr goes to 0, FDE approaches to

$$\left[\rho_s(1-\varepsilon_t)\left(c_{ps} + c_{pa}x - h_a\frac{\partial x}{\partial T}\right) + \varepsilon_t\rho_v c_{pv}\right]T_t = k_{eq}\left[T_{rr} + \frac{T_r}{r}\right] \tag{4.13}$$

It is nothing but the governing equation itself, consequently FTCS is a consistent approximation of the adsorption heat transfer equation with $O(\Delta t) + O(\Delta r)^2$.

4.3. Stability

The general behavior of the exact solution of the PDE must be considered. If the partial differential equation itself is unstable, then the numerical solution also must be

unstable. The concept of stability does not apply in that case. However, if the PDE itself is stable, then the numerical solution must be bounded. The concept of stability applies in that case.

Stability analysis can be performed only for linear PDEs. Consequently, nonlinear PDEs must be linearized locally, and the FDE which approximates the linearized PDE is analyzed for stability. For this study, the governing heat transfer equation is non-linear. On the other hand, stability criteria obtained for the FDE approximating the linearized PDE is also applied to the FDE approximating the nonlinear PDE in literature [30]. There are several methods to analyze stability for all the finite difference equation, and the von Neumann method, which is one of the most commonly used techniques, is used for this study. The details of the von Neumann method can be found anywhere in literature [30]. The steps for performing a von Neumann stability analysis of a finite difference equation are summarized below:

- Substitute the complex Fourier components for $f(i \pm 1, j)$ into FDE.
- Express $exp(\pm I\theta)$ in terms of $sin\theta$ and $cos\theta$, and determine the amplification factor, G.
- Analyze G (i.e., $|G| \leq 1$ to determine the stability criteria for the FDE.

$$T(i,j+1) = T(i,j) + A(i,j)\frac{\Delta t}{(\Delta r)^2}\left[T(i+1,j) - 2T(i,j) + T(i-1,j) + \frac{\Delta r}{2r(i)}\left(T(i+1,j) - T(i-1,j)\right)\right] \tag{4.14}$$

where $A(i,j)$ is given as:

$$A(i,j) = \frac{k_{eq}}{\rho_s(1-\varepsilon_t)\left(c_{ps} + c_{pa}x - h_a\frac{\partial x}{\partial \overline{T}}\right) + \varepsilon_t\rho_v c_{pv}} \tag{4.15}$$

The required Fourier components are given as:

$$T(i \pm 1, j) = T(i,j)exp(\pm I\theta) \tag{4.16}$$

Substituting these components into FDE gives:

$$T(i,j+1) = T(i,j) + A(i,j)\frac{\Delta t}{(\Delta r)^2}\Big[T(i,j)exp(I\theta) - 2T(i,j) + T(i,j)exp(-I\theta) + \frac{\Delta r}{2r(i)}\big(T(i,j)exp(I\theta) - T(i,j)exp(-I\theta)\big)\Big] \quad (4.17)$$

Introducing the relationship between the cosine and exponential functions, it yields:

$$T(i,j+1) = T(i,j)\left[1 + A(i,j)\frac{\Delta t}{(\Delta r)^2}\left(\frac{Isin\theta\Delta r}{r} + 2cos\theta - 2\right)\right] \quad (4.18)$$

Thus, the amplification factor G is defined as:

$$G = 1 + A\frac{\Delta t}{(\Delta r)^2}\left(\frac{isin\theta\Delta r}{r} + 2cos\theta - 2\right) \quad (4.19)$$

The amplification factor G is the single step exact solution of the finite difference equation for the general Fourier component, which must be less than unity in magnitude to ensure a bounded solution. $|G| \leq 1$ yields to

$$-1 \leq 1 + A\frac{\Delta t}{(\Delta r)^2}\left(\frac{isin\theta\Delta r}{r} + 2cos\theta - 2\right) \leq 1 \quad (4.20)$$

Note that A is always positive, since $\frac{\partial x}{\partial T}$ is always negative (an increase in temperature results in a decrease of adsorbate concentration in adorbent) and multiplication with $-h_a$ gives a positive result, the other terms existing in equation are always positive (i.e., k_{eq}, ρ_s, c_{ps}, ...). Therefore, the upper limit is always satisfied since $2cos\theta - 2$ varies between -4 and 0 as θ ranges from -∞ to +∞. From the lower limit,

$$c\frac{\Delta t}{(\Delta r)^2} \leq \frac{1}{2} \quad (4.21)$$

is the stability criteria, where

$$c = \frac{k_{eq}\left(-\frac{isin\theta\Delta r}{4r} - \frac{cos\theta}{2} + \frac{1}{2}\right)}{\rho_s(1-\varepsilon_t)\left(c_{ps} + c_{pa}x - h_a\frac{\partial x}{\partial T}\right) + \varepsilon_t\rho_v c_{pv}} \quad (4.22)$$

The structure of the amplification factor is an outcome of the problem geometry. The governing equation which is written in cylindrical coordinates contains symmetry as a result of physical domain of the adsorbent bed. θ varies in the range between 0° and 360° and for the problems in cylindrical coordinate it becomes to 180° and while $sin\theta$ terms is dropping, nominator of c parameter reduce to k_{eq}.

FTCS approximation of the governing equation is conditionally stable. The numerical analysis that is run by a MATLAB algorithm shows that when Δr is choosen as 2.5 mm, and Δt is chosen as 0.1 second, the solution complies with stability and convergence criteria. By changing grid size, and refining mesh temperature distribution is calculated and tabled in Appendix D.

In summary, the forward-time centered-space (FTCS) approximation of the governing heat transfer equation for adsorption of methanol on activated carbon is explicit, single step, consistent, $O(\Delta t) + O(\Delta r)^2$, conditionally stable. The adsorber is described with a grid is small enough to neglect the variations of the temperature and concentration. Then, the average values of the temperature, concentration and the heat transfer rate are calculated to assess the overall system performance. The average temperature and concentration refer to the average of the summation of all nodal points within the adsorption bed.

5. RESULTS AND DISCUSSIONS

5.1. Adsorbent Bed Temperature for Basic Cycle

The numerical solution is obtained under the listed operating parameters in Appendix B, using the proposed mathematical model and assumptions and finally the numerical approach introduced in the previous section.

Bed temperature distribution at distinct radial locations, $r = 60,\ 85,\ 100,\ 110\ mm$, with respect to time is plotted for activated carbon/ammonia, activated carbon/methanol, zeolite/water, and silica gel/water and listed in the following figures. The cycle is assumed to be complete when the average bed temperature has reached 98% of the generating temperature T_{g2}.

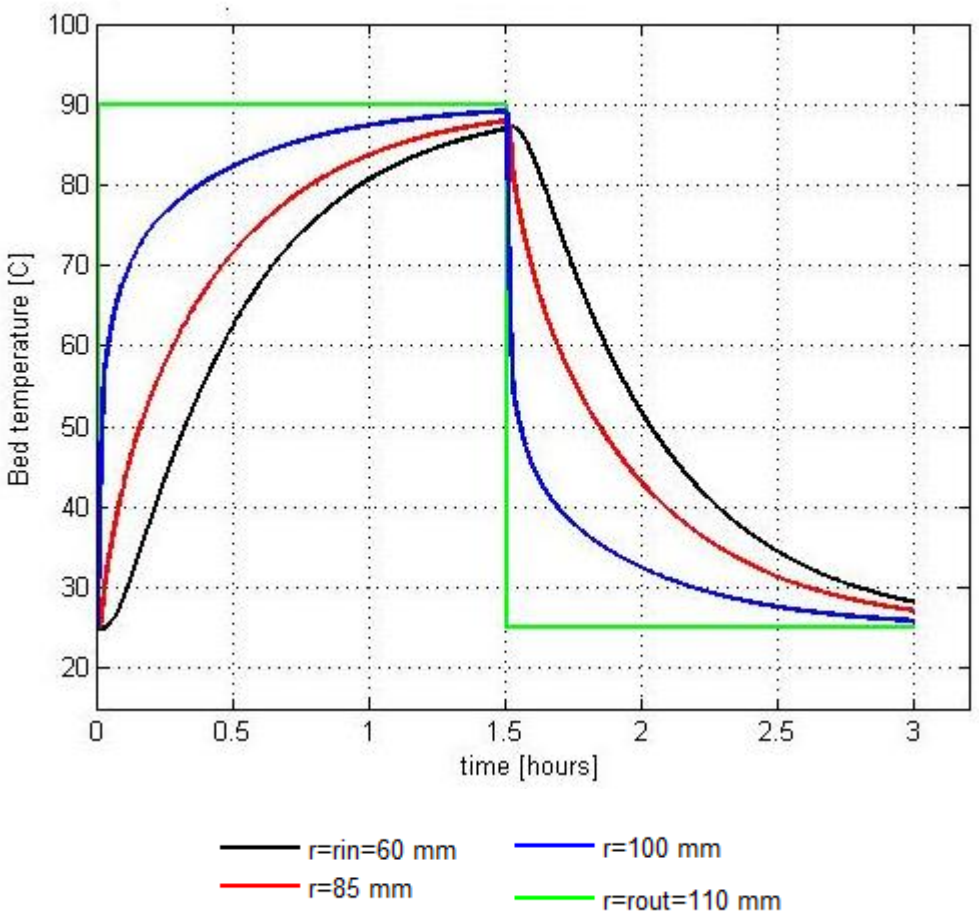

Figure 5.1. Bed temperature distribution vs time for AC/ammonia.

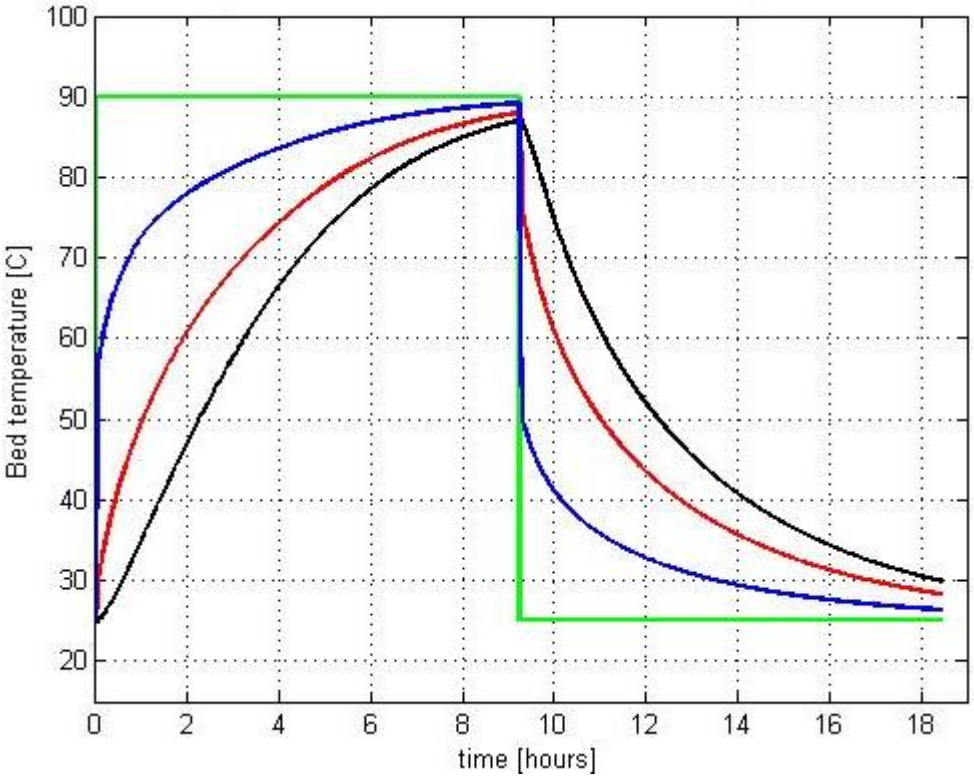

Figure 5.2. Bed temperature distribution vs time for AC/methanol.

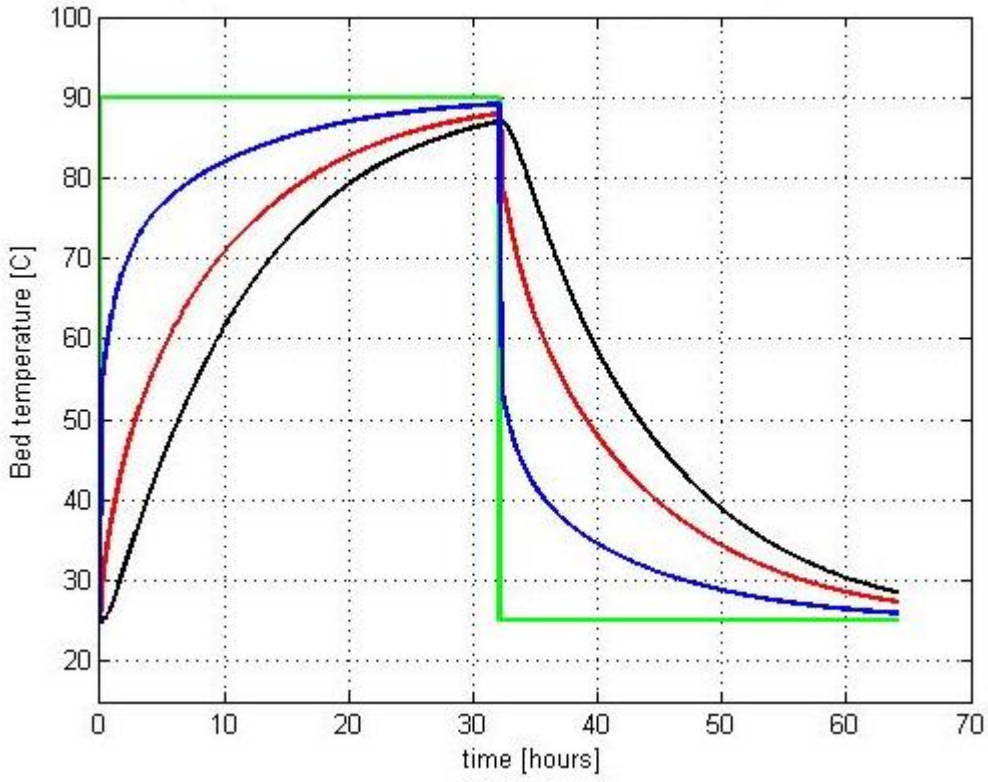

Figure 5.3. Bed temperature distribution vs time for silica gel/water.

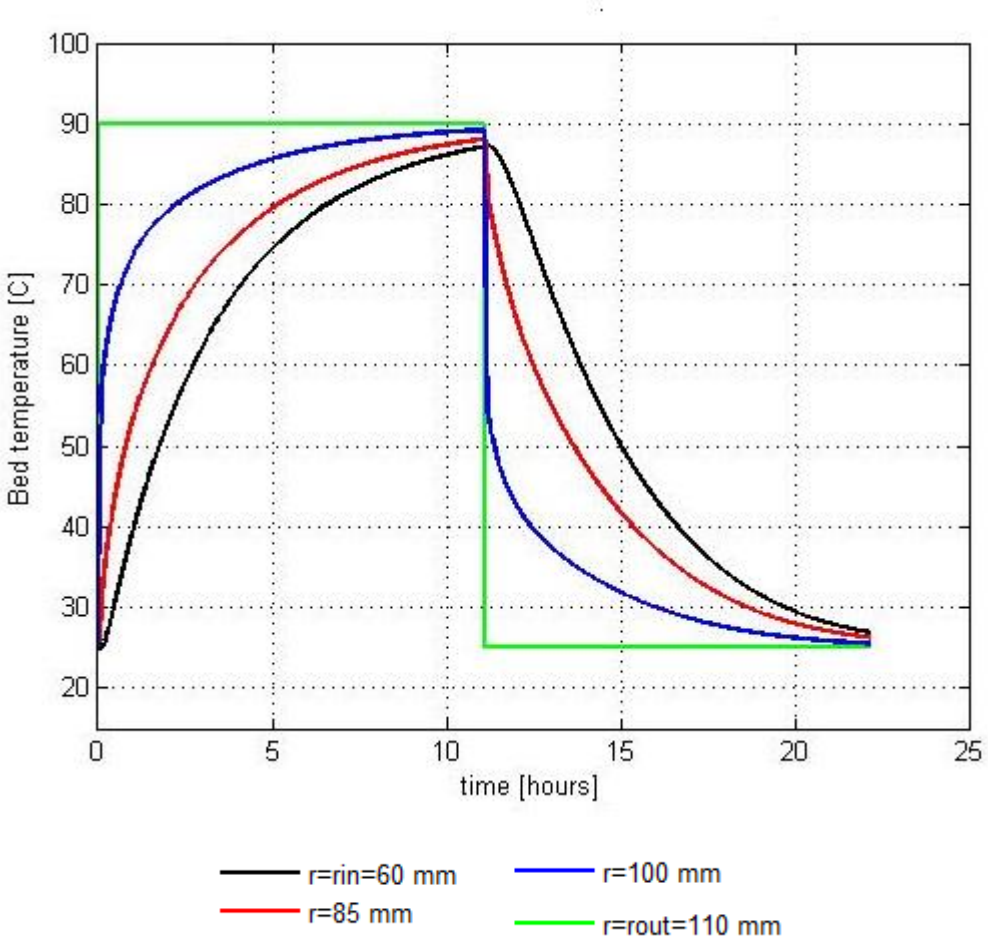

Figure 5.4. Bed temperature distribution vs time for zeolite/water.

There are two observations obtained as outcomes of the numerical analysis. One is that the temperature development is comprised of two stages as sharp climbing at the beginning within several minutes followed by the relatively slow rise during isosteric heating and desorption phase, respectively. The cause of this phenomenon is thought to be considerable part of the total heat input is supplied to the system during isobaric desorption, though the sensible heat, which is relatively small in comparison to the desorption heat, is consumed only to make the adsorbate be completely saturated and it results in sharp temperature increase within short part of the total cycle time. The other point is that the temperatures of the relatively inner positions of the cylindrical carbon bed are almost the same in the first minutes (i.e., 210 seconds for AC/methanol pair). It is an expected outcome since heating time is short and the bed thermal conductivity is poor; therefore, there should be a clear temperature difference between relatively inner radius and outer radius of the bed.

In order to validate the numerical results' compliance with literature, the algorithm written in MATLAB software is adopted for the data existing in literature [2] in Appendix E.

For adsorption refrigeration systems, there are two parameters utilized to evaluate system performance, i.e., COP and SCP. COP is basically related to operating parameters, which includes heat source and heat sink temperature, evaporating and condensing temperature. SCP is basically related to design parameters such as geometrical size of the adsorbent bed and thermodynamic properties such as thermal conductivity, heat of adsorption, and experimental parameters, i.e., K, n, x_0 used in proposed D-A adsorption equilibrium model which varies for each working pair. Especially, thermal conductivity and heat of adsorption are the basic parameters which affect the cycle time and consequently system performance.

5.2. Dimensionless Form of the Governing Equation

Before investigating the effects of listed parameters on COP and SCP, it will be useful to make the governing equation written in dimensionless form in order to determine the dimensionless variables if there exists. The governing equation, which was solved by utilizing FTCS numerical technique, was given as:

$$\left[\rho_s\left(c_{ps}+c_{pa}x\right)(1-\varepsilon_t)+\varepsilon_t\rho_v c_{pv}\right]\frac{\partial T}{\partial t} = k_{eq}\left(\frac{\partial^2 T}{\partial r^2}+\frac{1}{r}\frac{\partial T}{\partial r}\right)+(1-\varepsilon_t)\rho_s h_a\frac{\partial x}{\partial t} \tag{5.1}$$

To obtain the dimensionless form of the heat balance equation of the adsorber, the following dimensionless variables are introduced:

$\overline{\rho_{1,2,3}}=\frac{\rho_{1,2,3}}{\rho_0}$, which is dimensionless density and 1, 2, 3 denote to solid, liquid and vapor phase, respectively.

$\overline{c_{p1,2,3}}=\frac{c_{p1,2,3}}{c_{p0}}$, which is dimensionless specific heat and 1, 2, 3 denote to solid, liquid and vapor phase, respectively.

$\overline{h_a}=\frac{h_a}{\Delta H_{vap}}$, which is dimensionless heat of adsorption.

$\bar{T} = \frac{T}{T-T_{sat}}$, which is dimensionless temperature.

$\bar{t} = \frac{t}{t_0}$, which is dimensionless time.

$\bar{r} = \frac{r}{r_0}$, which is dimensionless radial length.

$\overline{k_{eq}} = \frac{k_{eq}}{k_0}$, which is dimensionless thermal conductivity.

It should be noted that total porosity, which is shown as ε_t, and sorption amount, which is shown as x, are dimensionless values.

When the new dimensionless variables are introduced into the governing equation and appropriate simplifications are done, the following dimensionless form is obtained:

$$\left[\overline{\rho_1}\left(\overline{c_{p1}} + \overline{c_{p2}}x\right)(1-\varepsilon_t) + \overline{\rho_3}\varepsilon_t\overline{c_{p3}}\right]\frac{\partial \bar{T}}{\partial \bar{t}} = (Fo)\overline{k_{eq}}\left(\frac{\partial^2 \bar{T}}{\partial \bar{r}^2} + \frac{1}{\bar{r}}\frac{\partial \bar{T}}{\partial r}\right) + \frac{1}{(Ja)}\overline{\rho_1}(1-\varepsilon_t)\overline{h_a}\frac{\partial x}{\partial \bar{t}} \tag{5.2}$$

where

$$Fo = \frac{k_0 t_0}{c_{p0}\rho_0 r_0^2} = \frac{\alpha_0 t_0}{r_0^2} \tag{5.3}$$

is Fourier number and defines the ratio of the heat conduction rate to the rate of thermal energy storage in a solid media.

$$Ja = \frac{c_{p0}(T - T_{sat})}{\Delta H_{vap}} \tag{5.4}$$

is Jakob number and defines the ratio of the sensible heat to latent heat energy adsorbed during liquid-vapor phase change.

Activated carbon/ammonia pair has the highest Fourier number which means has the lowest thermal energy storage capacity; therefore, it requires less cycle time. Whereas, silica gel/water has 8.5 times lower Fourier number due to its high energy storage capacity; that's why, its cycle duration is the highest. (i.e., $\frac{\alpha_0}{r_0^2}$ is $3.3\text{x}10^{-4}$ for AC/ammonia; whereas, it is $0.4\text{x}10^{-4}$ for silica gel/water)

The second outcome of the dimension analysis is that decrease on Jacob number results in higher cycle time duration. It is because required desorption energy is much more to make the adsorbate be desorbed. Due to relatively low heat conduction coefficient and relatively lower Jacob number of silica gel/water system, heat supply duration must be longer for it in comparison to other working pairs.

It should be also highlighted that concentration change for the cycle which utilizes activated carbon/ammonia as working pair is the lowest among the pairs under investigation. Lower concentration changes can be driven by lower heat input and at the system converges 98 % of heat source temperature rapidly. Porosity effect on the cycle time will be investigated in one of the following sections.

5.3. Parametric Analysis

5.3.1. Effect of Varying T_{g2} (T_{hw}) on COP for Basic Cycle

Depending on the values of T_{ev} and T_{con}, the COP has a maximum at some value of T_{g2}. This happens because as T_{g2} increases, x_{min} (or x_{dil}) decreases; therefore, a higher concentration change occurs which leads to increase on Q_{ev}.

On the other hand, higher concentration variation requires extra energy input to make the adsorbate be desorbed and so COP begins to decrease. In the analysis, COP is calculated for a range of heat source temperature starting from 50 °C to 180 °C with 10 °C temperature step, and it is observed that zeolite/water pair reaches its maximum COP which is 0.49 at 170 °C; activated carbon/ammonia, which has always the lowest COP over the range, reaches its maximum COP which is 0.40 at 160 °C; silica gel/water, which has always the highest COP over the range due to adsorbate's high latent heat of vaporization energy, reaches its maximum COP which is 0.69 at 110 °C; and finally activated carbon/methanol reaches its maximum COP which is 0.51 at 90 °C, while T_{ev} and T_{con} are 10 °C and 25°C, respectively.

It should be noted that among the analyzed working pairs zeolite/water requires the highest heat source temperature to reach maximum COP under certain evaporating and

condensing temperatures. This is because, zeolite needs higher heat source temperature to make the adsorbate be desorbed due to its high heat of desorption energy and consequently higher concentration change will result in higher COP.

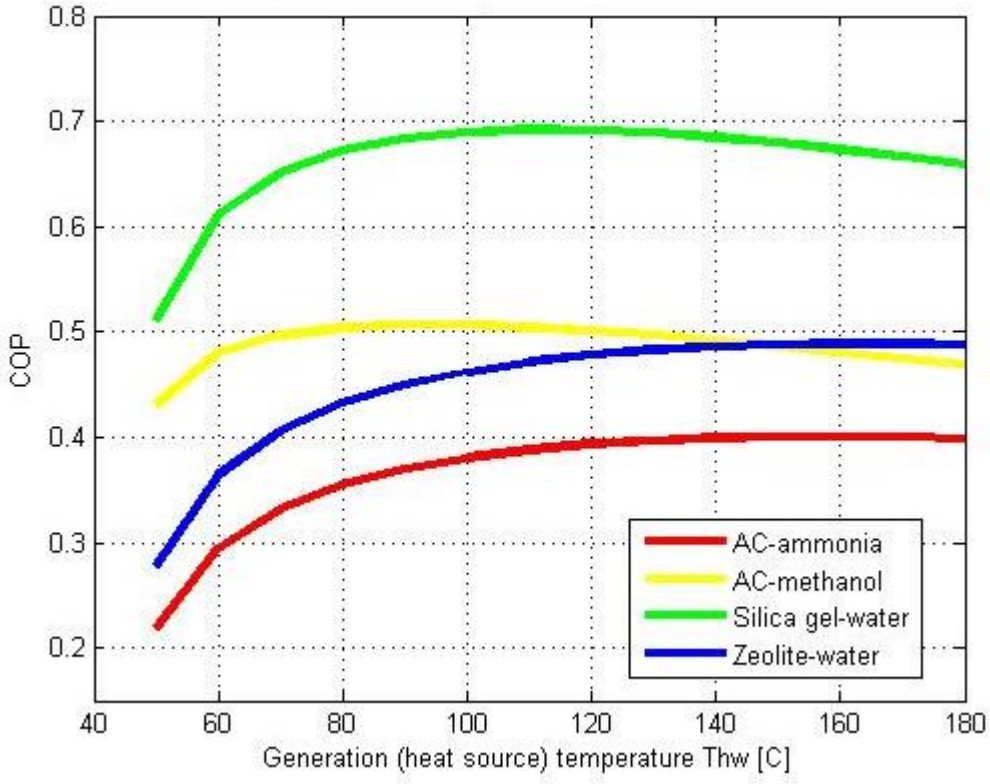

Figure 5.5. Influence of the heat source temperature on COP, $T_{con} = 25°C \;\; T_{ev} = 10°C$.

5.3.2. Effect of Varying T_{con} on COP for Basic Cycle

Minimum adsorbed amount depends on saturation temperature, which is condensing temperature, during desorption process. As T_{con} increases, the COP decreases. This is because when condenser temperature increases, x_{min} (or x_{dil}) at T_{g2} becomes a higher value as seen in Figure 5.6 (i.e., x_{min} is 0.08 at 15 °C condensing temperature, while it is 0.14 at 30 °C condensing temperature) . This means that for the same amount of heat input there is less of a concentration change which leads Q_{ev} to decrease and so does the COP. The second reason, which has minor effect in comparison to concentration change, is that when temperature difference is increased between condenser and evaporator by increasing condenser temperature with fixed evaporator temperature, required sensible heat demand is increased, so the COP decreases. In the analysis, COP is calculated for a range of condenser temperature starting from 15 °C to 50 °C with 5 °C temperature step,

and the results validates that as T_{con} increases so the COP decreases. While T_{ev} and T_{g2} are 10 °C and 90 °C, respectively, COP for silica gel/water, which has always the highest COP over the range, is 0.68; for activated carbon/methanol is 0.51; for zeolite/water is 0.45; for activated carbon/ammonia, which has always the lowest COP over the range, is 0.37 at 25 °C condensing temperature.

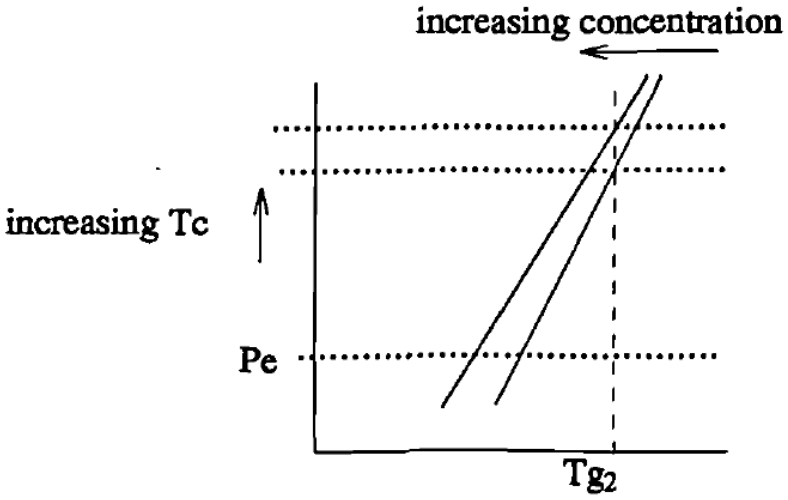

Figure 5.6. Schematic of the condenser temperature effect on concentration [16].

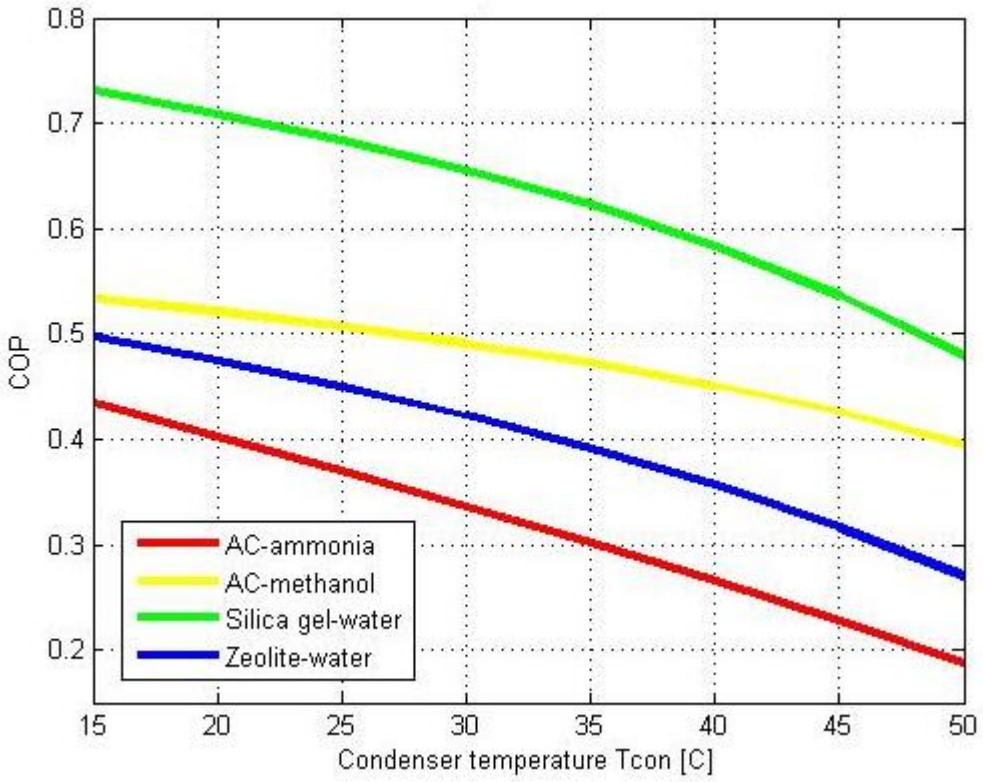

Figure 5.7. Influence of the condenser temperature on COP, $T_{hw} = 90°C$ $T_{ev} = 10°C$.

5.3.3. Effect of Varying T_{ev} on COP for Basic Cycle

Maximum adsorbed amount depends on saturation temperature, which is evaporating temperature, during adsorption process. As T_{ev} decreases, the COP decreases, too. This is because the value of T_{ev} determines on which isostere T_{a2} will follow. From the p-T-x diagram shown in Figure 5.8 it can be seen that as T_{ev} drops so does the x_{max} (i.e., x_{max} is 0.44 at 20 °C evaporating temperature, while it is 0.35 at 5 °C evaporating temperature). x_{min} (or x_{dil}), which depends on T_{con}, remains the same over the range of T_{ev} then Q_{ev} decreases due to lower concentration change as T_{ev} decreases. In the analysis, COP is calculated for a range of evaporating temperature starting from -15 °C to 20 °C with 5 °C temperature step, and the results validates that as T_{ev} increases so the COP increases. While T_{con} and T_{g2} are 25 °C and 90 °C, respectively, COP values were listed in the previous section for 10 °C evaporating temperature.

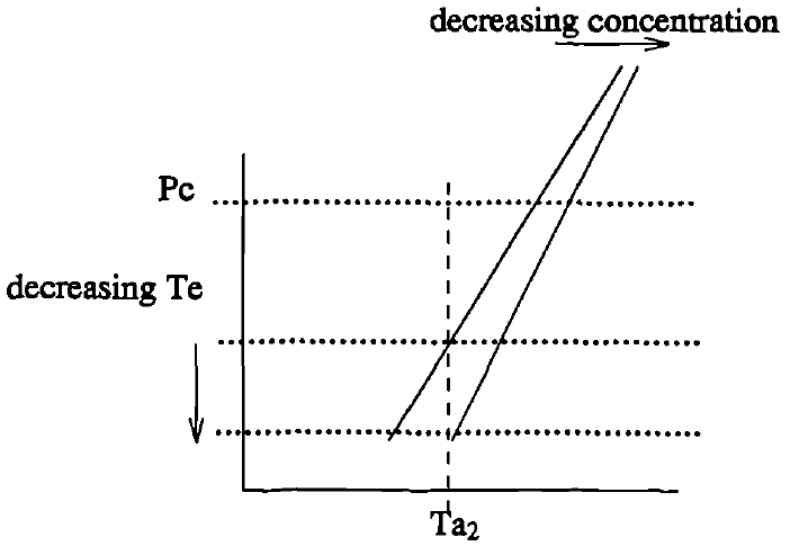

Figure 5.8. Schematic of the evaporator temperature effect on concentration [16].

As a result of COP analysis, silica gel/water gives the best performance, while activated carbon/ammonia gives the worst for all investigated operating parameters. In order to choose the working pair that should be used under certain operating conditions, SCP also should be taken into consideration.

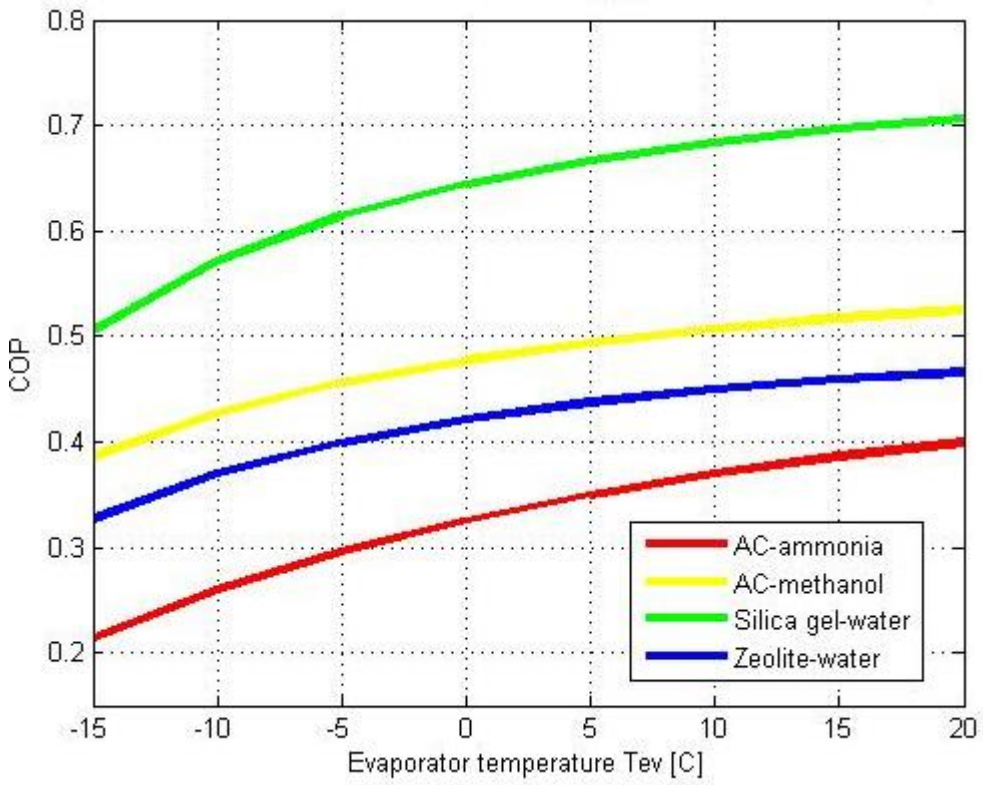

Figure 5.9. Influence of the evaporator temperature on COP, $T_{hw} = 90°C$ $T_{con} = 25°C$.

5.3.4. Effect of Varying T_{g2} (T_{hw}) on SCP for Basic Cycle

As a similar approach to the effect of varying T_{g2} on COP, SCP is calculated for a range of heat source temperature starting from 50 °C to 180 °C with 10 °C temperature step, and it is observed that when heat source temperature is increased, SCP also increases but with a decreasing slope. On the other hand, it should be noted that SCP begins to remain constant or even decrease after a certain heat source temperature which changes for all working pairs while keeping all other parameters fixed. It is because, the time during desorption process increases with an increase of heat source temperature. Since there is a higher temperature difference between initial case and end of desorption case while T_{g2} is increasing. In order to converge higher heat source temperature, external heat must be supplied longer to the adsorbent bed. Although cycled mass increases with heat source temperature, there is a limit showing minimum adsorbed amount. After this limit, diluted concentration amount begins to remain constant, consequently SCP becomes constant. In this analysis, maximum SCP is obtained at 180 °C for all working pairs. Maximum SCP

for activated carbon/ammonia is 22, for activated carbon/methanol is 6.6, for silica gel/water is 3.3, and finally for zeolite/water is 6.2 W/kg adsorbent.

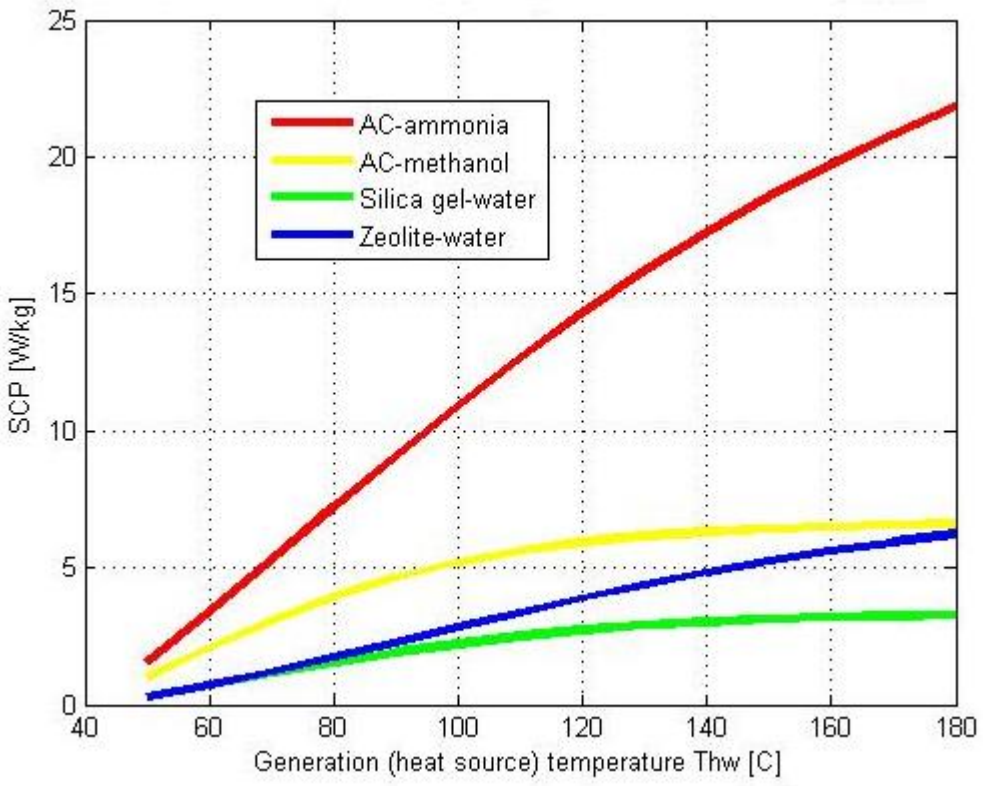

Figure 5.10. Influence of the heat source temperature on SCP per unit adsorbent mass, $T_{con} = 25°C \;\; T_{ev} = 10°C$.

5.3.5. Effect of Varying T_{con} on SCP for Basic Cycle

Regarding to the condenser temperature effect on SCP, a high condensing temperature results in a lower concentration variation; therefore, SCP is expected to decrease. On the other hand, lower concentration variation means less heat is needed to drive desorption and less heat will be released during adsorption, which results in a shorter cycle time and consequently SCP will increase. When these two distinct effects are taken into consideration and SCP is calculated with respect to condensing temperature which varies between 15 °C to 50 °C with 5 °C temperature step, and Figure 5.11 is obtained. It can be seen from Figure 5.11 that when condensing temperature increases, SCP decreases. It shows that higher condensing temperature has much more decreasing effect on cycled refrigerant mass in comparison to cycle time. While T_{ev} and T_{g2} are 10 °C and 90 °C, respectively, SCP for activated carbon/ammonia, which has always the highest SCP over

the range, is 9.1; for activated carbon/methanol is 4.6; for zeolite/water is 2.3; for silica gel/water, which has always the lowest SCP over the range, is 1.9 W/kg adsorbent at 25 °C condensing temperature.

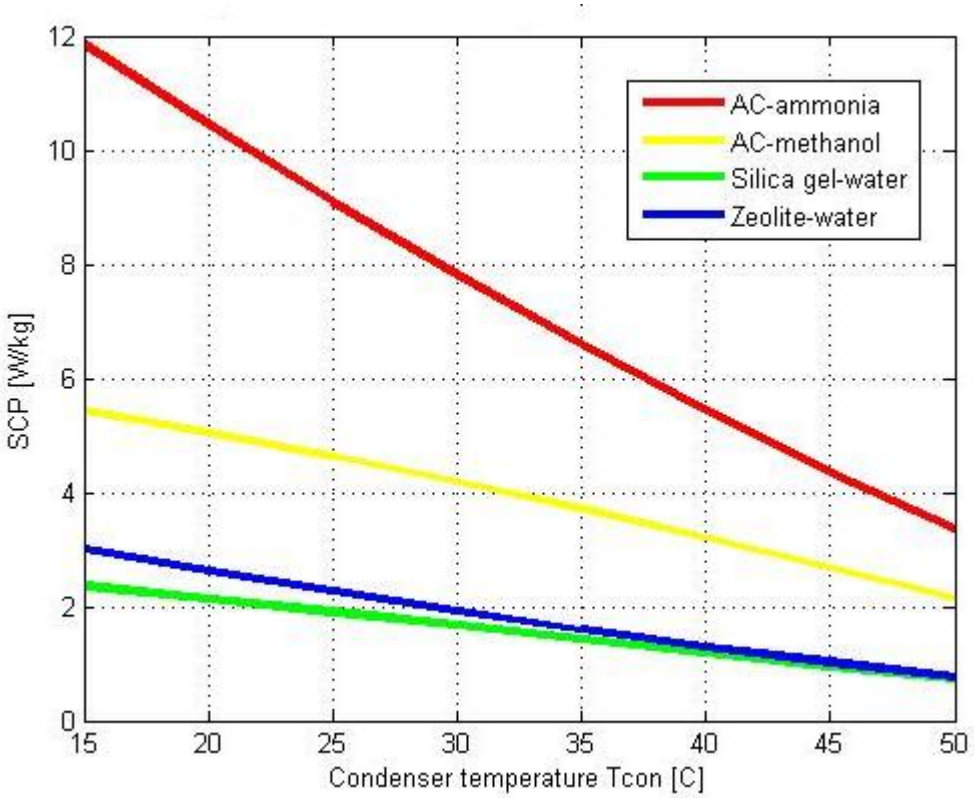

Figure 5.11. Influence of the condenser temperature on SCP per unit adsorbent mass, $T_{hw} = 90°C$ $T_{ev} = 10°C$.

5.3.6. Effect of Varying T_{ev} on SCP for Basic Cycle

Regarding to the evaporating temperature effect on SCP, a high evaporating temperature results in a higher concentration variation; therefore, SCP is expected to increase. On the other hand, higher concentration variation means more heat is needed to drive desorption and more heat will be released during adsorption, which results in a longer cycle time and consequently SCP will decrease. When these two distinct effects are taken into consideration and SCP is calculated with respect to evaporating temperature which varies between -15 °C to 20 °C with 5 °C temperature step and Figure 5.12 is obtained. It can be seen from Figure 5.12 that when evaporating temperature increases, SCP also increase but with a decreasing slope. While T_{con} and T_{g2} are 25 °C and 90 °C, respectively, SCP values were listed in the previous section for 10 °C evaporating temperature.

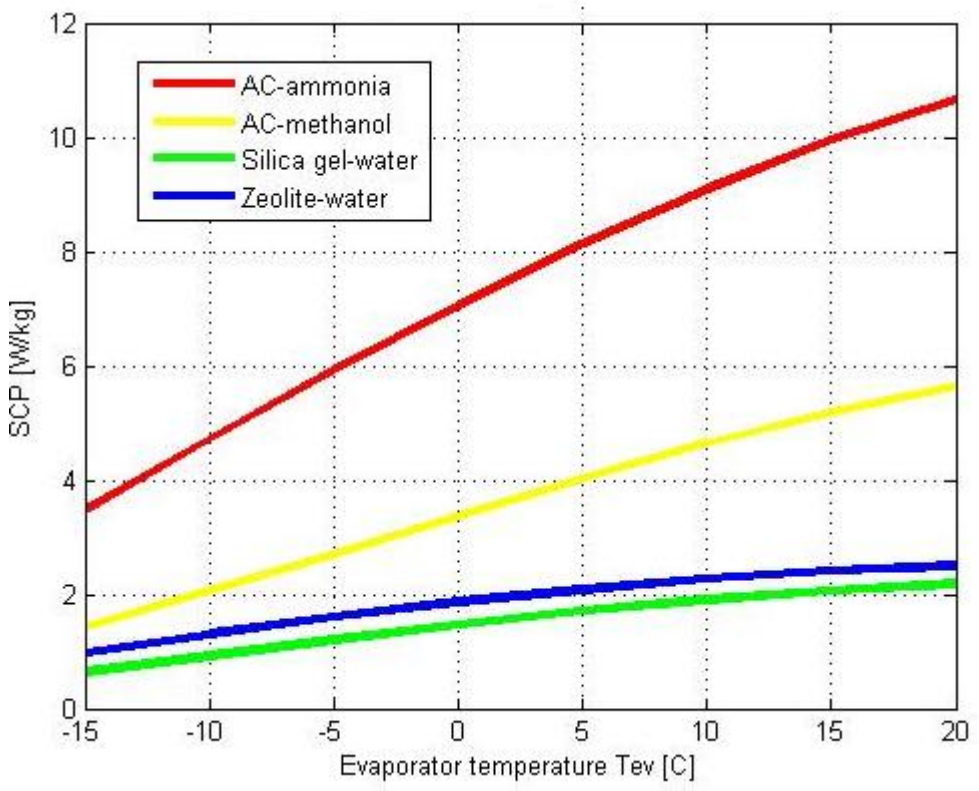

Figure 5.12. Influence of the evaporator temperature on SCP per unit adsorbent mass, $T_{hw} = 90°C$ $T_{con} = 25°C$.

In contrast to the COP analysis, activated carbon/ammonia pair gives the highest SCP, while silica gel/water pair gives the worst over the range for all investigated operating parameters. It is an expected result, since required time to reach heat source or heat sink temperature or in other words time during desorption and adsorption phase is much more for silica gel/water pair in comparison to activated carbon/ammonia due to its relatively low thermal conductivity, higher heat of desorption and higher thermal energy storage capacity.

Based on COP and SCP analysis done, it is needed to make a compromise to choose an appropriate adsorbate/adsorbent pair. The low pressure systems, which use the working pairs such as activated carbon-methanol, zeolite-water, silica gel-water, have the negligible interior pressure gradient and mass transfer velocity and comply with the uniform pressure gradient assumption. Since the effect of convection action in the energy equation is very little and can be neglected when solving the temperature field for the low pressure systems, it is appropriate to choose a pair among activated carbon-methanol, zeolite-water and silica gel-water, although activated carbon-ammonia gives higher SCP.

The most important drawback of the low pressure systems is due to weak mass transfer, which is a result of low pressure, cycle time is considerably larger in comparison to high pressure systems. Silica gel/water is the best pair for COP point of view, while it is the worst for SCP point of view. Therefore, activated carbon/methanol pair is selected for proposed mass and heat recovery adsorption refrigeration cycle as a good compromise while both COP and SCP as coupled are taken into consideration. Therefore, all analysis will be performed based on activated carbon/methanol pair in the following sections.

5.3.7. Porous Media Geometry Effect and Cycle Time Optimization

Cycle time is a significant parameter for operating an adsorption refrigeration system. Operating parameters such as generation temperature, condenser temperature and evaporator temperature have been evaluated in terms of their effects on cycle time and consequently SCP so far. These parameters affect cycle time due to their contribution on concentration variation change. Another significant parameter is geometrical size of the adsorbent bed. The inner radius is assumed to be constant as $r_{in} = 60\ mm$, and four outer radius, $r_{out} = 90, 100, 110, 120\ mm$, are selected to investigate the effect of bed geometrical size on cycle time. In order to simplify the analysis, the cycle is assumed to be complete when the average bed temperature has reached 90% of the generating temperature T_{g2}, which is 90 °C, and all other parameters used for activated carbon/methanol pair are fixed. Mesh size is kept as $\Delta r = 2\ mm$ and $\Delta t = 0.1\ s$. Figure 5.13 plots the effect of adsorbent size on cycle time. It is concluded from the Figure 5.13 that with an increase on the outer radius, the cycle time is prolonged. When the outer radius is 110 mm, which is the design case for two adsorbers, approximately 10.7 hours needed to reach 90% of the generating temperature, while outer radius is 90 mm, this time is shortened as 4.1 hours. It is an expected result, since when the thickness of the adsorbent bed is increased, heat transfer rate will decrease and the time necessary for the completion of each phase also increases and so the cycle duration.

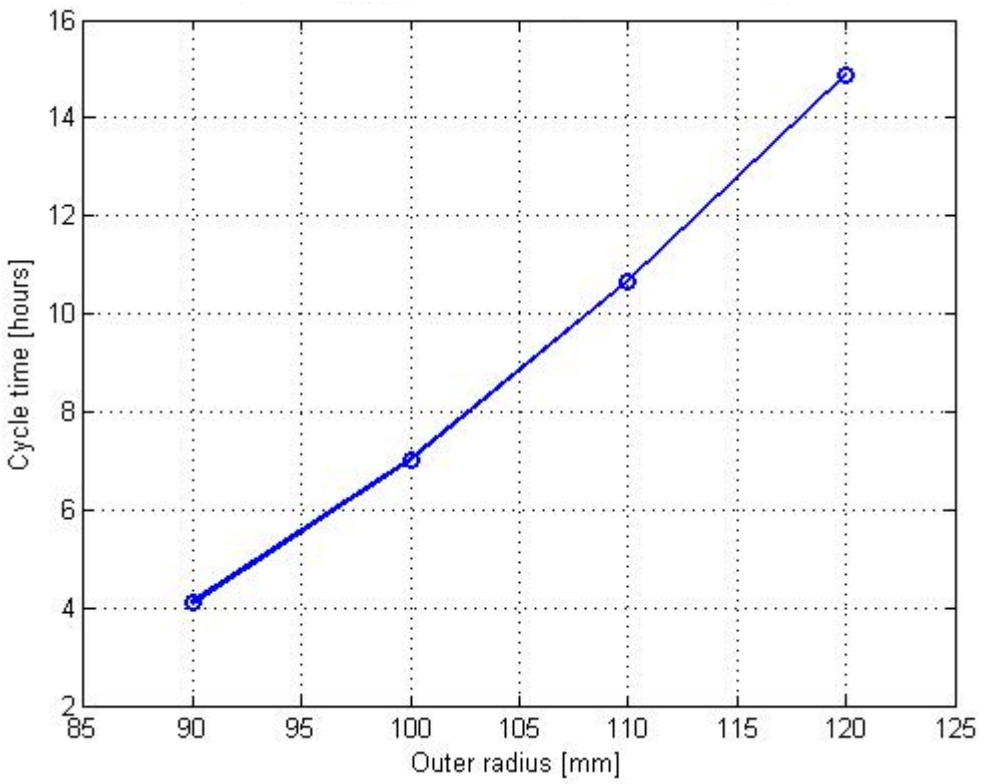

Figure 5.13. Adsorbent bed size effect on cycle time.

Cycle time requires an extra attention to obtain an optimized adsorption refrigeration system. Since when cycle time is increased apart from geometrical size of the adsorber, higher COP can be obtained due to the fact that more refrigerant can be desorbed leading to generate more refrigeration capacity, even though it leads to decrease on SCP. In order to determine these considerations cycle time will be deeply analyzed.

Firstly, all operating conditions that are $T_{hw} = 90$ ℃, $T_{cw} = 25$ ℃, $T_{con} = 25$ ℃, $T_{ev} = 10$ ℃ and geometrical size of the bed, $r_{in} = 60\ mm$ and $r_{out} = 110\ mm$ are kept as constant. At the begining, the cycle was assumed to be complete when the average bed temperature has reached 98% of the generating temperature T_{hw} and cycle time was found as 18.45 hours for activated carbon/methanol and it was quite high for an efficient cycle. For this time, cycle time will be independent and average bed temperature will be calculated depending on variable time parameter. After average bed temperature is calculated by FTCS method, system performance parameters, which are COP and SCP, will be plotted against total cycle time. As it was stated in the assumption section, the time during desorption and adsorption will be assumed as equal while performance of the cycle is analyzed.

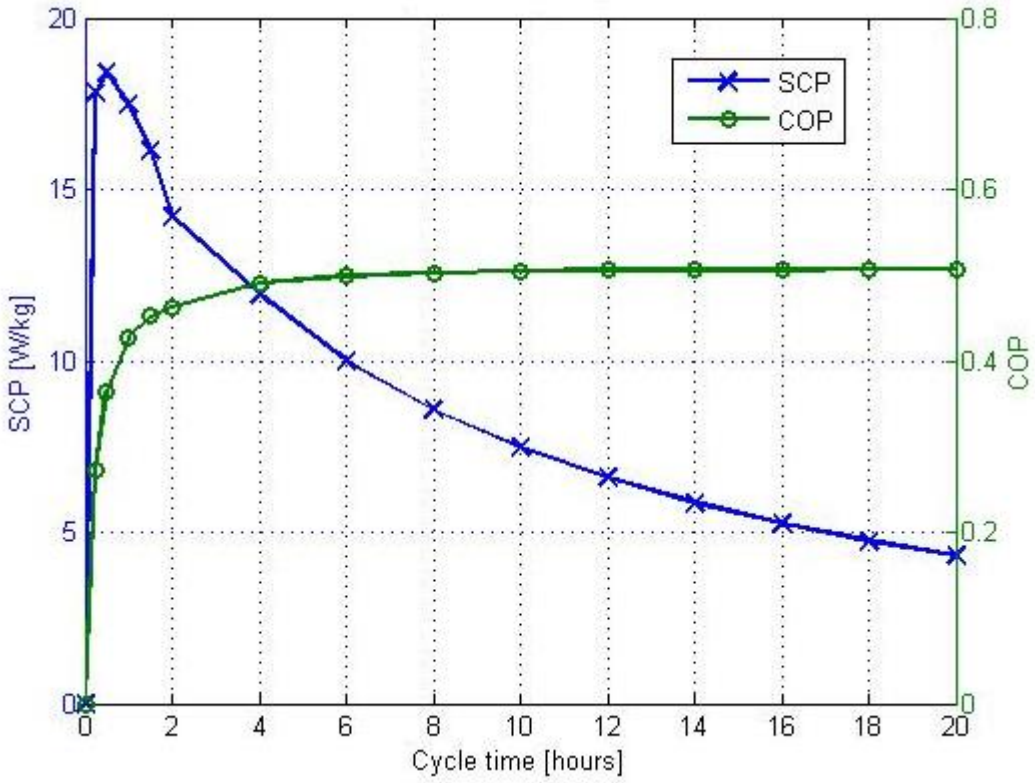

Figure 5.14. Cycle time optimization.

Regarding to the analysis, Figure 5.14 is obtained. As it was expected COP increases with an increase in cycle time, though SCP decreases. However, it is shown that there is no need to supply external heat to the bed after a certain time in terms of COP criteria to make the bed approach to 98% of the heat source temperature. COP begins to remain nearly constant after 4 hours. Hence, it is beneficial to make compromise between COP and SCP and consequently heat supply can be stopped after 2 hours, and cooling phase can be initiated. By this way it is possible to obtain higher SCP which may be more important according to the purpose of the application. This approach can be introduced for other working pairs such as silica gel/water and zeolite/water. These pairs requires much more heat supply due to relatively high heat of desorption capacity, which reduces *Jacob* number existing in the governing equation, and due to worse thermal conductivity and high thermal energy storage in comparison to activated carbon, temperature equilibrium is reached very slowly. On the other hand cycle time optimization eliminates long cycle time drawback.

5.3.8. Porosity Effect on Cycle Time

Porosity is a thermo physical property; however, it is possible to obtain different porous structures for the same adsorbent by using different and several manufacturing techniques. As a result of manufacturing process, types of pore may be different for each sample. Figure 5.15 shows different types of pore for activated carbon. Although adsorbent manufacturing techniques are out of thesis scope, the required information can be found anywhere in the literature [16].

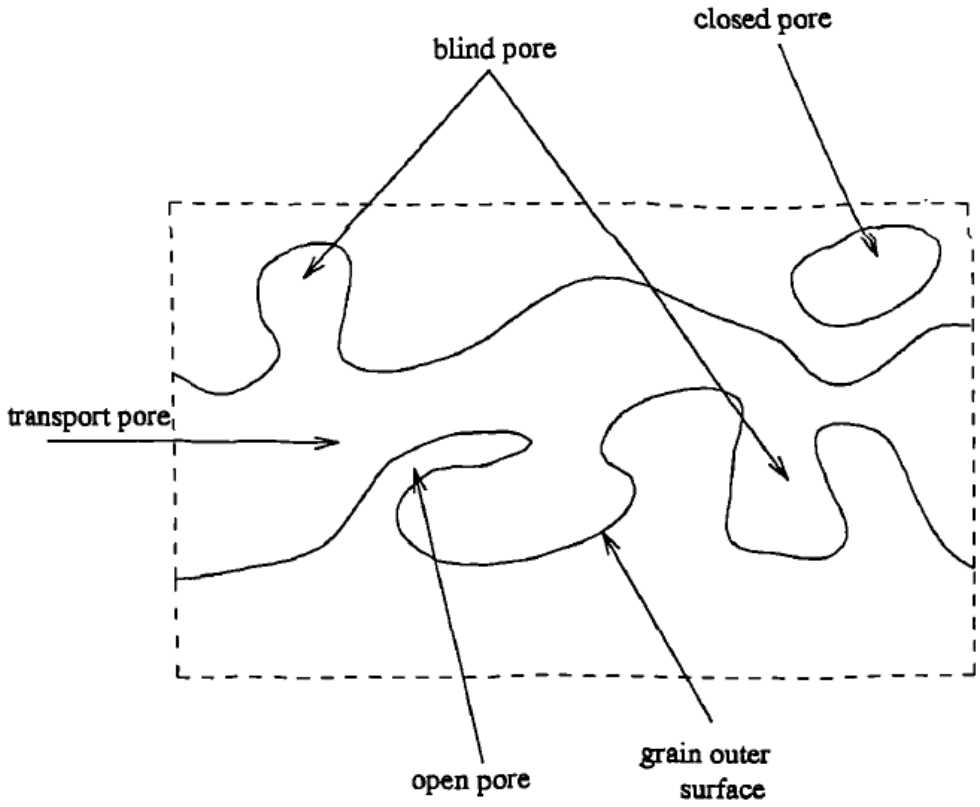

Figure 5.15. Porous structure [16].

For this study, porosity effect on system performance will be analyzed. By using different porosity values for activated carbon, its effect on cycle time will be determined. At the beginning solid, adsorbed liquid and vapor phases were assumed to be in equilibrium; therefore, an equilibrium temperature is used to solve heat balance equation.

In order to determine porosity effect on cycle time all operating parameters and geometrical size of the adsorbent bed are kept constant as was done in cycle time optimization analysis. While porosity will be varied between 0 and 1 with 0.2 step,

required cycle time is plotted by assuming cycle is complete when the average bed temperature has reached 90% of the generating temperature T_{hw}.

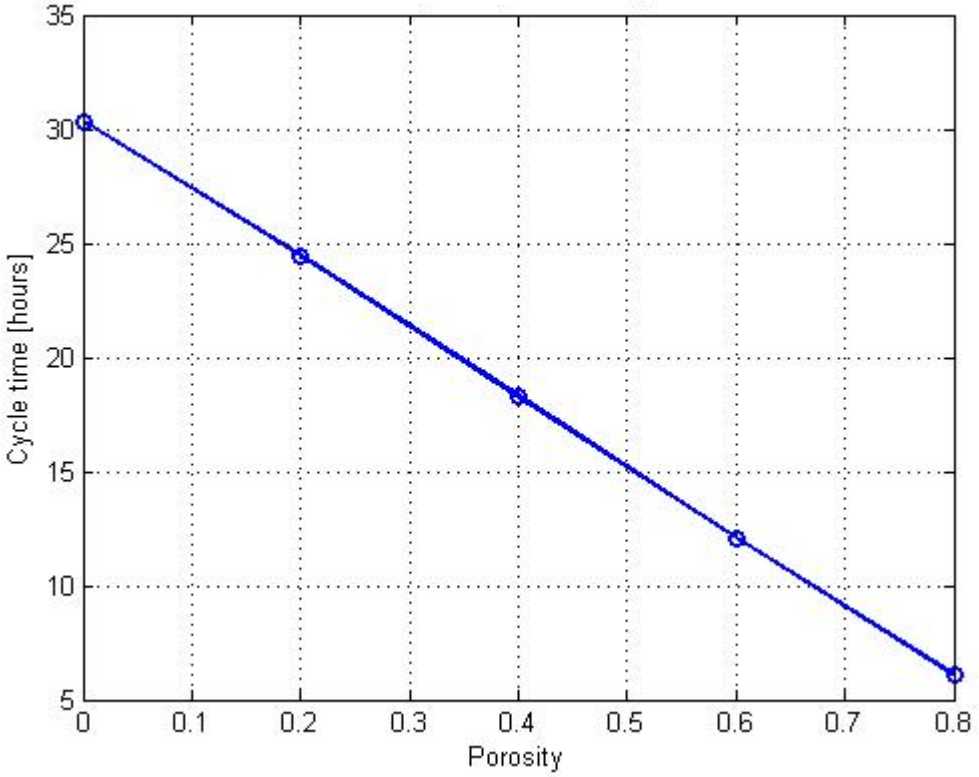

Figure 5.16. Adsorbent porosity effect on cycle time.

As a result of the analysis, Figure 5.16 is obtained. It is clearly seen that when porosity increases, required cycle time decreases linearly. $(1-\varepsilon_t)$ is the coefficient of heat of adsorption or desorption in the governing equation; therefore when porosity approaches to 1, latent heat supply or release duration, in other words desorption or adsorption duration decrease. Desorption and adsorption times consist of majority of the whole cycle time; therefore, increase on porosity result in decrease on cycle time. $\varepsilon_t = 1$ is a special case, which means that no adsorption/desorption occurs and against the fundamental of problem, so it is not shown on the Figure 5.16.

5.4. Second Law Efficiency for Basic Cycle

The second law efficiency is calculated by:

$$\eta_{II} = \frac{COP}{COP_{Carnot}} \tag{5.5}$$

The allowable maximum COP for an adsorption system is obtained by assuming the cycle is completely reversible. Suppose that external heat input (Q_{hw}) supplied to the adsorption system is given to a Carnot heat engine. Work output would be $W = \eta_{Carnot} Q_{hw}$. By utilizing this amount of work, it is possible to take $Q_{ev} = WCOP_{Carnot,refrigeration}$ amount of heat from the space to be cooled. Then, Carnot COP, which is completely reversible, for an adsorption refrigeration system is given as [31]:

$$\mathrm{COP_{Carnot}} = \frac{Q_{ev}}{Q_{hw}} = \eta_{Carnot} COP_{Carnot,refrigeration} = \frac{1 - \frac{\mathrm{T_{cw}}}{\mathrm{T_{hw}}}}{\frac{\mathrm{T_{con}}}{\mathrm{T_{ev}}} - 1} \tag{5.6}$$

While T_{ev}, T_{con}, T_{hw} and T_{cw} are 10 °C, 25 °C, 90 °C, 25 °C, respectively, COP for activated carbon/methanol was calculated as 0.5065. Then, the second law efficiency is found as 0.15 for the basic cycle.

5.5. Dynamic Sorption Amount

Dynamic sorption amount at distinct radial locations with respect to time is plotted for activated carbon/ammonia in Figure 5.17 and Figure 5.18.

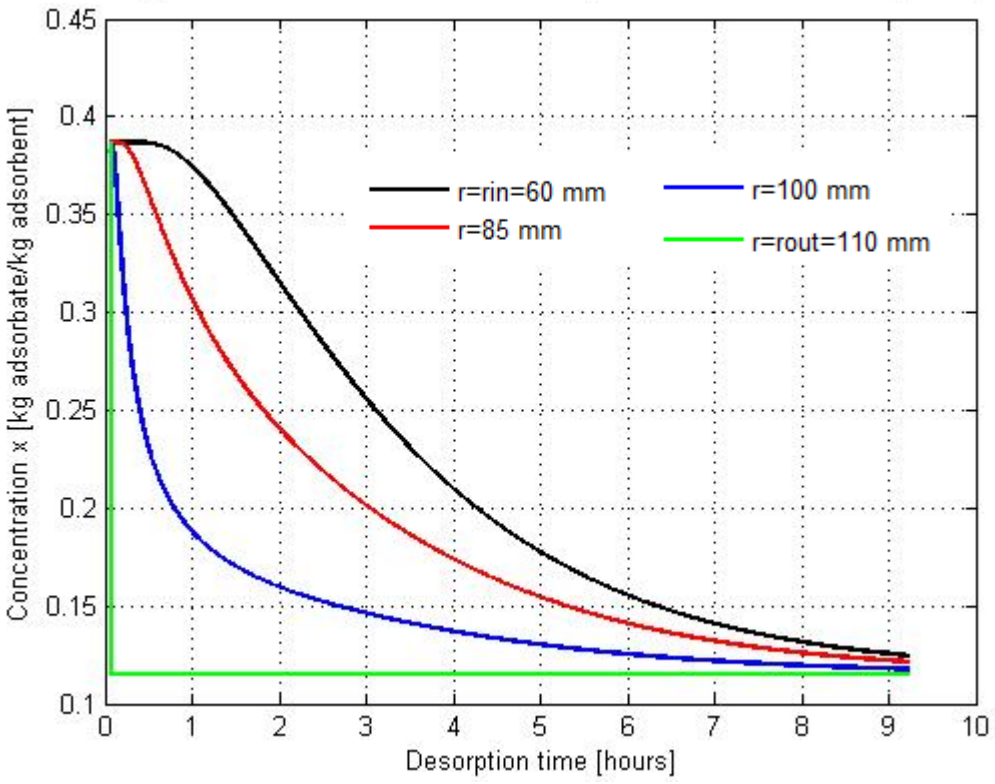

Figure 5.17. Concentration variation vs time during isosteric heating and desorption phase for activated carbon/methanol.

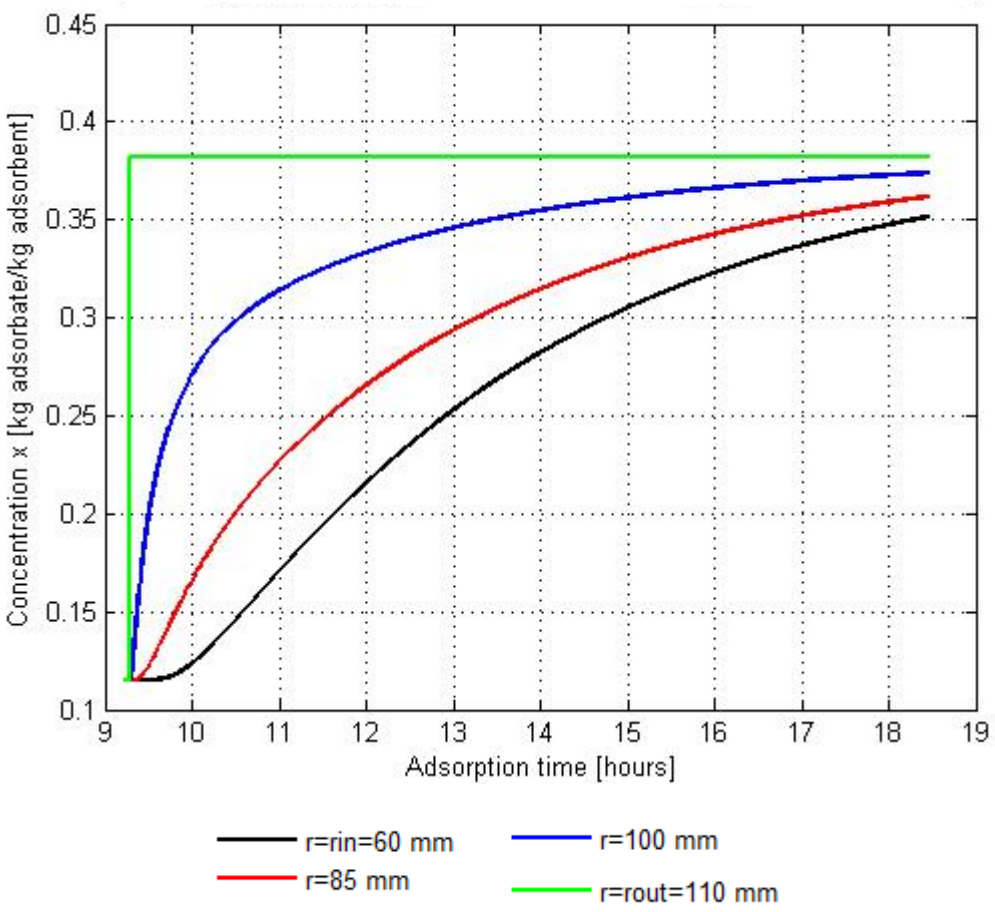

Figure 5.18. Concentration variation vs time during isosteric cooling and adsorption phase for activated carbon/methanol.

Regarding to the dynamic sorption amount, concentration does not change throughout the bed, until the bed reaches saturation temperature corresponding to condensing pressure, since during this phase adsorbate try to reach saturation condition while being heated and no desorption takes place at the beginning within several minutes. This result also complies with one of the assumptions which were listed. Indeed, concentration changes from point to point in radial direction during isosteric heating/cooling. During isosteric heating (or cooling) process, temperature difference between outer radius and relatively inner radius is high and this temperature gradient force vapor to be adsorbed by the relatively inner radius where temperature is lower. Therefore, vapor around outer positions of the bed starts to travel into inner positions of the bed and consequently adsorbed. However, the total adsorbed amount throughout the bed remains constant. This vapor migration can be neglected, since required time to reach saturation conditions for desorption and adsorption is accomplished rapidly and isosteric phases only

represent small amount of the total cycle time. (i.e., 0.6% for AC/methanol pair and much lower for Silica gel/water or zeolite/water)

Average bed concentration and temperature versus time are plotted and given by Figure 5.19 and Figure 5.20, respectively.

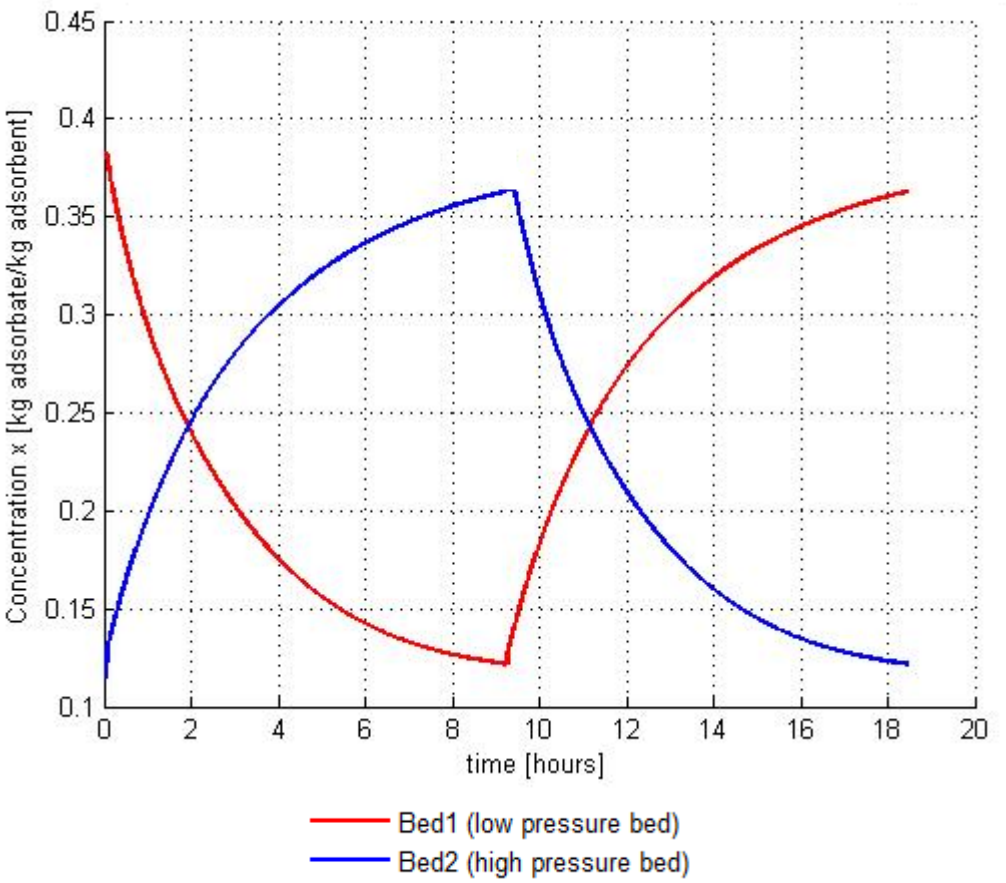

Figure 5.19. Average bed concentration vs time for activated carbon/methanol, $T_{hw} = 90°C,\ T_{con} = 25°C,\ T_{ev} = 10°C.$

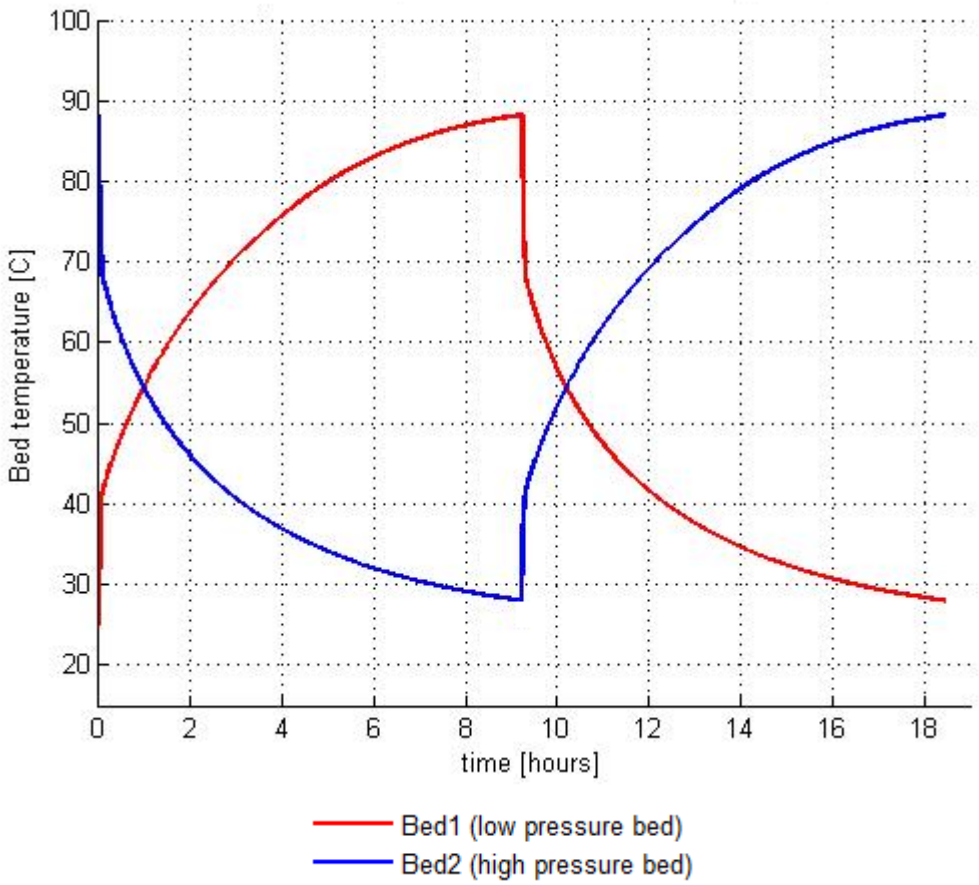

Figure 5.20. Average bed temperature vs time for activated carbon/methanol, $T_{hw} = 90°C$, $T_{con} = 25°C$, $T_{ev} = 10°C$.

5.6. Two Dimensional Plots

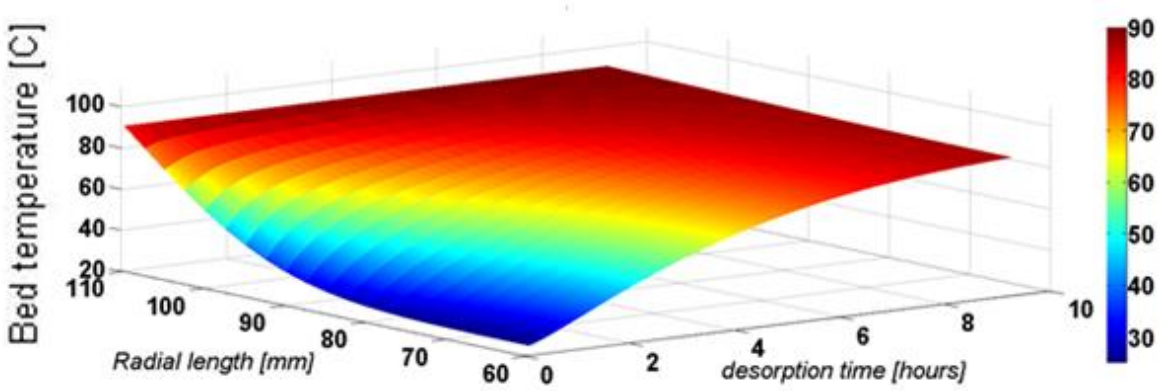

Figure 5.21. Bed 1 temperature distribution during heating for activated carbon/methanol.

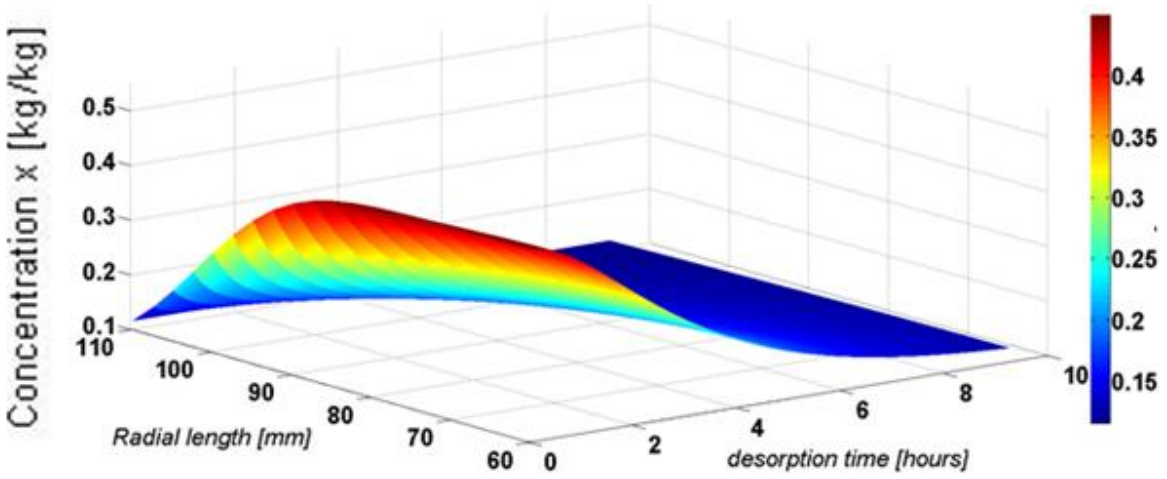

Figure 5.22. Bed 1 concentration distribution during heating for activated carbon/methanol.

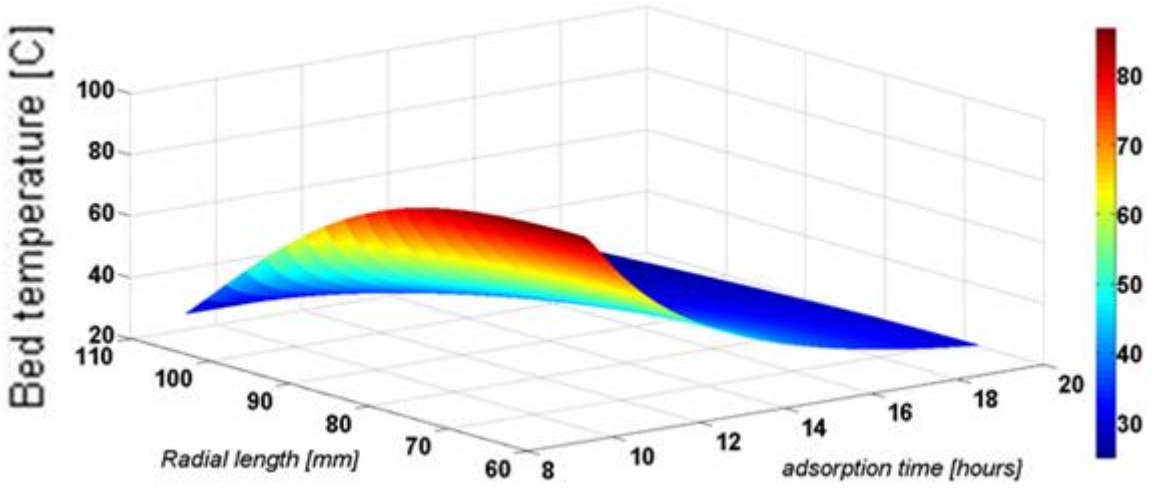

Figure 5.23. Bed 1 temperature distribution during cooling for activated carbon/methanol.

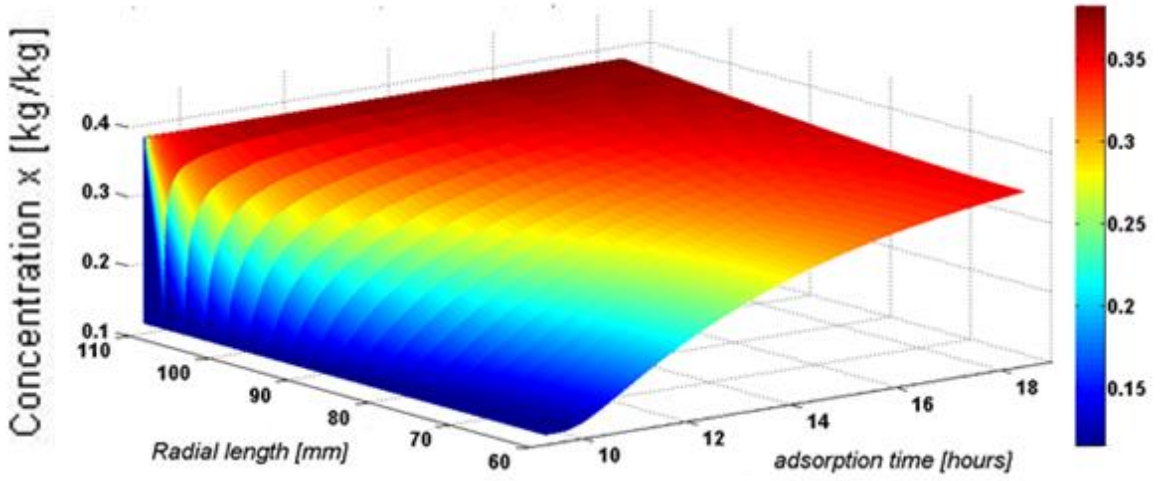

Figure 5.24. Bed 1 concentration distribution during cooling for activated carbon/methanol.

5.7. Mass and Heat Recovery Cycle Analysis

Activated carbon/methanol is adopted for combined mass and heat recovery cycle. All operating parameters' effect on COP and SCP are analyzed and presented in the following sections.

5.7.1. Mass Recovery Effect

δx/Δx, which is the ratio of enlarged cycle concentration over the concentration variation without mass recovery, is plotted to determine the operating parameters effect. It is concluded from Figure 5.25 that lower heat source temperature gives more enlarged refrigerant capacity and increase the system performance. This is because when heat source temperature increases, concentration variation increases (i.e., Δx is 0.06, 0.18, 0.27 at 50 °C, 70 °C, 90 °C heat source temperature) while enlarged cycle concentration remains constant, so the ratio becomes smaller when heat source temperature increases. After a certain heat source temperature, which is approximately 95-100 °C, there is no need to increase heat source temperature, since the ratio begins to remain constant.

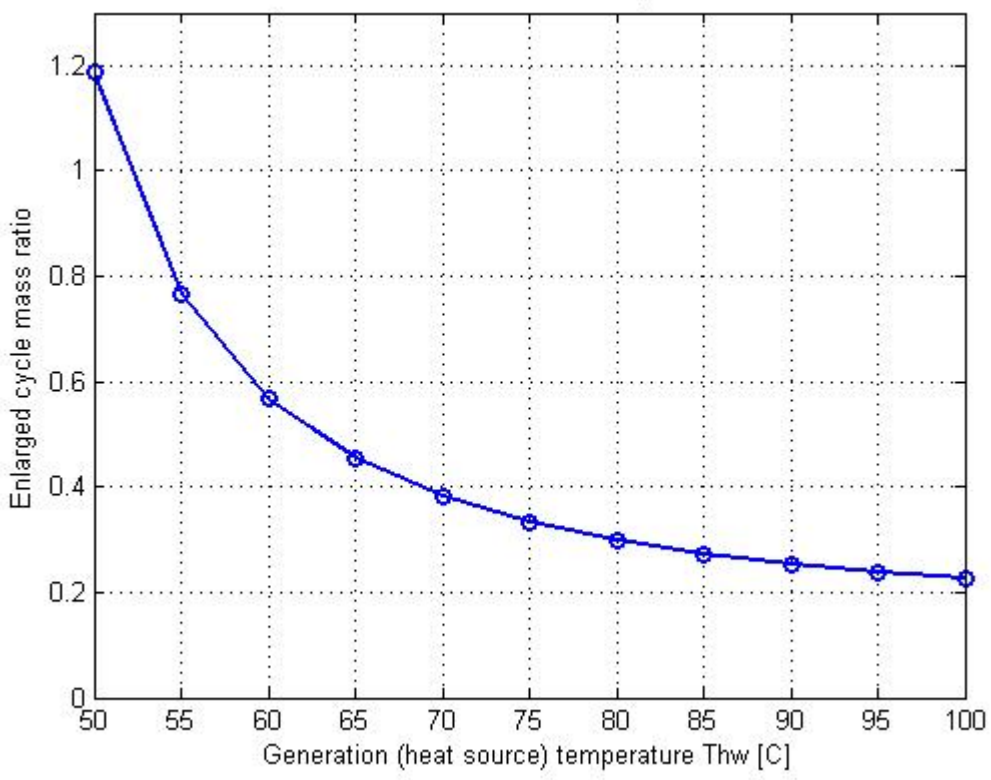

Figure 5.25. Heat source temperature effect on mass recovery ratio, $T_{con} = 25°C,\ T_{ev} = 10°C$.

Heat source temperature is the most effective parameter on mass recovery ratio in comparison to condenser and evaporator temperature. When Figure 5.26 is analyzed, it is concluded that although mass recovery is enhanced with an increase on condenser temperature due to decrease on denominator of δx/Δx; this effect is small, and can be negligible in comparison to heat source temperature and may be assumed as constant.

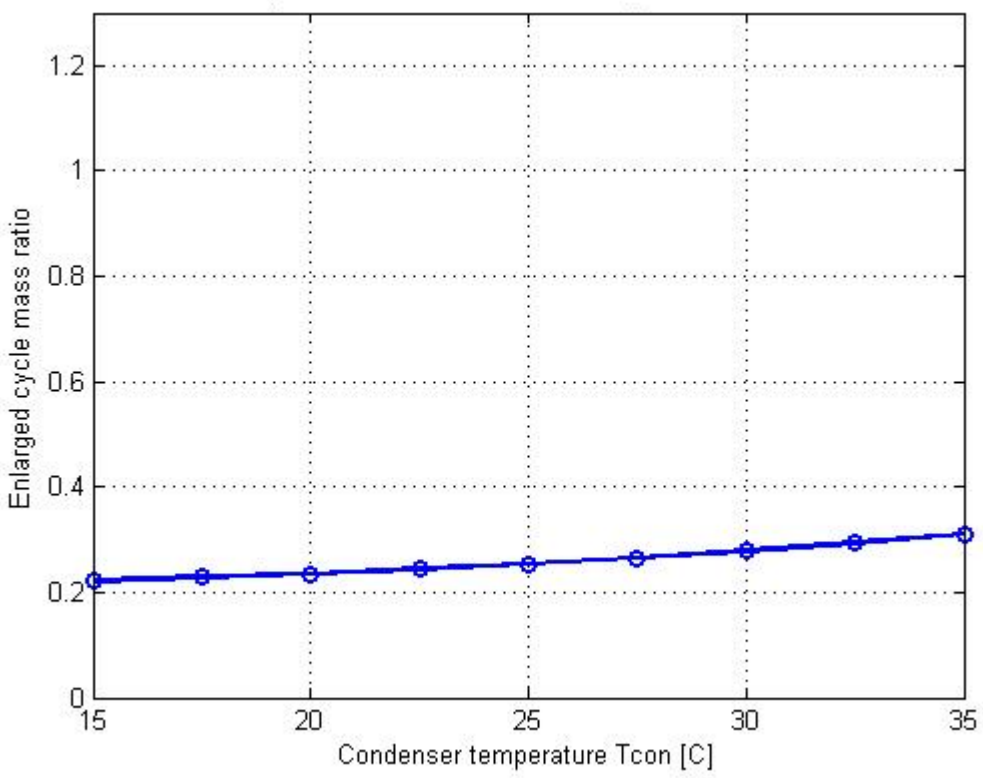

Figure 5.26. Condenser temperature effect on mass recovery ratio, $T_{hw} = 90°C,\ T_{ev} = 10°C$.

On the other hand, Figure 5.27 shows that mass recovery can be enhanced at lower evaporation temperatures. It is because decrease on evaporation temperature, which forces the system to operate under low pressure conditions, results in lower concentration change; therefore, δx/Δx ratio becomes higher. The second reason is that when evaporator temperature increases, pressure difference between condenser and evaporator becomes smaller which decreases mass transfer between adsorbers and consequently enlarged cycle mass ratio drops.

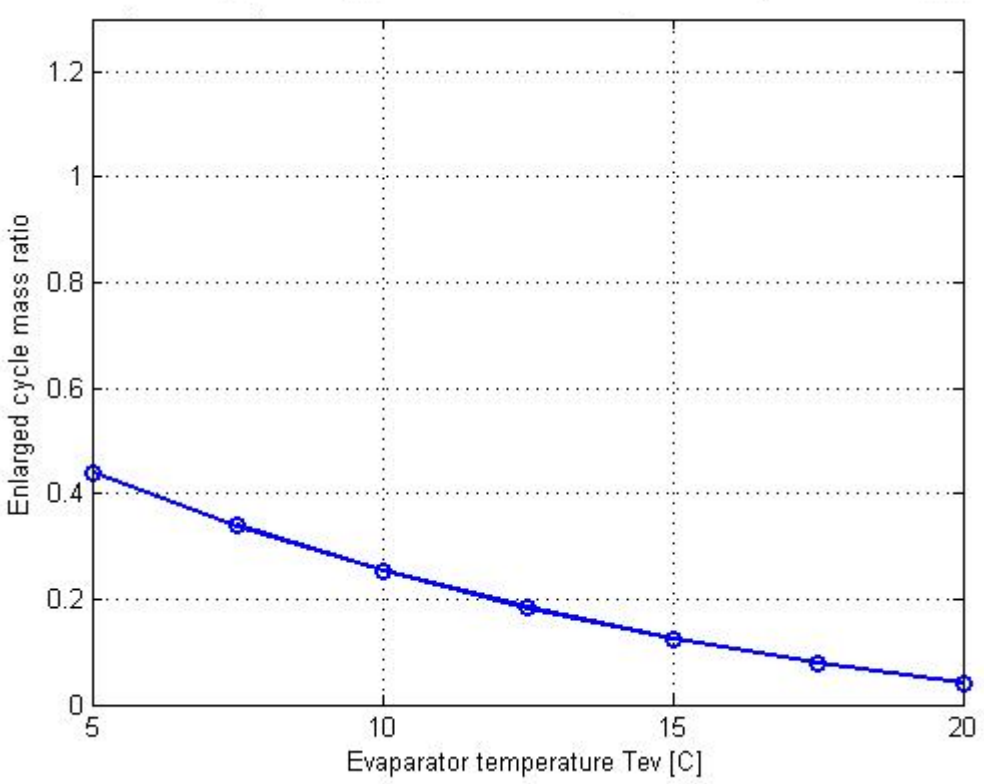

Figure 5.27. Evaporator temperature effect on mass recovery ratio, $T_{hw} = 90°C,\ T_{con} = 25°C$.

5.7.2. Mass and Heat Recovery Combined Effect

It can be easily seen from Figure 5.28 to Figure 5.33 that the combined mass and heat recovery cycle gives larger COP and SCP, which are approximately 1.25 times more than that of the basic cycle, while heat source temperature, condenser temperature and evaporator temperature are 90 °C, 25 °C, 10 °C, respectively. It is concluded that COP is enhanced by heat recovery, while SCP is increased by mass recovery effect.

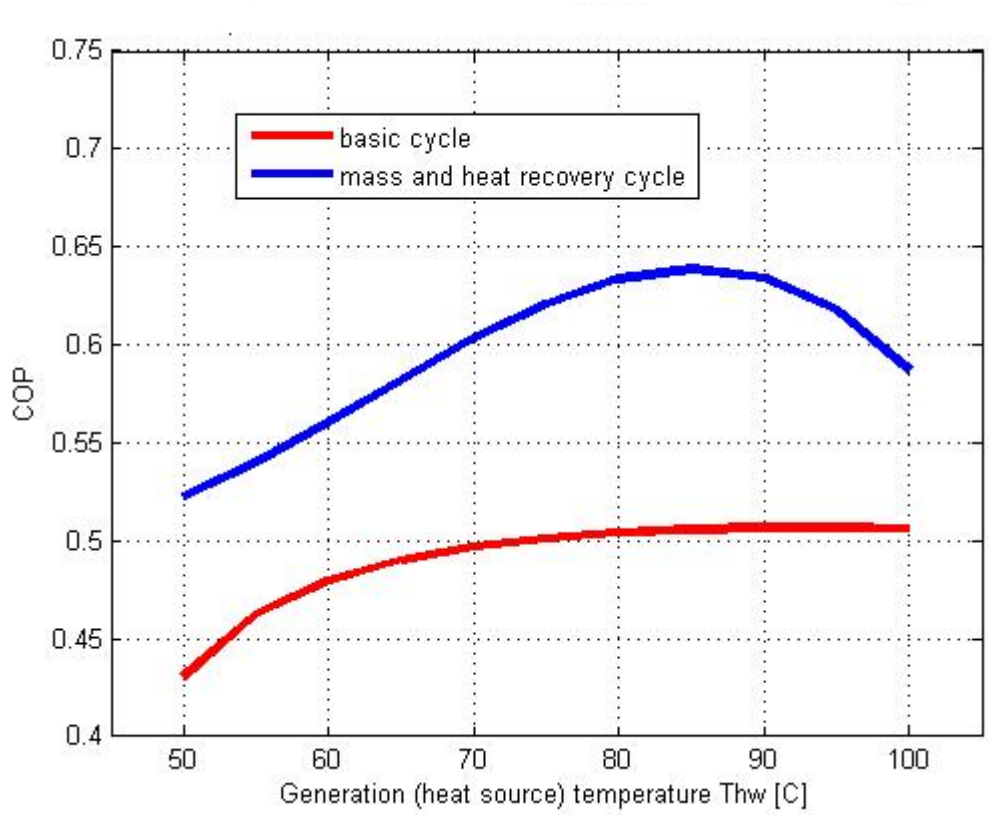

Figure 5.28. Basic and combined cycle COP comparison, $T_{con} = 25°C,\ T_{ev} = 10°C.$

It was shown that mass recovery will increase cycled mass which is benefit for system performance. But due to increase on cycled mass, required heat input during desorption will also increase; therefore mass recovery does not have important role on COP. It was also shown that increase on heat source temperature, decreases enlarged cycle mass, however Figure 5.28 shows that due to pure heat recovery effect, COP tends to increase until around 90 °C. After this temperature heat recovery ratio becomes insufficient and external heat input becomes effective leading to decrease on COP.

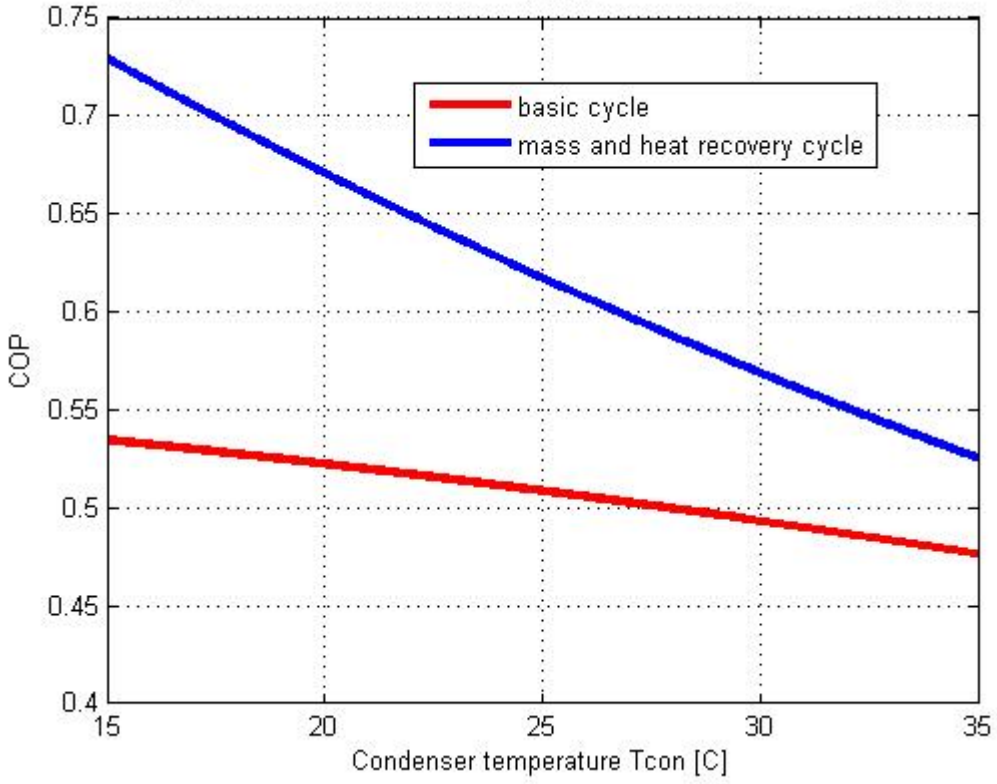

Figure 5.29. Basic and combined cycle COP comparison, $T_{hw} = 90°C,\ T_{ev} = 10°C$.

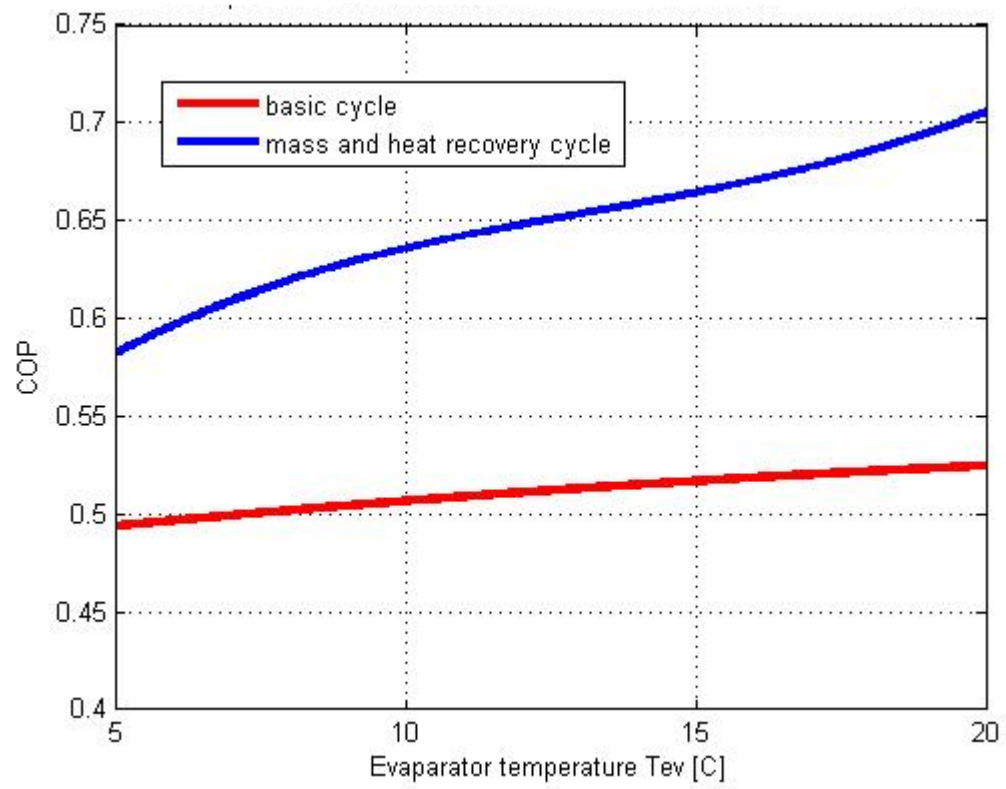

Figure 5.30. Basic and combined cycle COP comparison, $T_{hw} = 90°C,\ T_{con} = 25°C$.

Regarding to Figure 5.29 and Figure 5.30, the reason of condenser temperature and evaporator temperature effect on COP for the combined cycle is exactly the same with the listed reasons for basic cycle in sections 5.3.2 and 5.3.3. Due to heat recovery's decreasing effect on sensible and latent heat input, COP is larger than that of basic cycle.

Mass and heat recovery cycle analysis gives a significant outcome regarding to its effect on SCP. It is observed that combined cycle's performance increasing effect in terms of COP is dominant in comparison to SCP, especially at high generation temperatures where enlarged mass ratio begins to remain constant (Figure 5.25). This is because SCP depends on cycle time. During heat recovery process, heat input is not supplied by an external heat source. Cycle is driven due to the temperature difference of the two adsorbent beds. However the temperature gap between the two adsorbers is not high compared to the gap between the adsorber and external heat source or heat sink. Hence, the heat exchange rate during the heat recovery phase is small compared to the basic cycle. The total cycle time will then increase leading to a penalty in terms of a reduction in SCP for heat recovery cycle.

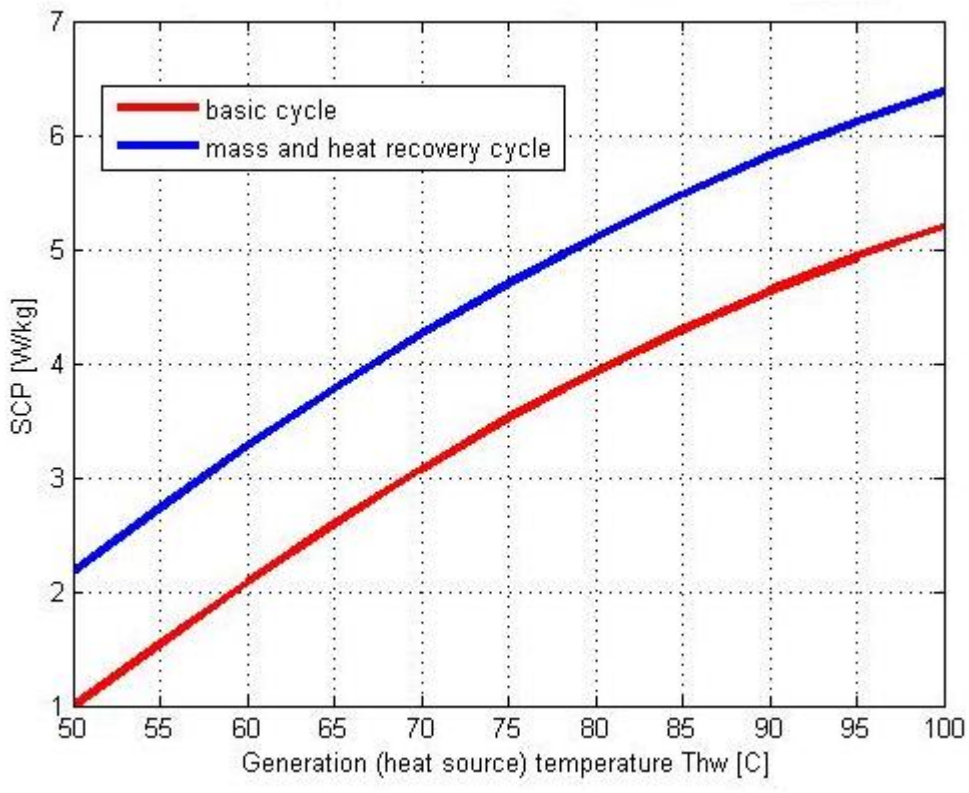

Figure 5.31. Basic and combined cycle SCP comparison, $T_{con} = 25°C,\ T_{ev} = 10°C$.

On the other hand, when Figure 5.31 is evaluated, it is shown that enlarged cycled mass, which was achieved by mass recovery process; compensate this reduction and increases SCP. Therefore heat recovery cycle should be used with mass recovery cycle, which operates quickly (pressure balance is achieved rapidly compared to temperature balance) and has negligible effect on cycle time.

The second recommendation is that heat recovery should not be kept on until two beds reach an equilibrium temperature (ideal heat recovery). Although ideal heat recovery case increases COP, it will result in even less SCP compared to basic cycle especially at high generation temperatures. Therefore, heat recovery process is finalized when temperature difference between two beds decreases and becomes 20 °C in this study.

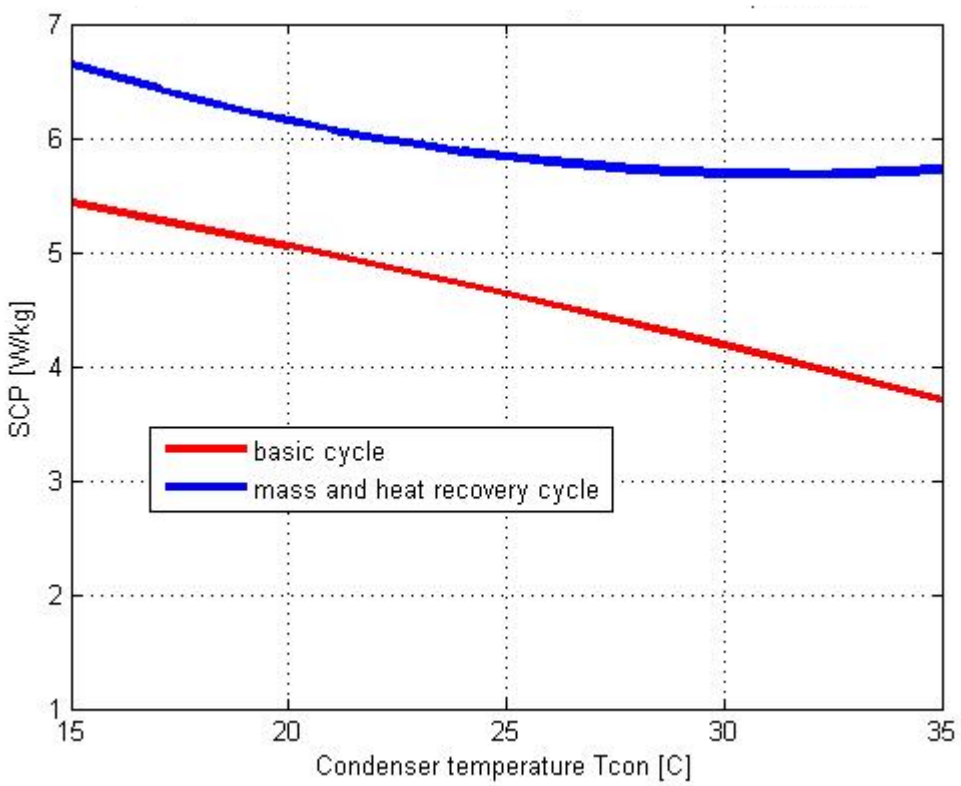

Figure 5.32. Basic and combined cycle SCP comparison, $T_{hw} = 90°C,\ T_{ev} = 10°C$.

Figure 5.32 and Figure 5.33 shows condenser temperature and evaporator temperature effect on SCP, respectively.

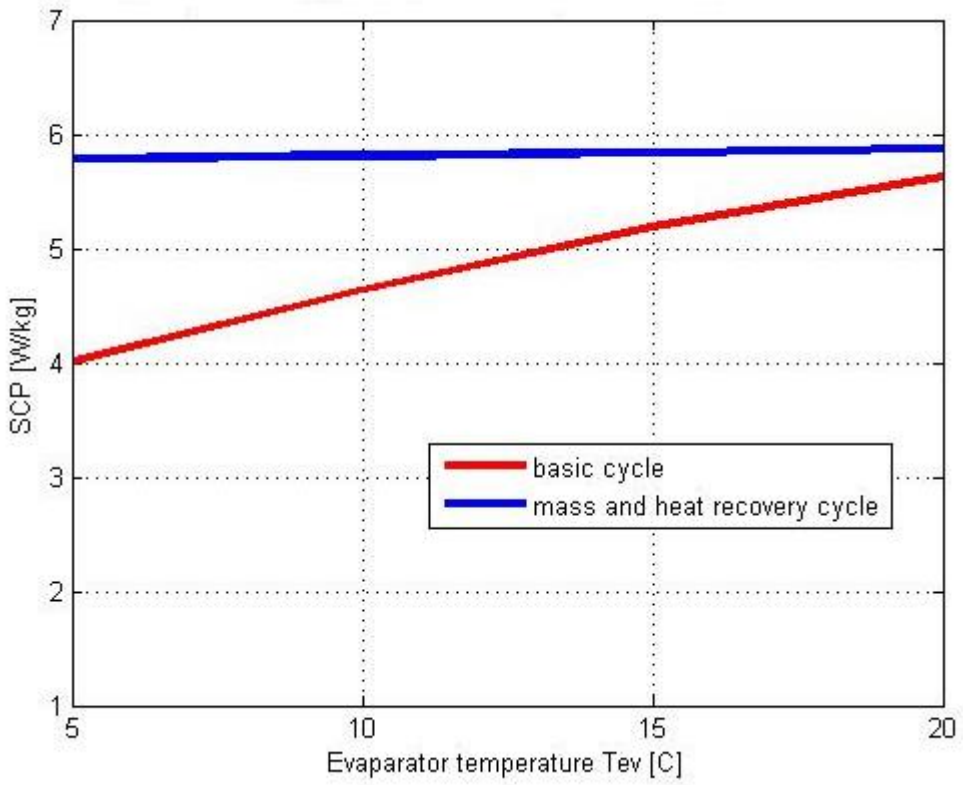

Figure 5.33. Basic and combined cycle SCP comparison, $T_{hw} = 90°C,\ T_{con} = 25°C$.

Figure 5.33 shows that SCP difference between basic and combined cycles decreases when evaporator temperature increases. This is an expected result, since while evaporator temperature increases, cycled mass also increases; however, in order to desorb these enlarged mass, cycle time must be prolonged. Therefore, these two distinct effects compensate each other and SCP seems to be constant while evaporator temperature is increasing.

6. CONCLUSIONS AND RECOMMENDATIONS

6.1. Conclusions

This thesis involved the thermodynamic investigation of a two-beds adsorption refrigeration cycle with mass and heat recovery, which resulted in enhancement on system performance as 1.25 times in terms of COP and SCP than that of the basic cycle.

A non-uniform temperature/uniform pressure mathematical model was adopted by several assumptions for an external-heated generator to describe the transient heat and mass transfer within adsorbent bed. The governing heat transfer equation take into account detail adsorption phenomena was solved numerically by writing an algorithm in MATLAB, which utilizes the forward-time centered-space (FTCS) method in the time and radial space domain and takes account stability and convergence criteria. A grid sensitivity analysis was performed for three cases by changing grid size, and refining mesh. When Δr and Δt were chosen as 2.5 mm, and 0.1 second, respectively, the solution complied with stability and convergence criteria and remained to be constant. The detailed temperature and concentration profiles were obtained for different working pairs such as activated carbon/ammonia, activated carbon/methanol, silica gel/water and zeolite/water.

Firstly, basic adsorption refrigeration cycle performance was investigated by parametric analysis. Heat source temperature, condenser temperature and evaporator temperature effects on COP and SCP were analyzed step by step for all suggested working pairs. As a result of COP analysis, silica gel/water gave the best performance, while activated carbon/ammonia gave the worst; however, it was contrast as an outcome of SCP analysis. Throughout the COP and SCP analysis for the basic cycle, it was concluded that when condenser temperature increases, COP and SCP decreases, too, although when evaporator temperature increases, COP and SCP increases. Regarding to the heat source temperature effect, maximum COP and SCP were obtained at different points. It was also concluded that zeolite/water requires the highest heat source temperature around 180 °C to reach its maximum COP under certain evaporating and condensing temperatures.

Secondly, after a compromise between COP and SCP, activated carbon/methanol pair was selected and adopted for the refrigeration cycle with mass and heat recovery and the same analysis was carried out. Under certain operating conditions and problem geometry, COP and SCP of the cycle were calculated as 0.64 and 5.8 W/kg adsorbent, respectively. While heat recovery effect increases COP, SCP is mainly enhanced due to mass recovery effect. It was observed that combined cycle's performance increasing effect in terms of COP was dominant in comparison to SCP, especially at high generation temperatures. Since heat recovery itself decreases SCP due to the fact that it leads to noticeable increase on total cycle time. In order to eliminate this penalty, heat recovery must be used with mass recovery. Another significant outcome was that after a certain heat source temperature, which was approximately 95-100 °C, there is no need to increase heat source temperature. Since the recovered mass begins to remain constant. Heat source temperature is the most effective parameter on enhanced mass recovery ratio in comparison to condenser and evaporator temperature. It was concluded that although mass recovery was enhanced with an increase on condenser temperature, this effect can be negligible and assumed to be constant, while increase on evaporator temperature yields to decrease on mass recovery ratio.

Thirdly, the effect of bed geometry on cycle performance was examined. It was concluded that when the thickness of the adsorbent bed was increased, heat transfer rate decreased and the time necessary for the completion of each phase also increased and so the cycle duration. It was also clearly figured out that when porosity increases, required cycle time decreased linearly.

Another outcome of this thesis was obtained by making the governing equation written in dimensionless form, and the system behavior was found as depending on dimensionless Fourier and Jakob number.

Finally, cycle time optimization was performed. It was shown that there is no need to supply external heat to the bed after a certain time in terms of COP criteria to make the bed approach to the heat source temperature. COP begins to remain nearly constant after 4 hours. Therefore, heat supply can be stopped after 2 hours, and cooling phase can be initiated. By this way it was possible to obtain higher SCP as 12 W/kg adsorbent and total

cycle time could be reduced 77.8% for the basic cycle utilizing activated carbon/methanol pair.

6.2. Recommendations

In order to promote further research toward improving and developing adsorption refrigeration systems, following recommendations may be listed.

- Non-uniform pressure model may be adopted to take convection effect into account while temperature and concentration fields are determined.
- Local thermal non-equilibrium between solid adsorbent and vapor adsorbate may be employed to take internal diffusion effect into account and develop a more accurate model.
- Cycle time should be reduced by optimizing related parameters to reach higher cooling power.
- Exergy analysis may be carried out for adsorption refrigeration cycle.
- If required data available in literature other working pair alternatives may be employed to have higher cooling power.

APPENDIX A: TAYLOR SERIES EXPANSION

If we want to write $T(i+1,j)$, $T(i-1,j)$, and $T(i,j+1)$ by utilizing Taylor series expansion, it yields to

$$T(i+1,j) = T(i,j) + \frac{\partial T(i,j)}{\partial r}\Delta r + \frac{1}{2!}\frac{\partial^2 T(i,j)}{\partial r^2}(\Delta r)^2 + \frac{1}{3!}\frac{\partial^3 T(i,j)}{\partial r^3}(\Delta r)^3 + \cdots \quad \text{(A.1)}$$

,

$$T(i-1,j) = T(i,j) - \frac{\partial T(i,j)}{\partial r}\Delta r + \frac{1}{2!}\frac{\partial^2 T(i,j)}{\partial r^2}(\Delta r)^2 - \frac{1}{3!}\frac{\partial^3 T(i,j)}{\partial r^3}(\Delta r)^3 + \cdots \quad \text{(A.2)}$$

$$T(i,j+1) = T(i,j) + \frac{\partial T(i,j)}{\partial t}\Delta t + \frac{1}{2!}\frac{\partial^2 T(i,j)}{\partial t^2}(\Delta t)^2 + \frac{1}{3!}\frac{\partial^3 T(i,j)}{\partial t^3}(\Delta t)^3 + \cdots \quad \text{(A.3)}$$

For small Δt and Δr, higher order terms (H.O.T) can be neglected, which yields to

$$\frac{\partial T(i,j)}{\partial r} = \frac{T(i+1,j) - T(i,j)}{\Delta r} - \frac{\partial^2 T(i,j)}{\partial r^2}\frac{\Delta r}{2!} - \frac{\partial^3 T(i,j)}{\partial r^3}\frac{(\Delta r)^2}{3!} - \cdots \quad \text{(A.4)}$$

which is known as forward difference formula with neglecting truncation error $O(\Delta r)$

$$\frac{\partial T(i,j)}{\partial r} = \frac{T(i,j) - T(i-1,j)}{\Delta r} + \frac{\partial^2 T(i,j)}{\partial r^2}\frac{\Delta r}{2!} - \frac{\partial^3 T(i,j)}{\partial r^3}\frac{(\Delta r)^2}{3!} + \cdots \quad \text{(A.5)}$$

which is known as backward difference formula with neglecting truncation error $O(\Delta r)$

When Equation A.2 is extracted from Equation A.1, and added to Equation A.1; it yields to Equation A.6 and Equation A.7, respectively:

$$\frac{\partial T(i,j)}{\partial r} = \frac{T(i+1,j) - T(i-1,j)}{2\Delta r} - \frac{\partial^3 T(i,j)}{\partial r^3}\frac{(\Delta r)^2}{3!} - \cdots \quad \text{(A.6)}$$

which is known as centered difference formula with neglecting truncation error $O(\Delta r)^2$

$$\frac{\partial^2 T(i,j)}{\partial r^2} = \frac{T(i+1,j) - 2T(i,j) + T(i-1,j)}{(\Delta r)^2} + O(\Delta r)^2 \qquad \text{(A.7)}$$

which is known as centered difference formula for second order derivative with neglecting truncation error $O(\Delta r)^2$.

Exact partial time derivative can be written as:

$$\frac{\partial T(i,j)}{\partial t} = \frac{T(i,j+1) - T(i,j)}{\Delta t} - \frac{\partial^2 T(i,j)}{\partial t^2}\frac{\Delta t}{2!} - \frac{\partial^3 T(i,j)}{\partial t^3}\frac{(\Delta t)^2}{3!} - \cdots \qquad \text{(A.8)}$$

which is known as forward difference formula with neglecting truncation error $\mathrm{O}(\Delta t)$

APPENDIX B: THERMODYNAMIC AND OPERATING PARAMETERS

Table B.1. Thermodynamic and operating parameters utilized in analysis (extracted from [1, 2, 13, 28, 32, 33]).

	Activated carbon/Ammonia	**Activated carbon/Methanol**	**Silica gel/Water**	**Zeolite/Water**
r_{in} [mm]	60			
r_{out} [mm]	110			
T_{hw} [°C]	90			
T_{cw} [°C]	25			
T_{con} [°C]	25			
T_{ev} [°C]	10			
T_{in} [°C]	25			
k_{eq} [W/mK]	0.431	0.18	0.198	0.2
h_d [kJ/kg]	1600	1900	2800	3750
ε_t	0.7	0.65	0.64	0.603
ρ_s [kg/m^3]	620	620	2027	960
c_{ps} [J/kgK]	836	836	1000	920
c_{pa} [J/kgK]	4800	2530	4200	4200
L_e (T_{ev}) [kJ/kg]	1225.58	1191.15	2477.3	2477.3

APPENDIX C: CONSISTENCY OF NUMERICAL METHOD

$$T(i,j+1) = T(i,j) + T_t(i,j)\Delta t + \frac{1}{2}T_{tt}(i,j)(\Delta t)^2 + \frac{1}{3!}T_{ttt}(i,j)(\Delta t)^3 + \cdots \quad \text{(C. 1)}$$

$$\begin{aligned} T(i \pm 1,j) = \; & T(i,j) \pm T_r(i,j)\Delta r + \frac{1}{2}T_{rr}(i,j)(\Delta r)^2 \pm \frac{1}{3!}T_{rrr}(i,j)(\Delta r)^3 \\ & + \frac{1}{4!}T_{rrrr}(i,j)(\Delta r)^4 \pm \frac{1}{5!}T_{rrrrr}(i,j)(\Delta r)^5 + \frac{1}{6!}T_{rrrrrr}(i,j)(\Delta r)^6 \\ & \pm \cdots \end{aligned} \quad \text{(C.2)}$$

where T_t and T_r are the time and space derivatives of temperature, respectively.

When the above Taylor expansions are substituted into the FDE, and dropping the notation (i, j) for clarity, it gives:

$$\begin{aligned} & \left[\rho_s(1-\varepsilon_t)\left(c_{ps} + c_{pa}x - h_a\frac{\partial x}{\partial T}\right)\right. \\ & \left. + \varepsilon_t\rho_v c_{pv}\right]\frac{-T + T + T_t\Delta t + \frac{1}{2}T_{tt}(\Delta t)^2 + \frac{1}{3!}T_{ttt}(\Delta t)^3 + \cdots}{\Delta t} \\ & = k_{eq}\left[\frac{-2T + 2T + T_{rr}(\Delta r)^2 + \frac{2}{4!}T_{rrrr}(\Delta r)^4 + \frac{2}{6!}T_{rrrrrr}(\Delta r)^6 + \cdots}{(\Delta r)^2}\right. \\ & \left. + \frac{1}{r}\frac{2T_r\Delta r + \frac{2}{3!}T_{rrr}(\Delta r)^3 + \frac{2}{5!}T_{rrrrr}(\Delta r)^5 + \cdots}{2\Delta r}\right] \end{aligned} \quad \text{(C.3)}$$

Rearranging the last expression (C.3) gives:

$$\left[\rho_s(1-\varepsilon_t)\left(c_{ps}+c_{pa}x-h_a\frac{\partial x}{\partial T}\right)+\varepsilon_t\rho_v c_{pv}\right]\left[T_t+\frac{1}{2}T_{tt}\Delta t+\frac{1}{3!}T_{ttt}(\Delta t)^2+\cdots\right]$$

$$=k_{eq}\left[T_{rr}+\frac{2}{4!}T_{rrrr}(\Delta r)^2+\frac{2}{6!}T_{rrrrrr}(\Delta r)^4+\cdots\right. \tag{C.4}$$

$$\left.+\frac{T_r+\frac{1}{3!}T_{rrr}(\Delta r)^2+\frac{1}{5!}T_{rrrrr}(\Delta r)^4+\cdots}{r}\right]$$

As Δt and Δr goes to 0, FDE approaches to

$$\left[\rho_s(1-\varepsilon_t)\left(c_{ps}+c_{pa}x-h_a\frac{\partial x}{\partial T}\right)+\varepsilon_t\rho_v c_{pv}\right]T_t=k_{eq}\left[T_{rr}+\frac{T_r}{r}\right] \tag{C.5}$$

APPENDIX D: GRID SENSITIVITY ANALYSIS

By utilizing activated carbon/methanol pair and refining mesh size, temperature distribution within adsorbent bed at three different locations, where T1, T2 and T3 denote the temperature at 70 mm, 85 mm and 100 mm, respectively, is given by Table D.1 and Figure D.1.

Table D.1. Grid sensitivity analysis of temperature development within adsorbent bed for three different meshes.

	Δr=5 mm Δt=1 s			Δr=2.5 mm Δt=0.1 s			Δr=0.5 mm Δt=0.05 s		
Time [s]	**T1 [°C]**	**T2 [°C]**	**T3 [°C]**	**T1 [°C]**	**T2 [°C]**	**T3 [°C]**	**T1 [°C]**	**T2 [°C]**	**T3 [°C]**
Isosteric Heating Phase									
0	25	25	25	25	25	25	25	25	25
100	25.012	25.939	45.245	25.005	25.752	45.254	25.003	25.675	45.247
200	25.351	30.049	56.337	25.286	29.891	56.418	25.260	29.828	56.438
Desorption Phase									
2210	32.341	43.556	68.784	32.370	43.593	68.834	32.385	43.605	68.848
4210	39.580	52.011	73.807	39.610	52.080	73.843	39.585	52.098	73.853
6210	46.402	58.242	76.842	46.383	58.293	76.867	46.296	58.289	76.872
8210	52.627	63.227	79.042	52.547	63.241	79.054	52.399	63.202	79.047
10210	58.232	67.422	80.804	58.101	67.395	80.801	57.902	67.319	80.779
12210	63.235	71.041	82.289	63.067	70.979	82.271	62.834	70.871	82.236
14210	67.659	74.190	83.566	67.470	74.101	83.537	67.218	73.970	83.492
16210	71.526	76.923	84.671	71.331	76.819	84.634	71.076	76.675	84.582
18210	74.864	79.276	85.622	74.675	79.167	85.582	74.429	79.020	85.527
20210	77.707	81.281	86.434	77.532	81.174	86.393	77.305	81.033	86.339
22210	80.096	82.967	87.118	79.941	82.869	87.080	79.738	82.738	87.029
24210	82.078	84.368	87.689	81.945	84.281	87.654	81.769	84.165	87.609
26210	83.702	85.519	88.158	83.592	85.445	88.129	83.443	85.344	88.089
28210	85.021	86.454	88.541	84.931	86.392	88.516	84.807	86.308	88.482
30210	86.080	87.207	88.849	86.009	87.157	88.829	85.907	87.087	88.801

Table D.1. Grid sensitivity analysis of temperature development within adsorbent bed for three different meshes (cont.).

32210	86.926	87.808	89.096	86.869	87.768	89.080	86.788	87.712	89.057
33210	87.281	88.060	89.200	87.231	88.025	89.186	87.158	87.975	89.165
Isosteric Cooling Phase									
33310	87.390	85.094	61.473	87.381	85.226	61.355	87.330	85.255	61.316
33410	85.967	77.587	51.217	86.018	77.603	51.139	85.998	77.588	51.106
33420	85.716	76.873	50.568	85.768	76.883	50.494	85.749	76.865	50.462
Adsorption Phase									
35420	75.396	63.630	42.574	75.067	63.531	42.509	74.741	63.440	42.478
37420	66.831	56.124	38.572	66.329	55.915	38.496	65.928	55.748	38.446
39420	60.132	50.793	36.028	59.617	50.532	35.934	59.239	50.338	35.867
41420	54.801	46.711	34.181	54.322	46.437	34.078	53.986	46.241	34.005
43420	50.460	43.453	32.749	50.028	43.186	32.645	49.736	43.002	32.574
45420	46.860	40.784	31.597	46.476	40.535	31.498	46.223	40.368	31.431
47420	43.833	38.560	30.648	43.493	38.332	30.556	43.275	38.183	30.495
49420	41.262	36.684	29.854	40.962	36.478	29.771	40.774	36.346	29.716
51420	39.062	35.087	29.183	38.798	34.902	29.108	38.635	34.787	29.060
53420	37.170	33.718	28.611	36.937	33.555	28.544	36.797	33.454	28.502
55420	35.537	32.541	28.120	35.332	32.396	28.061	35.211	32.309	28.024
57420	34.124	31.525	27.698	33.944	31.397	27.645	33.839	31.322	27.614
59420	32.900	30.647	27.334	32.741	30.534	27.287	32.651	30.468	27.260
61420	31.838	29.886	27.019	31.698	29.786	26.978	31.620	29.730	26.954
63420	30.917	29.227	26.746	30.793	29.139	26.710	30.726	29.090	26.690
65420	30.117	28.655	26.510	30.009	28.578	26.478	29.951	28.535	26.460
66420	29.758	28.398	26.404	29.657	28.326	26.374	29.603	28.287	26.358

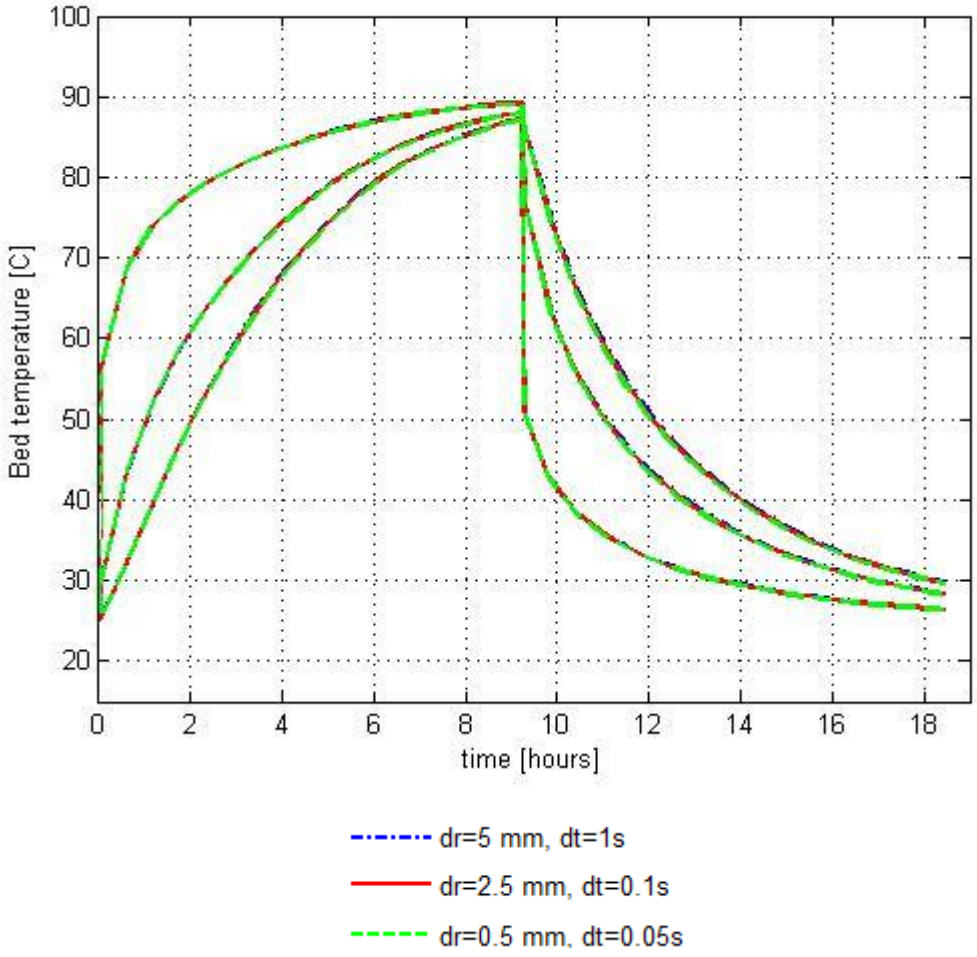

Figure D.1. Grid sensitivity analysis of temperature development within adsorbent bed for three different meshes.

APPENDIX E: LITERATURE COMPARISON

In order to validate the numerical results' compliance with literature, the algorithm written in MATLAB software was adopted for the study existing in literature and published by A. El Fadar, A. Mimet, and M. Perez Garcia [2] who had studied continuous adsorption refrigeration system consisting of two adsorbent beds and powered by parabolic trough solar collector. Activated carbon as adsorbent and ammonia as refrigerant had been selected. Their model was based on non-uniform temperature, uniform pressure and local thermal equilibrium between solid adsorbent and adsorbate vapor. They had also verified the numerical result with experiment. All operating parameters used by A. El Fadar, A. Mimet, and M. Perez Garcia were conducted into the algorithm, and Figure E.1 was plotted and compared with Figure E.2, which exists in literature [2]. As it can be easily seen, the algorithm used in this thesis study complies with both numerical and experimental results obtained by A. El Fadar, A. Mimet, and M. Perez Garcia.

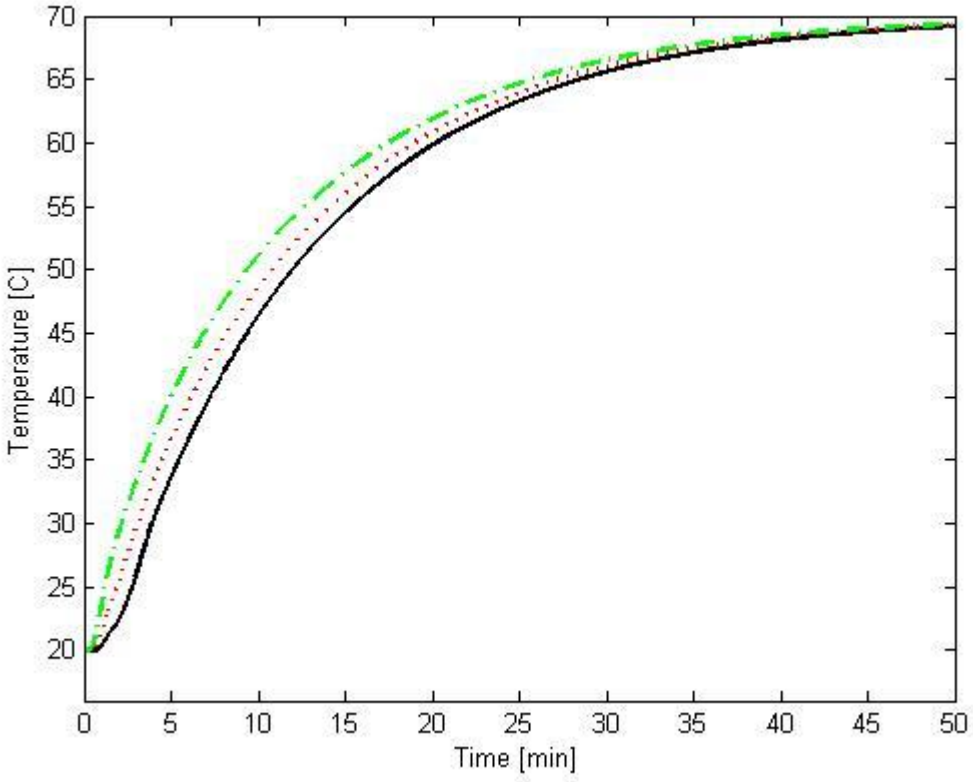

Figure E.1. Adsorbent bed temperature profile comparison.

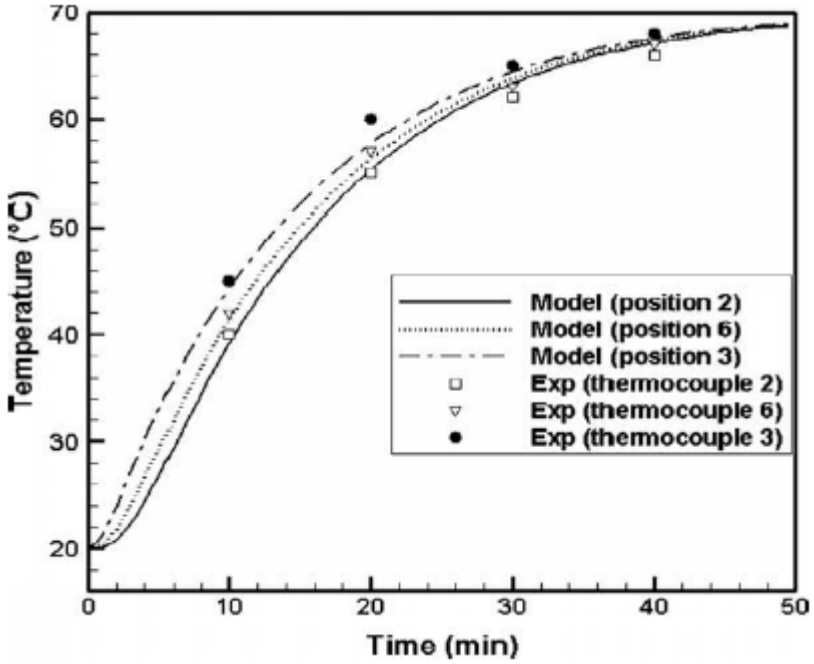

Figure E.2. Comparison of the predicted transient temperature distributions with experimental data [2].

REFERENCES

1. Leong, K. C., Y. Liu, "Numerical Study of A Combined Heat and Mass Recovery Adsorption Cooling Cycle", *International Journal of Heat and Mass Transfer,* Vol. 47, No. 22, pp. 4761-4770, 2004.
2. Fadar, A. E., A. Mimet, M. P. Garcia, "Modelling and Performance Study of A Continuous Adsorption Refrigeration System Driven by Parabolic Trough Solar Collector", *Solar Energy,* Vol. 83, No. 6, pp. 850-861, 2008.
3. Aghbalou, F., A. Mimet, F. Badia, J. Illa, A. E. Bouardi, J. Bougard, "Heat and Mass Transfer During Adsorption of Ammonia in A Cylindrical Adsorbent Bed, Thermal Performance Study of A Combined Parabolic Solar Collector, Water Heat Pipe and Adsorber Generator Assembly", *Applied Thermal Engineering,* Vol. 24, No. 17, pp. 2537-2555, 2004.
4. Wang, D. C., Z. Z. Xia, J. Y. Wu, "Design and Performance Prediction of A Novel Zeolite–Water Adsorption Air Conditioner", *Energy Conversion and Management,* Vol. 47, No. 5, pp. 590-610, 2006.
5. Qu, T. F., R. Z. Wang, W. Wang, "Study on Heat and Mass Recovery in Adsorption Refrigeration Cycles", *Applied Thermal Engineering,* Vol. 21, No. 4, pp. 439-452, 2001.
6. Qu, T. F., W. Wang, R. Z. Wang, "Study of The Effects of Mass and Heat Recovery on The Performances of Activated Carbon/Ammonia Adsorption Refrigeration Cycles", *Journal of Solar Energy Engineering,* Vol. 124, No. 3, pp. 283-290, 2002.
7. Bansal, R. C., M. Goyal, *Activated Carbon Adsorption*, Taylor & Francis Group, Oxford, 2005.
8. Boor, L. B., *Adsorption and Activated Carbon*, M.S. Thesis, University of Wisconsin-Madison, 1992.
9. Wang, R. Z., Q. B. Wang, "Adsorption Mechanism and Improvements of The Adsorption Equation for Adsorption Refrigeration Pairs", *International Journal of Energy Research,* Vol. 23, No. 10, pp. 887-898, 1999.
10. Wang, L. W., R. Z. Wang, R. G. Oliveira, "A Review on Adsorption Working Pairs for Refrigeration", *Renewable and Sustainable Energy Reviews,* Vol. 13, No. 3, pp. 518-534, 2009.

11. Zhao, Y., *Study of Activated Carbon/Methanol Adsorption Refrigeration Tube and System Integration*, M.S. Thesis, The University of Adelaide, 2011.
12. Teng, Y., R. Z. Wang, J. Y. Wu, "Study of The Fundamentals of Adsorption Systems", *Applied Thermal Engineering*, Vol. 17, No. 4, pp. 327-338, 1997.
13. Sumathy, K., K. H. Yeung, L. Yong, "Technology Development in The Solar Adsorption Refrigeration Systems", *Progress in Energy and Combustion Science*, Vol. 29, No. 4, pp. 301-327, 2003.
14. Alghoul, M. A., M. Y. Sulaiman, B. Z. Azmi, M. A. Wahab, "Advances on Multi-Purpose Solar Adsorption Systems for Domestic Refrigeration and Water Heating", *Applied Thermal Engineering*, Vol. 27, No. 5, pp. 813-822, 2007.
15. Strand, G., "Activated Carbon for Purification of Alcohol", 2001, homedistiller.org/activated_book1.pdf, accessed at May 2002.
16. Turner, L., *Improvement of Activated Charcoal-Ammonia Adsorption Heat Pumping/Refrigeration Cycles Investigation of Porosity and Heat/Mass Transfer Characteristics*, Ph.D. Thesis, University of Warwick, 1992.
17. Wang, R. Z., "Adsorption Refrigeration Research in Shanghai Jiao Tong University", *Renewable and Sustainable Energy Reviews*, Vol. 5, No. 1, pp. 1-37, 2001.
18. Wang, R. Z., "Performance Improvement of Adsorption Cooling by Heat and Mass Recovery Operation", *International Journal of Refrigeration*, Vol. 24, No. 7, pp. 602-611, 2001.
19. Szarzynski, S., Y. Feng, M. Pons, "Study of Different Internal Vapor Transports for Adsorption Cycles with Heat Regeneration", *International Journal of Refrigeration*, Vol. 20, No. 6, pp. 390-401, 1997.
20. Marletta, L., G. Maggio, A. Freni, M. Ingrasciotta, G. Restuccia, "A Non-uniform Temperature Non-uniform Pressure Dynamic Model of Heat and Mass Transfer in Compact Adsorbent Beds", *International Journal of Heat and Mass Transfer*, Vol. 45, No. 16, pp. 3321-3330, 2002.
21. Chua, H. T., K. C. Ng, W. Wang, C. Yap, X. L. Wang, "Transient Modeling of A Two Beds Silica Gel/Water Adsorption Chiller", *International Journal of Heat and Mass Transfer*, Vol. 47, No. 4, pp. 659-669, 2004.
22. Liu, Y., K. C. Leong, "Numerical Study of A Novel Cascading Adsorption Cycle", *International Journal of Refrigeration*, Vol. 29, No. 2, pp. 250-259, 2006.

23. Cortes, F. B., F. Chejne, J. M. Mejia, C. A. Londono, "Mathematical Model of The Sorption Phenomenon of Methanol in Activated Coal", *Energy Conservation and Management*, Vol. 50, No. 5, pp. 1295-1303, 2009.
24. Khattab, N. M., "Simulation and Optimization of A Novel Solar Powered Adsorption Refrigeration Module", *Solar Energy*, Vol. 80, No. 7, pp. 823-833, 2006.
25. Hu, J., R. H. B. Exell, "Simulation and Sensitivity Analysis of An Intermittent Solar Powered Charcoal/Methanol Refrigerator", *Renewable Energy*, Vol. 4, No. 1, pp. 133-149, 1994.
26. Maggio, G., A. Freni, G. Restuccia, "A Dynamic Model of Heat and Mass Transfer in A Double Bed Adsorption Machine with Internal Heat Recovery", *International Journal of Refrigeration,* Vol. 29, No. 4, pp. 589-600, 2006.
27. Wu, W. D., H. Zhang, D. W. Sun, "Mathematical Simulation and Experimental Study of A Modified Zeolite 13X/Water Adsorption Refrigeration Module", *Applied Thermal Engineering,* Vol. 29, No. 4, pp. 645–651, 2009.
28. Mers, A. A., A. Azzabakh, A. Mimet, H. E. Kalkha, "Optimal Design Study of Cylindrical Finned Reactor for Solar Adsorption Cooling Machine Working with Activated Carbon/Ammonia Pair", *Applied Thermal Engineering,* Vol. 26, No. 16, pp. 1866-1875, 2006.
29. Liu, Y., K. C. Leong, "The Effect of Operating Conditions on The Performance of Zeolite/Water Adsorption Cooling Systems", *Applied Thermal Engineering* Vol. 25, No. 10, pp. 1403-1418, 2005.
30. Hoffman J. D., *Numerical Methods for Engineering and Scientists*, Purdue University, 2001.
31. Pons, M., F. Meunier, G. Cacciola, R. E. Critoph, M. Groll, L. Puigjaner, B. Spinner, F. Ziegler, "Thermodynamic Based Comparison of Sorption Systems for Cooling and Heat Pumping", *International Journal of Refrigeration,* Vol. 22, No. 1, pp. 5-17, 1999.
32. Demirocak, D. E., *Thermodynamic and Economic Analysis of A Solar Thermal Powered Adsorption Cooling System,* M.S. Thesis, Middle East Technical University, 2008.

33. Taylan, O., *Numerical Modelling and Performance Analysis of A Solar Powered Ideal Adsorption Cooling Systems*, M.S. Thesis, Middle East Technical University, 2010.